Master of Science in Space Engineering – *Politecnico di Milano*

Cursus ingénieur, filière OTSU – *ISAE SUPAERO*

Centre National d'Etudes Spatiales

Lunar Modes Feasibility Analysis for MicroCarb Mission

Master Thesis

Student:

Tommaso CAPANO

ID number: 899986

CNES supervisor:

Isabelle SEBBAG

ISAE supervisor:

David MIMOUN

Academic Year:

2029- 2020

Politecnico di Milano supervisor:

Camilla COLOMBO

Thursday, December 3, 2020

This content is original, written by the Author, Tommaso Capano. All the non-original information, taken from previous works, are specified and recorded in the bibliography.
When referring to this work, full bibliographic details must be given, i.e:
Tommaso Capano, “Lunar modes feasibility analysis for MicroCarb mission”. 2020, Politecnico di Milano, Faculty of industrial Engineering, Department of Aerospace Science and Technologies, Master in Space Engineering, Supervisor: Camilla Colombo, Co-supervisor: Isabelle Sebbag.

Acknowledgments

This internship was carried out in a challenging period marked by social distancing and restrictions to face a global pandemic crisis currently spreading worldwide. In such a context, it was not easy to dive into a new working environment and establish solid bounds with people around me. I would like to personally thank my tutor Isabelle for doing her best to create a warm environment and put me at ease in every possible situation. She showed me the importance of human connection, especially in a formal working context. Special thanks to Miguel, Nicolas and the rest of the *MP* team for the extraordinary support they offered me: I found the strongest motivation in their passion and interest that prompted me to do my best. My gratitude equally goes to Ms. Camilla Colombo and Mr. David Mimoun who supervised the internship since the earliest developments, giving me precious advices on technical aspects.

To all my dear friends that I met in Toulouse, I owe you the merit to have turned my life into a dream. Thanks for these two breath-taking years. Thanks to all of you from the deep of my soul. Home is wherever you feel home, nothing else.

Infine, rivolgo il pensiero e il cuore ai miei genitori.
Nonostante tutte le difficoltà incontrate in questi anni, siete sempre stati in grado di darmi sostegno, fiducia e affetto anche nei momenti più bui. Questa esperienza lontano da casa mi ha insegnato ad apprezzare gli enormi sforzi che ognuno di voi ha fatto per rendermi la persona che desideravo essere. Tutti noi commettiamo errori, ogni giorno. Siamo lontani dall'essere perfetti e non esistono né cattivi figli né buoni genitori. Ciò che davvero importa, personalmente, è che io abbia potuto contare su di voi quando ne ho avuto bisogno. D'ora in avanti, perciò, contate pure su di me.

Abstract

Carbon dioxide is recognised as the main driver of human-induced climate change. Its evolution in time is therefore scrutinised with attention by the global scientific community. Today there is a lack of understanding of the vegetation dynamics, and its response to increasing CO_2 and changing climate. This lack of understanding limits our ability to anticipate the carbon budget and thus the rate of climate change. There is therefore a strong need for a better understanding of the carbon cycle and the processes that control the exchanges of carbon between the atmosphere, the vegetation, and the soil. Within this framework, the MicroCarb mission proposed by French Space Agency CNES represent the European contribution to CO_2 remote sensing measurement, providing a continuous monitoring of our globe and serving as technological pathfinder for future missions. This thesis contributes to the feasibility assessments of three calibration modes based on lunar observations; they are crucial to characterise the behavior of the on-board spectrometer, the main instrument responsible for scientific measurements. In particular, lunar calibrations aim at quantifying the components of the random error in measurements due to uncertainties in the real radiometric gain of the instrument, as well as geometrical distortions introduced by spectral decomposition of the light. This allow to increase its precision to satisfy the mission requirements which impose a random error lower than one part per million in measurements of CO_2 concentration at surface level.

The key points of investigation concern the identification of the optimal conditions, in terms of lunar phase as well as spacecraft configurations, to perform such guidance modes in compliance with the attitude constrains defined for the mission. The associated acquisition legs were thus simulated and analysed over all the possible scenarios defined by the mission analysis to ensure their feasibility and determine the criticality associated to each specific configuration.

The analysis showed that calibrations are feasible within a portion of lunar cycle corresponding to one week, where optimal performances are found; furthermore, it was showed that performances on long term were strictly dependent on the relative elevation of the Moon, which can arise visibility problems during observations.

Table of Contents

List of acronyms

AOCS	Attitude and Orbit Control System
ACT	ACross Track Direction
ALT	ALong Track direction
cal/val	calibration and validation phase
CNES	Centre National des Etudes Spatiales
CO_2	Carbon dioxide
DSO	Direction Systèmes Orbitaux
DV	sous-direction Dynamique du Vol
ESA	European Space Agency
FOV	Field Of View
GOSAT	Greenhouse gasses Observing SATellite
IFOV	Instantaneous Field Of View
JAXA	Japanese Aerospace eXploration Agency
LEOP	Launch and Early Orbit Phase
MCV	Miroir de Changement de Visée (line-of-sight rotation mirror)
MLTAN	Mean Local Time of Ascending Node
MP	Service Programmation Mission et guidage en attitude
NASA	National Aeronautics and Space Administration
NIR	Near InfraRed region
OCO	Orbital Carbon Observatory
O_2	molecular oxygen
OHP	Orbit horizon plane
PLGS	PayLoad Ground Segment
ppm	part per million
SI	sous-direction Systèmes Instrumentaux
SNR	Signal-to-Noise Ratio
SWIR	Short Wave Infrared Region
VIS	Visible spectral region
VTS	Visualisation Toolkit for Space data

List of Symbols

α	Approach angle
β	Orbit plane angle with respect to Earth-Sun direction
δ	Moon relative elevation
δ^*	Average Moon relative elevation
$\boldsymbol{n}$	Normal to the orbit horizon plane
$\boldsymbol{h}$	Angular momentum direction
$\boldsymbol{k}$	Normal to the ecliptic plane
λ	Spectral wavelength
X	Column-averaged concentration
P	Atmospheric pressure
φ	Lunar phase
ρ	MCV roll
w	Weight function of column concentration

1. Introduction

The latest scientific assessment by the Intergovernmental Panel on Climate Change [1] states that climate warming is unequivocal. Many recent changes are unprecedented over decades to millennia. The atmosphere and ocean have warmed, snow and ice have diminished, and sea level has risen. Changes such as these have resulted from positive radiative forcing caused by increased concentrations of atmospheric greenhouse gases. Carbon dioxide (CO_2) makes the largest contributions to radiative forcing. With concentrations now the highest since 800 000 years [1], and continuing to rise, reducing the emission of this gas is considered the most important environmental challenge in the 21st century. The evolution of CO_2 emissions in time is therefore scrutinised with attention by the international scientific community. The current global carbon budget [2] indicates that in the period from 2005 to 2018, an average of 11.03 GtC (Giga tonnes of carbon dioxide per year) is produced every year, 82% of which is due to fossil fuel combustion. Once released in the environment, CO_2 is absorbed by the atmosphere (45%), oceans (24%) and terrestrial vegetation (29%); acting as natural sinks and continuously interacting in a mutual way, they give rise to the environmental process commonly known as carbon cycle. As of today, many questions on this topic remains open: 2% of the global budget remains unattributed, indicating overestimated emissions and/or underestimated sinks. Also, there is a lack of understanding of the vegetation dynamic, and its response to increasing CO_2 within the next century. Studies performed by Potsdam Institute for Climate Impact Research [3] show that, by 2100, the increase in CO_2 emissions can lead to an overall net reduction of carbon sink capacity, from land vegetation, that could drop from 3.0 $GtCyr^{-1}$ to 0.6 and 0.3 $GtCyr^{-1}$ for a moderate and strong climate change scenarios (2.9 K and 5.3 K temperature increase over present), respectively. However, there is no consensus on whether the land sink is mostly in the tropics, mid-latitudes, or boreal regions. This lack of understanding of the vegetation processes limits our ability to anticipate the carbon budget and thus the rate of climate change in future decade. A better

comprehension of the carbon cycle can be obtained through a continuous monitoring of CO_2 fluxes at the land-atmosphere interface and the analysis of its response to inter-annual climate anomalies.

This objective suggests the development of a satellite monitoring system as recognised by the scientific community and several space agencies. In this sense, SCIAMACHY instrument, embarked on ESA's Envisat mission [4] and launched in 2006, pioneered the ability to remotely sense greenhouse gases with good sensitivity throughout the atmosphere boundary layer. It provided the first measurements of CO_2 column concentration (X_{CO_2}) with a spatial resolution of 40 km^2, providing insights into how CO_2 fluxes in northern ecosystem respond to interannual surface-temperature variability [4]. SCIAMACHY's single measurement precision has been assessed against the Total Carbon Column Observing Network (TCCON), and is estimated within 2-5 parts-per-million (ppm). The estimated relative bias is around 1 ppm at regional scales [4]. An important step forward in measurement accuracy was done with GOTSAT [5], designed by the Japanese Aerospace eXploration Agency (JAXA), launched in 2009. The on-board spectrometer ANSO-FTS allows to perform measurements on spatial scales of 10 km, with circular footprints. However, the drawback is a reduced spatial coverage and resolution. This limits the use of the data, only constraining the variability of CO_2 fluxes at continental scale. GOSAT single measurement precision assessed against TCCON is 2-3 ppm [5]. A second mission GOSAT-2 [6], launched in 2018 and currently operative, represents the successor of GOSAT. In addition to an improved version of the imager for cloud detection, the FTS-2 spectrometer features a wider spectral range, including two additional bands in the ultra-violet region which are very effective in the characterisation of aerosols over urban areas. The improved signal-to-noise ratio and extended along-track pointing angle for sun glint measurement over oceans will also contribute to an increase in gas concentration data yield [6]. The Orbiting Carbon Observatory 2 (OCO-2) mission [7], developed by NASA, is the first Earth remote sensing mission entirely dedicated to CO_2 emissions. After the loss of its predecessor (OCO) on February 2009 [7], caused by a failure in fairing separation during launch phase, the mission was successfully launched in 2014 and it is currently active in data acquisitions. The system is equipped with three grating spectrometers working independently but fed by a common telescope: this innovative solution enables higher performances in terms of Signal to Noise Ratio (SNR>400) with a precision of 0.5 ppm [7].The Chinese Space Agency is also active in CO_2 remote sensing activities with its TanSat mission, successfully launched in 2016. It features an optical spectrometer working over three spectral bands with a spatial resolution of 2 km and a Cloud and Aerosol Polarisation Imager (CAPI) to compensate CO_2 measurement errors by high-resolution measurement of cloud and aerosol. Single measurements precision assessed against TCCON is 4 ppm [8].

Within this framework, the MicroCarb mission proposed by the French Space Agency CNES (Centre National d'Etudes Spatiales) represents a European contribution to CO_2 remote sensing measurement, serving as both a technological pathfinder for future operational systems and as a continuity link to support data collected by previous missions. The main technological challenge that MicroCarb will face consists in the design a new carbon emission tracker, with objectives and performances comparable with those of larger missions (precision of the order of 1 ppm), using a 200 kg-class microsatellite. Particularly, studies performed by Airbus Defense and Space [9] for CNES demonstrated that the level of performances required can be attained with a miniaturised spectrometer to integrate on an already-existing platform product (MYRIADE) at very affordable costs [10]. The overall budget is estimated by Airbus to be approximately 160 M€ (including 14 M€ for the spectrometer production), that is one-third of the amount spent for OCO-2 (435 M€) and less than one half of the GOSAT budget (340 M€) [10].

Mission requirements defined for MicroCarb [11] impose that CO_2 column concentration should be measured with high precision, limiting random errors between 0.5 ppm (goal), and 1.5 ppm (threshold) and bias between 0.1 ppm (goal) and 0.2 ppm (threshold). To achieve such level of accuracy, it is necessary to characterise the real transfer function of the spectrometer by performing a series of calibration tests both before the scientific data acquisition phase and during it, to monitor its performances over the time. The accuracy of the instrument is assessed by comparison of on-board measurements against data provided by TCCON located on ground. Its precision is instead assessed by using a variety of targets: oceans by night and deep space observations, for example, are used to quantify the effect of dark current. Internal lamps, lunar and solar observations are instead exploited to perform spectral, radiometric and geometric calibrations. One hand, this process determines the actual response of the spectrometer for each spectral channel; on the other hand, it determines the exact position of the vertex and the centre of its field of view.

The content of this thesis is the result of a 6-months internship developed within the flight dynamics and mission planning department at CNES, and constitutes the end-of-studies master thesis for a double degree exchange program with Politecnico di Milano and ISAE–SUPAERO. The main objective is to analyse three guidance modes scheduled in the MicroCarb mission profile to perform lunar calibrations. They involve the observation of the Moon surface which is sampled with a scan sequence across its clear side. A feasibility analysis is required to identify which are the most suitable conditions to perform such calibration measurements, in terms of lunar phase, period of the year as well as satellite attitude. Results should be compatible with all possible scenarios, considering that four orbits have been selected as possible candidate for the mission. The contributions provided by this work consist in:

- Improving the existing guidance algorithms that allow to simulate the guidance legs, both in terms of performances and robustness. The additional contributions will be integrated as part of the official library code defined for the mission;
- Define the possible configurations of interest in terms of Moon/spacecraft relative orientations; then simulate the acquisition legs all over the temporal widespan corresponding to calibration/validation phase, where lunar mode performances are particularly critical;
- Analyse the obtained results and justify their temporal evolution with appropriate models, in order to define the optimal conditions to be considered for mission planning;

The thesis is structured as follows: section 1 provides an overview of Earth-remote sensing principles, describing data acquisition and post-processing processes; section 2 focuses on MicroCarb mission, presenting the mission analysis and a description of the main instruments referred in the following; section 3 provides a description of the models and tools exploited for analyses; section 4 describes the strategy developed to perform the feasibility analysis of lunar modes; section 5 presents the results obtained; section 6 illustrates conclusions and further developments.

2. Earth remote sensing for air quality overview

Although traditional ground-based observation methods have the advantages of high precision and reliability, they are constrained by the distribution and number of the sites, and the lack of ability of a wide range of real-time monitoring [3]. Satellite remote sensing of atmospheric CO_2 concentration offers stable, continuous, large-scale observation and many other advantages, so in the monitoring of CO_2, satellite has played an increasingly important role. This chapter provides a description of the methods adopted by already-existing missions, focusing on the OCO-2 [12] mission by NASA, GOSAT-2 [13] by JAXA and TanSat [14] by the Chinese Space Agency, which represent the state of the art in earth remote sensing mission technologies. Section 2.1 provides general definitions for CO_2 remote sensing activities. Section 2.2 presents the different technologies available for on-board spectrometers describing the details the instruments embarked on previous missions as well as MicroCarb, pointing out the main innovations that it features.

2.1. Definitions and terminology

This paragraph provides a series of definitions of interest for CO_2 remote sensing activities, explaining the concepts of carbon sources, sinks and column concentration and introducing the absorption spectral bands typically considered.

CO_2 Sinks and Sources

The sinks and sources of CO_2 are controlled by physical and biological processes. CO_2 fluxes at the surface that can be either positive (sources) or negatives (sinks). The surface fluxes will be determined [15] by the inversion of a global circulation model including surface flux processes. This inversion is based on optimal estimation using a priori knowledge on fluxes.

CO_2 column concentration

Column concentration is defined as the averaged dry air mole fraction, which is the fraction of the number of CO_2 moles over the total number of moles of gas (the water vapor being excluded) contained in the same volume (column). The term “column” represents the vertical extension of a given area at earth surface, from ground level to space.

The average should be seen as a “weighted average”: the vertical weighting function is a function of atmospheric pressure and is provided within Level 2 together with the X_{CO_2} estimate. The weighting function expresses the relative sensibility of the column concentration product to the CO_2 molecules at a given level in the atmosphere. The integrated CO_2 concentration is defined [15] by the equation:

$$X_{CO_2} = \frac{1}{P_{surf}} \int_0^{P_{surf}} w(P) X_{CO_2}(P) dP$$

where *w(P)* is the CO_2 column concentration weighting function, *P* is the atmospheric pressure, P_{surf} is the pressure at ground level and $X_{CO_2}(P)$ is the concentration at the level *P*.

Typical CO_2 and O_2 absorption bands

Column concentrations can be measured starting from the knowledge of the ratio between CO_2 and O_2 molecular abundance in the atmosphere. In earth remote sensing missions, this information is in turn inferred by the absorption spectra of the light reflected by the Earth surface, analysing the top of atmosphere reflectance. Observations are generally made [2] in visible and infrared regions (Figure 2.1), selecting the spectral bands corresponding to highest absorption by a specific molecule. The four spectral lengths of interest are reported in Table 2.1 [2] .

Name	Region	Wavelength (μm)
O_2-A	Visible	0.76
O_2-B	Near visible IR	1.27
WCO_2	Near IR	1.64
SCO_2	Short-wave IR	2.0

Table 2.1: Absorption bands for CO_2 and O_2 monitoring [2].

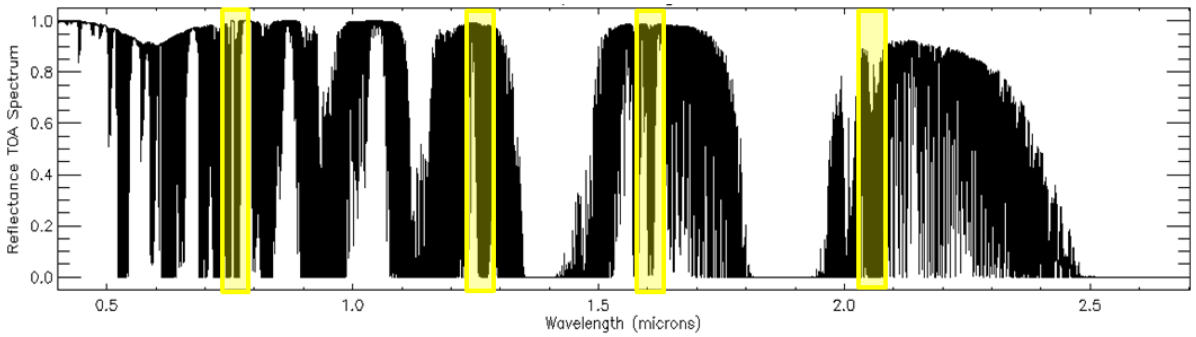

Figure 2.1: Atmospheric transmission in VIS, NIR and SWIR domains. Yellow areas are the spectral bands of MicroCarb [15].

2.2. State of the art spectroscopy for carbon dioxide remote sensing

The spectrometer technologies designed for monitoring CO_2 emissions can be divided in two categories, based on the mechanism of spectral decomposition technique: Fourier-Transform Spectrometers (FTS) and grating (optical) spectrometers [16]. Fourier-transform spectroscopes are based on measurements of the coherence of a radiative source [13]. The incoming beam is initially decomposed in a Michelson spectrograph with a mobile mirror; by changing the position of the mirror it is possible to modify the interference pattern acquired by the detector, thus generating a series of interferograms centered at different wavelengths. In a second moment, these raw data are elaborated by means of computer processing to determine the absorption spectra using a Fast Fourier Transform algorithm (Figure 2.2).

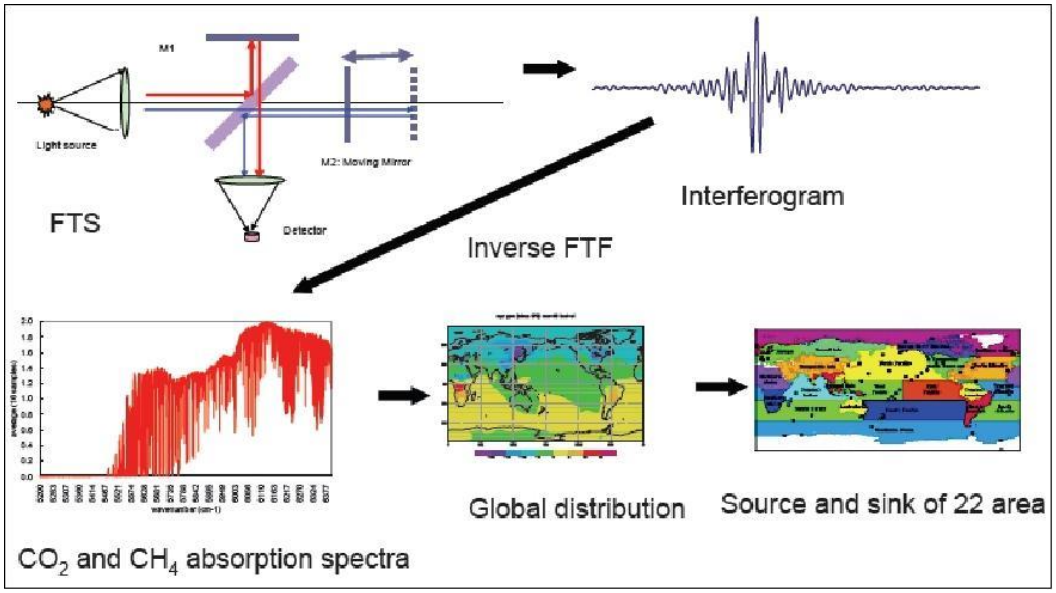

Figure 2.2: Process of realisation of absorption spectra using a FTS spectrometer [13]

This is the technology at the basis of TANSO-FTS [13], the spectrometer embarked on GOSAT mission. It has a mass of 250 kg and a power consumption of 310W and operates over four spectral bands centered at 0.76 µm (O_2-A), 1.64 µm (WCO_2), 2 µm (SCO_2) and 9.85 µm (for CH_4 concentration). The main TANSO-FTS elements, are: a scanning/pointing mechanism, relay optics, FTS spectrograph, and detector arrays in the focal plane. The maximum optical path difference of 2.5 cm provides a spectral resolution of 0.2 cm^{-1} across a wide spectral range going from 0.75 - 15 µm [13]. The scan arm motion is induced by a voice coil actuator driven by a sophisticated control algorithm. The on-board system generates and collect the interferograms pattern which are sent to the ground stations for processing. On the ground, the FTS interferograms are transformed into absorption spectra using fast Fourier transform algorithms [13].

The second category of spectrometers are based on a grating system for light decomposition [16]. The grating is a plane surface composed by a set of slits equally spaced that generate an interference pattern in the reflected wave fronts by optical diffraction. The OCO-2 instrument [12] is based on such principle. It consists of 3 imaging grating spectrometers optimized for the O_2-A band, SCO_2 and WCO_2 bands. It has a mass of 104 kg and a power consumption of 105 W. A representation of the instrument is provided in Figure 2.3. The 3 spectrometers use similar optical designs and are integrated into a common structure to improve system rigidity and thermal stability. They share a common housing and a common telescope. The telescope consists of an 11 cm aperture, as well as a primary and a secondary mirror. Each spectrometer consists of a slit, a two-lens collimator, a grating, and a two-lens camera. Each of the three spectrometers has essentially an identical layout. Minor differences among the spectrometers, such as the coatings, the lenses and the gratings, account for the different band passes that are characteristic of each channel.

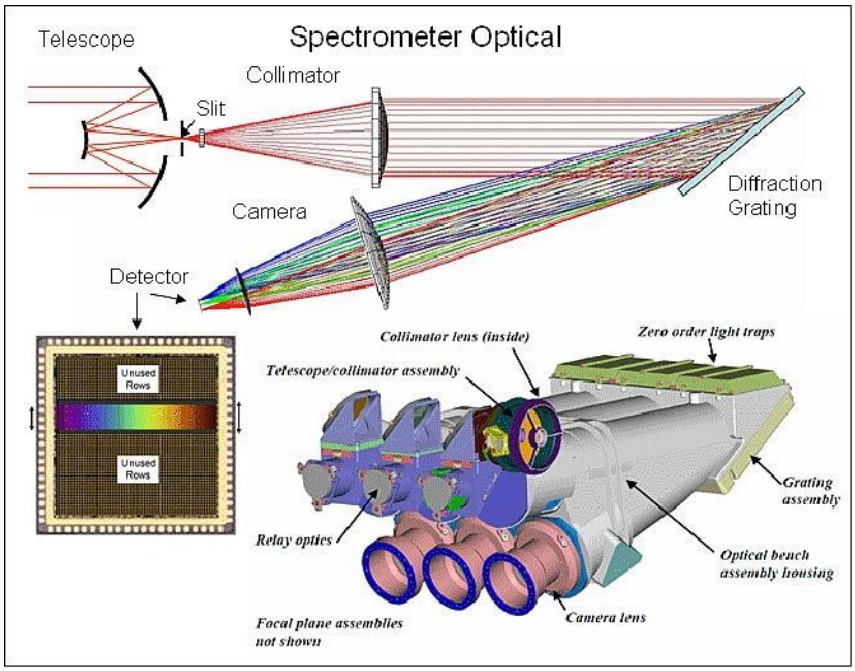

Figure 2.3: Representation of the three OCO-2 spectrometers [12].

A similar architecture was designed for CarbonSpec [14], the carbon dioxide spectrometer embarked on TanSat mission. Based on a grating diffraction technology, it has a mass of 204 kg and a power consumption of 225 W. As shown in Figure 2.4, CarbonSpec is composed of a single pointing mechanism, a telescope subsystem and a beam splitter that divides the incoming light into three beams directed toward the three diffraction grating spectrometer. An upgrade with respect to OCO-2 instrument consists in the imaging subsystem, embarked for clouds detection (CAPI).

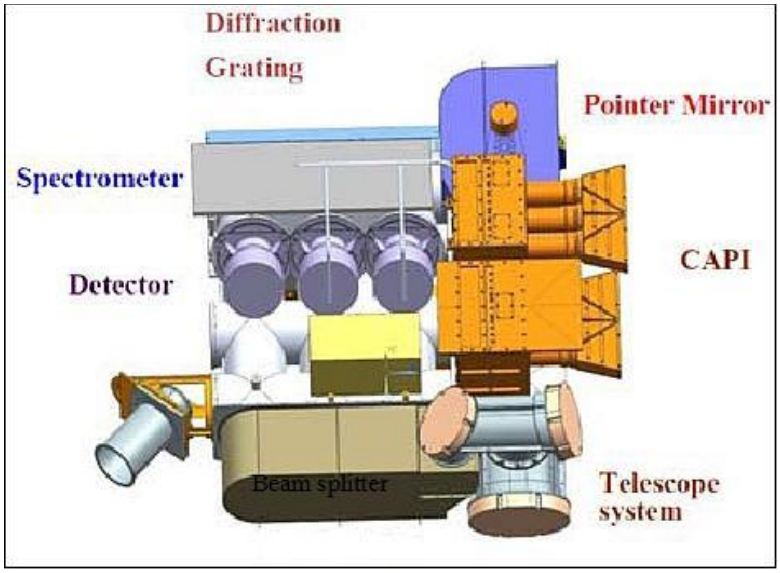

Figure 2.4: Representation of the three spectrometers of CarbonSpec [14].

The grating and FTS techniques both offer unique advantages for this application. For example, as it can be observed in Table 2.2 [13] [12] [14] [15] , TANSO-FTS provides greater spectral coverage and slightly higher spectral resolution, while the OCO-2 instrument and TanSat provide greater spatial resolution and slightly higher signal-to-noise ratios in each sounding. Comparisons of XCO_2 retrievals from these two measurement techniques could help to identify and correct subtle measurement biases that might otherwise be missed.

Parameter	**GOSAT**	**OCO-2**	**TanSat**	**MicroCarb**
Gases measured	CO_2, CH_4, O_2, O_3	CO_2, O_2	CO_2, O_2	CO_2, O_2
Instrument mass [kg]	250	104	204	63
Power consumption [W]	310	105	225	60
Nominal mission life [yr]	5	2	3	50
Spectral Coverage in O_2-A band (µm)	0.748-0.785	0.750-775	0.758-0.778	758.4- 768.4
Spectral resolution in O_2-A band (cm^{-1})	0.5	0.047	0.044	0.06
Spatial resolution [km]	0.5x0.5	1 km x 1 km	1 km x2 km	2x2
SNR in O_2-A band	180	600	360	200

Table 2.2: Performance comparisons between different CO_2 tracker spectrometers [13] [12] [14] [15].

MicroCarb mission relies on a miniaturised grating spectrometer with a mass of 63 kg and a consumption of 60 W. It is made of a telescope, a single slit-grating-detector system, filters and focusing optics [15]. Observations are made over four spectral bands: wavelengths of 1.6 and 2.0 µm are used to detect CO_2 absorptions lines, while wavelengths of 0.76 and 1.27 µm are rich in O_2 absorption lines. Using two spectral windows for O_2 measurements reduces the overall random error on CO_2 concentration. Indeed, the 0.76 µm O_2 band may be polluted by the fluorescence due to photosynthesis, whereas the 1.27 µm band is polluted by an airglow stratospheric emission due to the photolysis of O_3. All these phenomena have to be taken into account in the inversion and are sources for secondary products. A miniaturization of the instrument is made possible by relying on a single detector for all the four spectral bands; this solution reduces the overall complexity of the spectrometer design ensuring at the same time performances comparable with already-existing missions.

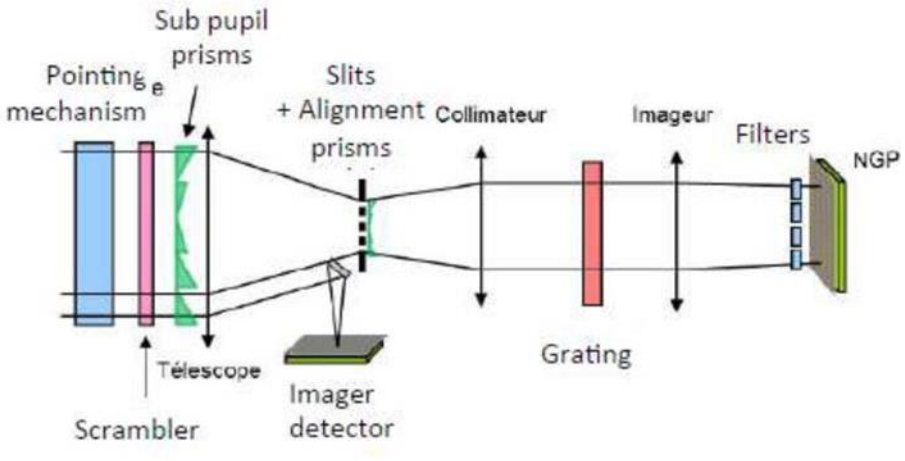

Figure 2.5: Representation of the MicroCarb spectrometer [15]

3. MicroCarb mission architecture overview

This chapter provides the technical description of the MicroCarb mission as delivered during design phases B and C. A general overview of the mission analysis and proposed orbits are given subsequently (section 3.1); the ground segment and guidance modes are illustrated in section 3.2 and 3.3. Section 3.4 describes the data processing architecture defined for MicroCarb; section 3.5 focuses on the calibration mission requirements. Then, the spacecraft configurations and the payload are described in sections 3.6 and 3.7, respectively.

3.1. Mission Analysis

The MicroCarb mission has a nominal duration of 5 years. The launch is expected for mid-2022 from Kourou Space Centre, in French Guiana [15]. Details about the launcher are yet not available since the satellite will fly as an auxiliary payload: it has therefore to adapt to primary mission launch schedules. It is of paramount importance to ensure a good flexibility in operational terms, to maximise the launch opportunities. To this aim, four orbits have been identified as possible candidates for the mission. They are phased, frozen and Sun-synchronous to meet observation and coverage mission required. This kind of solution, typical among Earth remote sensing missions, offer several advantages:

- Full coverage of the globe (thanks to nearly-polar inclination of the orbital plane);
- Periodical passages over same locations on ground, at least once per month (phased orbit);
- Constant altitude and constant illuminating conditions (frozen, sun-synchronous orbit);

Table 3.1 summarises the main features for the four orbits selected.

Orbit type	Phased frozen Sun-Synchronous
Orbits per day	14 +18/25
Inclination [deg]	98
Average altitude [km]	649
Orbit period [h]	1.75
Phased cycle length [days]	25
Orbits per cycle	368
Mean local time of the ascending node	10:30 pm (design) 13:30 pm 10:30 am 01:30 am

Table 3.1: Candidate orbits main features for MicroCarb mission [15].

The orbital planes form an angle (β) with the Earth-Sun direction, as shown in figure Figure 3.2, with an average value of 22.5° (or 1 h 30 min, equivalently). Its real value, however, oscillates periodically due to the non-uniform speed of the Earth in orbit around the Sun. A one-year trend evolution of ***β*** angle is given in Figure Figure 3.1 for 01.30 pm and 10.30 pm orbits.

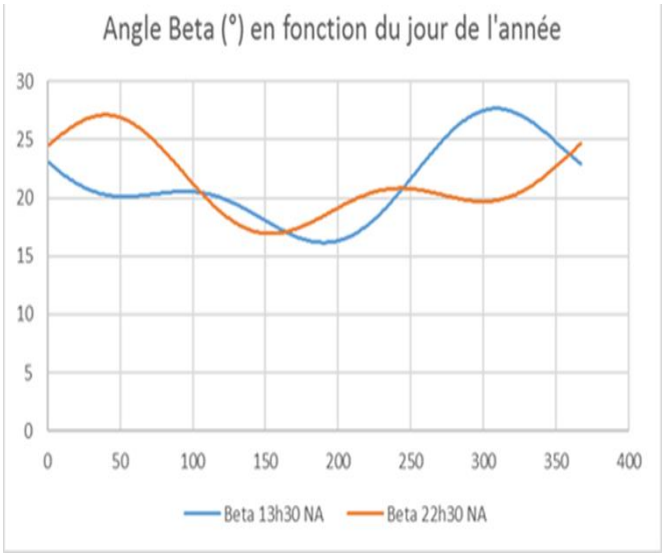

Figure 3.1: Evolution of the β angle for 01:30 pm and 10:30 pm orbits (left) [11].

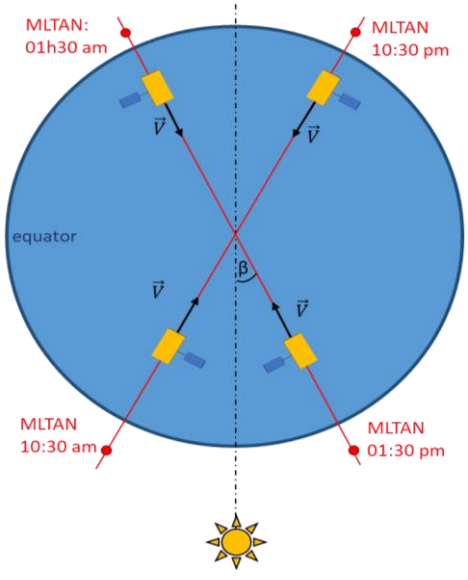

Figure 3.2 : Schematic representation of the four candidate orbits as seen from the North Pole.

The ascending node of the four orbits, in the four cases, has a Mean Local Time (MLTAN) of 01.30 am/pm, and 10.30 am/pm respectively[1]. The spacecraft's orientation along the orbit is defined such that the solar panel is always oriented on the side of the orbit enlighten by Sun. As it can be seen in Figure 3.2, this means that for 01.30 pm and 10.30 pm orbits the spacecraft's body axis $\mathbf{X_{sat}}$ is parallel to the velocity vector $\mathbf{V}$ (FORWARD configuration), whereas for 01.30 am and 10.30 am $\mathbf{X_{sat}}$ and $\mathbf{V}$ have opposite direction (BACKWARD configuration). As of today, the design orbit corresponds to the 10.30 pm. However, all the 4 possible scenarios should be covered to ensure that any result can equally apply to each one of them.

3.2. Ground segment

The ground segment is divided between three main elements: the mission control ground segment, the Payload Ground Segment (PLGS), and the CNES ground stations network (CNES Earth Terminal Multi-Mission Network) [17].

The Mission control ground segment is based on elements shared with other missions. It is responsible for the satellite as an orbiting object and must therefore make sure that it keeps operating in a stable and safe state to accomplish its mission. The Payload ground segment is dedicated to the mission and is therefore responsible for anything that has to do with mission data on the satellite. It is itself divided between several centres, each one being responsible for different activities with regards to scientific telemetry. The Command-Control Centre is common to other Myriade and Proteus series missions and is located in the Toulouse Space Centre of CNES. Both communications in S-band and X-band exploit the CNES multi-mission 2-GHz and 8-GHz ground station network located all around the globe to provide respectively, telemetry and mission data communications capabilities.

3.3. Guidance modes

A guidance mode (or acquisition mode) is defined by the pointing direction of the instrument during data acquisition. Several acquisition modes are identified for MicroCarb. The pointing can be provided

[1] In the following sections these four orbits will be referred by their MLTAN: a "10.30 pm orbit", for example, corresponds to the orbit with MLTAN=10.30 pm. Also, the notation 10.30 generally refers to the two orbits with MLTAN =10.30 am/pm.

either through the satellite Attitude and Orbit Control System (AOCS) or by the instrument itself, using its mobile mirror.

Table 3.2 shows main modes defined for MicroCarb activities: they are classified as routine modes, if their scope is to collect scientific data during acquisition, and calibration modes if they're required for calibration. Probationary modes, instead, can be seen as "extra" modes that were originally not defined in the mission plan but that can be exploited to gain useful insights on specific targets (an urban area for example).

Type	Name
MISS : routine	MISS_NADIR
	MISS_OFFNADIR
	MISS_SCAN
	MISS_GLINT
PROB : probationary	PROB_CITY
	PROB_REGION
	MISS_SCAN
	MISS_GLINT
CAL : calibration	CAL_OFFNADIR
	CAL_FIXEDTARGET
	CAL_DARKINST
	CAL_LAMP
	CAL_SUNPOLE
	CAL_SUNORB
	CAL_MOON
	CAL_LIMB
	CAL_COLDSPACE
	CAL_DARKOCEAN
	CAL_DAYOCEAN

Table 3.2: Main guidance modes defined for MicroCarb mission.

The principal modes are illustrated in Figure 3.3:

- The **nadir mode** (MISS_NADIR) consists in performing the measurement pointing in the direction orthogonal to the local horizon. It is considered as the default mode and it is used for acquisitions over lands above sea level;

- The **glint mode** (MISS_GLINT) consists in performing the measurement in the Sun-specular direction. Geometrically, this condition is met when the Viewer Zenith Angle (VZA) is equal to the Sun Zenith Angle (SZA). This configuration is used for acquisitions over oceans and seas;
- The **target mode** consists in performing successive measurements of a same target (TCCON stations, for example) at different VZA as the satellite flies over the target. Two target modes are defined with different objectives:
    - The fixed target (CAL_FIXEDTARGET) mode is defined by several acquisitions of a given target by maintaining the instrument line of sight permanently pointed in the target direction. This mode provides many acquisitions useful for aerosols characterisation.
    - The *scan mode* (MISS_SCAN) consists in increasing the ACT field by acquiring in the across-track direction, implying a reduction of the sampling along-track.
- The **city mode** (PROB_CITY) is a mapping capability over specific areas, using ALT forward and backward pointing.

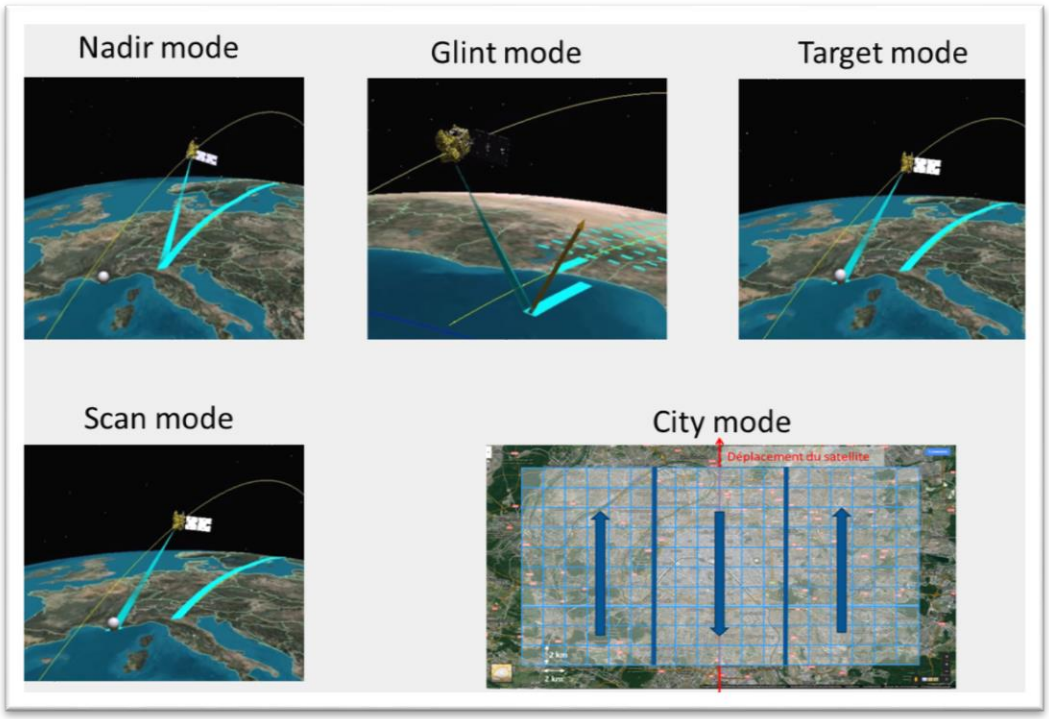

Figure 3.3: Nadir, glint, target, scan and city modes illustration [11].

The present report focuses on the analysis of three lunar modes defined for the mission:

- The **radiometric lunar mode** (CAL_MOONRADI) consists in performing a series of scan of the lunar surface to study the response of the instrument in terms of radiometric gain (see section 5.1.2)

- The **geometric lunar modes** (CAL_MOONGEAC, CAL_MOONGEAC) consists in performing a series of scan of the lunar surface to study the inter-band and intra-band coregistration process (parallel acquisition in multiple spectral bands) of the instrument; the two modes differ for the orientation of the instrument with respect to the scan direction: in one case its field of view is perpendicular to the scan direction whereas in the other is parallel (see section 5.1.1).

3.4. Scientific data processing

Measures obtained by the spectrometer provide raw data that are collected and analysed to infer the CO_2 surface fluxes map, considered as the target product. Data post-processing therefore undergoes a specific procedure divided into four processing levels [15], as shown in Figure *3.4*, to provide commercial products accessible by users:

- **Level 1 (L1):** radiometrically, spectrally and geometrically calibrated radiance spectra together with housekeeping data.
- **Level 2 (L2):** column integrated CO_2 concentrations estimates (X_{CO_2}), together with the vertical weighting function and other parameters that may help the data interpretation. The X_{CO_2} estimates are expressed in ppm.
- **Level 3 (L3):** spatio-temporal averages of the L2 products.
- **Level 4 (L4):** global CO_2 surface fluxes.

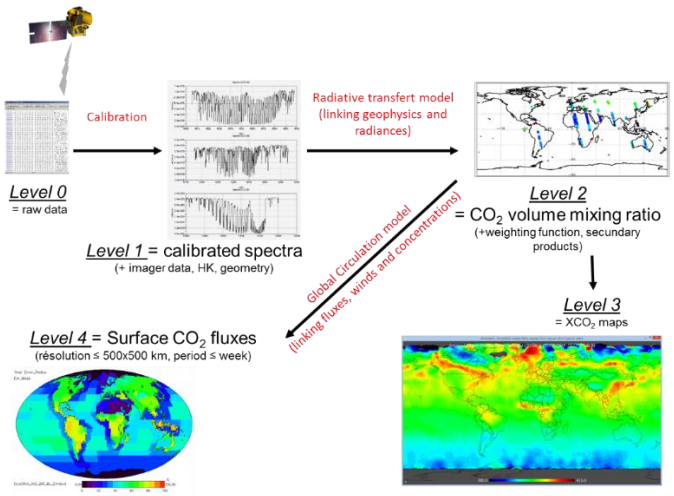

Figure 3.4: Product levels for MicroCarb mission *[15]*.

Level 1 products will mainly be used to compute integrated columns of CO_2 concentration, whereas level 2 products are derived from level 1 products provided that the geophysical conditions are appropriate (clear sky, sufficient incoming flux, limited aerosol amount…). In the context of MicroCarb mission, both L1-L2 and L2-L3 processes are under the responsibility of CNES.

Level 4 products are based on level 2 products and are obtained using a technique defined as model inversion, which provides global CO_2 surface fluxes from X_{CO_2} with the use of physical (atmospheric transport) and statistical (component errors) models to. Elaboration of products 4 will require additional means and data with respect to those developed in the frame of the MicroCarb mission and is therefore not considered as part of the mission.

3.5. Calibration activities

Activities in the initial months following the spacecraft launch are dedicated to calibration measures. This part of the mission, referred as calibration and validation phase (cal/val), takes place immediately after Launch and Early Orbit Phase (LEOP) and has a duration of approximately 9 months [11].

Calibrations are based on the comparison of the measures provided by the instrument in precise conditions with the expected output which is generally known a priori. Reference targets includes TCCON stations, Sun and Moon surfaces or internal lamps with constant luminosity. The main type of calibrations defined [11] for MicroCarb mission are:

- radiometric calibration: it consists in determining the actual value of the instrument's gain, expressing the measurement in energy units (usually [W]/[m^2]/[µm] for grating spectrometers).
- spectral calibration: it provides a wavelength value for each band of the spectrum, as well as the Instrumental Spectral Response Function, giving the dependency of each channel to any input wavelength.
- geometrical calibration: it provides the coordinates of the centre and four vertices of each Field of View.

Calibrations are introduced to satisfy the mission requirements [11] about the precision and accuracy levels, reported in Table 3.3. In particular, requirements CARB-MIS-REQ-4030 and CARB-MIS-REQ-4040 define the admissible tolerances for random errors and regional bias, respectively, for the level 2 data. The calibration and validation phase also consists in correcting instrumental artifacts such as residuals in non-linearity, channel to channel relative calibration and polarisation. In routine phase, calibration measurements will be performed periodically to monitor any phenomena of aging within the measurement chain that could lead to bias in measurements.

#	Requirement	Justification
CARB-MIS-REQ-4010	The MicroCarb level 2 mission centre shall generate level 2 products that include column-integrated CO_2 mixing ratio with respect to dry air, expressed in part per million (ppm). Level 2 products are generated from the MicroCarb level 1 individual measurements.	This is the product that is needed to estimate the fluxes through atmospheric transport inversion. The ppm unit is standard. Note that, in addition to the best estimate of the column concentration, there is a need for an uncertainty and a vertical weighting function.
CARB-MIS-REQ-4035	A weighting function (w) will be part of the level 2 product. The normalised weighting function shall have a value greater than 0.5 in the mixing layer of the atmosphere (between 850 and 1013 hPa).	This is to insure significant sensitivity to the low atmospheric layers which are directly connected to the surface fluxes
CARB-MIS-REQ-4030	The precision requirement (random error) for the level 2 mixing ratio estimate depends on the value of the weighting function close to the surface w_{surf}=w(Psurf): the precision shall be better than 0.5* w_{surf} ppm (goal) or 1.5* w_{surf} ppm (threshold) (1 standard deviation).	Literature requirements for individual FOV are 1 ppm (see for example RD-19). The L2 performance is however strongly linked to the L1 SNR, which is dependent on radiance. The range between 0.5* w_{surf} and 1.5* w_{surf} give the possibility to deal with this natural variability.
CARB-MIS-REQ-4040	A regional bias is defined as a systematic error over a given region with similar surface and atmospheric conditions at the scale of 1 week and 1000 km. Regional bias on level 2 product shall not exceed 0.1* w_{surf} ppm (goal) or 0.2* w_{surf} ppm (threshold) after correction and calibration.	The strong advantage of the satellite is the number of observations that it provides. Even if individual measurements are much less accurate than surface in situ samples, the large number of observations can compensate the higher noise, but only if the noise has little bias. The scientific community expressed a need at 0.2 ppm for individual measurement. With a w_{surf} =1, this value is our threshold.
CARB-MIS-REQ-5040	The MicroCarb level 1 products performances in terms of SNR, spectral widths and centres of the bands, spectral resolution and sampling, number of FOV, radiometric calibration, spectral calibration, geometric calibration and pseudo-noises must be driven by the compliance in L2 requirements in terms of random error and regional biases	A large pixel leads to a high SNR but will make the processing more complex (mainly homogeneity in surface altitude within FOV) and will lead to a higher probability of clear sky. Trade-off needs to be made.

Table 3.3: Measurements performances defined by mission requirements [11].

3.6. Spacecraft configuration

The structure of the spacecraft was designed from a generic miniaturised satellite platform called Myriade, provided by CNES in partnership with the European Aeronautic Defence and Space Company (EADS). Developed since 1998, this platform is conceived for small satellites with mass ranging from 50kg to 200kg and has been used for 19 satellites, 17 of which have already been launched (as of end 2020) and successfully completed their mission [18]. It has a cubical shape of 60x60x60cm^3 and it features a solar generator of 0.8m^2 to provide up to 200W of electric power to the system. With respect to the standard version of the platform, a series of upgrades were implemented *ad hoc* for MicroCarb Mission to meet manoeuvrability and on-board data storage requirements [17], including:

- New-generation on-board computer with greater capacity;
- Extension of mass memory storage capacity and telemetry rate;
- Use of inclined reaction wheels with the aim of optimising agility and reliability;
- Implementation of gyro-less AOCS;
- Compliance with the latest space debris mitigation requirements (propulsion, passivation);

The spacecraft's body frame is centred on its theorical barycentre, considering the satellite in launch configuration. The Z_{sat} axis is defined in the direction of the Earth port line of sight, the Y_{sat} axis is opposite to the side containing the solar panel. The X_{sat} axis completes the frame, according to right-hand convention (Figure 3.5). Payload components for MicroCarb mission were integrated on the top side (+X_{sat}) of the structure and include a grating spectrometer, the opening slit referred as Earth port and a radiator surrounded by a cryogenic thermal baffle.

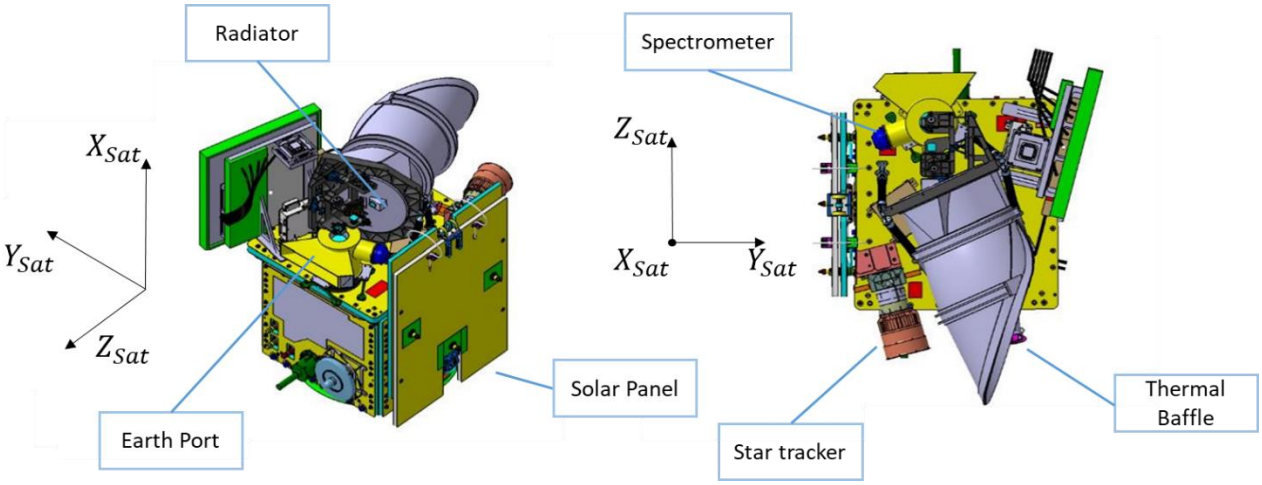

Figure 3.5: 3D and top views of the MicroCarb satellite structure in launch configuration [11].

The Attitude an Orbit Control System (AOCS) is composed by an optical star tracker, a magnetorquer and four reaction wheels, providing up to 0.12 Nms torque, inclined with respect to the satellite axis to increase its agility in pitch rotations. The presence of a fourth wheel is required for redundancy in safe mode.

The main features of the MicroCarb platform are summarised in Table 3.4.

dry/launch mass	170 /200 kg
Size	600x800x1000 mm
Solar array power	200 W;
Propulsion	Hydrazine
AOCS	Star trakcer, 4 reaction wheels
Data storage capacity	800 Gb
Reliability (5 years)	0.85

Table 3.4: MicroCarb's platform main features.

3.7. The MicroCarb payload

The only scientific instrument for data acquisition embarked on MicroCarb is the passive infrared spectrometer, operating over four different wavelengths and based on the use of a scaled network to ensure spectral dispersion (see section 0 for a more detailed description of the acquisition fundamentals). In order to work within its operational environment, the spectrometer must be kept at low temperatures (*150 K*) with a very high stability (*±1K*). For this reason, a passive cooling system is introduced, consisting of a radiator surrounded by a protective thermal shield, referred as thermal baffle. It must be ensured that the radiator exchanges energy by radiation with deep space only, with no perturbation from other celestial bodies. As it can be seen in Figure 3.6, the baffle is shaped as a hollow, truncated cylinder with an additional opening referred as notch-Earth. The longer side of the baffle is designed to protect the radiator from Sun. The smaller side, instead, protects the radiator from Earth albedo. Particularly, it must be ensured that no direct incoming beams nor reflected ones reach the bottom of the shield [19].

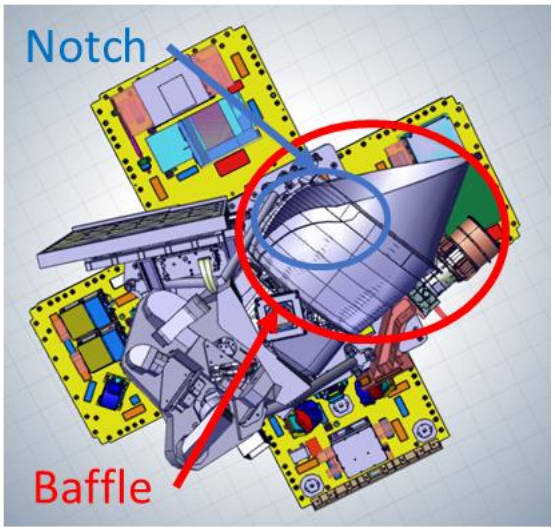

Figure 3.6: Thermal baffle illustration (red). The earth notch is highlighted in blue [19].

Observations are made analyzing the incoming photons collected by a narrow nest, referred as Earth port, that allow the light from the Earth surface to reach the detector. Inside the Earth port, a mirror mechanism (Mirroir de Changement de Visée, MCV) is inserted to enable the system to change the instrument's line-of-sight direction without changing the satellite's attitude. The MCV is free to rotate around the spacecraft's roll axis; its orientation is defined by the variable ρ and provides the system with an additional degree of freedom; this can be exploited to:

- point at the Earth's surface through the Earth port, for $\rho \in [-35°; 35°]$;
- put the *MCV* in shutter position, $\rho = 180°$;
- point at solar diffuser[2] to perform solar calibrations;
- point at the internal lamp for radiometric calibrations;

In terms of attitude control, the MCV increases the system manoeuverability. This feature can be exploited to perform off-track acquisitions as well as pointing at a given target with several different attitudes of the platform. This last feature is particularly important for dazzling avoidance and is largely exploited in the context of lunar acquisition modes.

[2] The solar diffuser is an internal opening that enables to observe the Sun while keeping the platform in Nadir configuration. This reduce the complexity of the operation since no spacecraft manoeuvre is required.

The projection on the ground of its Instantaneous Field of View (IFOV) is composed by three rectangular fens, covering an overall ACT widespan of 13.5 km. Considering that an elementary acquisition requires an integration time of approximately 1.4s and that the ground displacement in this interval is 8.9 km, during an acquisition in Nadir mode the instruments scans a rectangular region of 13.5x8.9 km^2.

Each vertex of the FOV is labelled with a letter (A-G); the *FOV* orientation is by convention [11] given by the $\overline{M_{2,ext}M_1}$ direction (Figure 3.7).

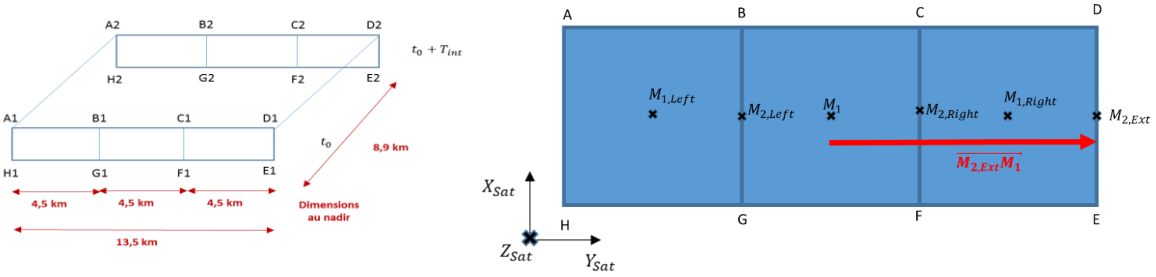

Figure 3.7: FOV schematic representation and orientation vector.

4. Models and tools

This section contains the description of all the models required to analyse the lunar calibration modes over time. Section 4.1 details the orientation of the inertial reference frame considered to describe the relative position of celestial bodies in space; section 4.2 illustrates how the thermal baffle and star tracker fields of view are modeled to monitor that they are correctly oriented in space avoiding dazzling phenomena; in section 4.3 all the conventions and models introduced to describe the Moon motion in space are detailed; section 4.4 gives an overview on the main programs and tools used to implement and simulate the guidance sequences associated to lunar calibrations.

4.1. Inertial reference frame

The EME2000 (also referred as J2000) was selected as the Earth-centred inertial frame. It is defined with the Earth's Mean Equator and Equinox at 12:00 Terrestrial Time on 1 January 2000. The x-axis is aligned with the mean equinox. The z-axis is aligned with the Earth's rotation axis or celestial North Pole. The y-axis is rotated by 90° East about the celestial equator.

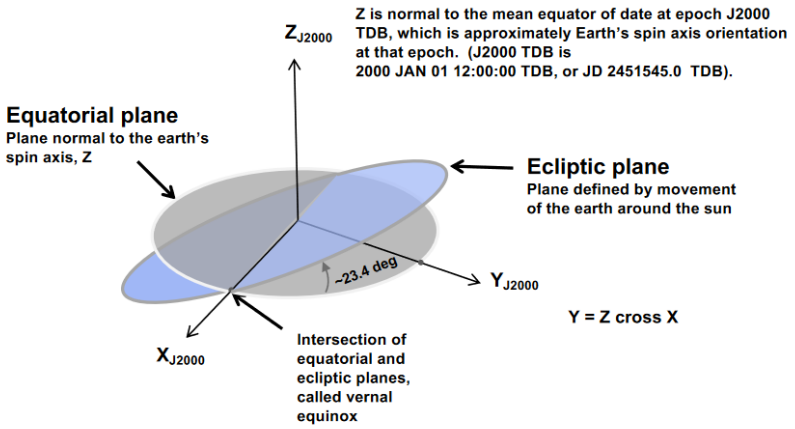

Figure 4.1: EME2000 reference frame [15].

4.2. Sensor modelling and attitude constrains

All over the mission, it must be ensured that the spacecraft's attitude is compatible with the orientation constraints given by the thermal baffle and the star tracker. In fact, during a guidance leg the attitude of the satellite is imposed by the target to observe as well the FOV relative orientation with respect to it, though in a general case this could generate dazzling problems. In such a case the leg is said to be not feasible and cannot therefore be scheduled for the actual mission plan. For this reason, each leg must be simulated to assert the validity all over its interval of definition.

With this scope, the star tracker field of view is modeled as a conical shape (Figure 4.2) centred around its pointing axis with three different exclusion angles. They are introduced to consider the possibility of dazzling by indirect light beams that reach the detector after multiple reflections. The star tracker pointing axis in satellite body frame, as well as the values of the three exclusion angles, are given in Table 4.1.

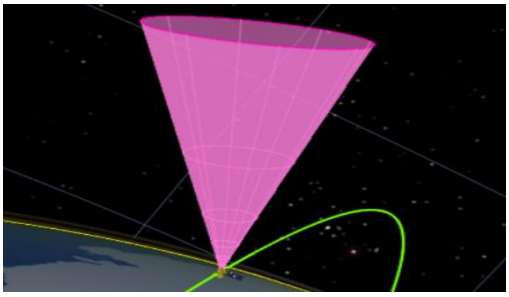

Figure 4.2: Star tracker Earth exclusion angle, illustrated with a VTS representation.

	Value
Pointing axis in body frame	{0, 0.26, -0.97}
Earth exclusion half angle	18.9°
Sun exclusion half angle	26°
Moon exclusion half angle	19.5°

Table 4.1: Star tracker pointing axis in satellite body frame and Sun, Earth and Moon exclusion angles.

Concerning the thermal baffle, due to its complex shape, it is not straightforward to provide a criterion to determine under which conditions it is dazzled. An efficient solution consists in introducing an equivalent system of three fictitious sensors, defined so that the baffle is not dazzled if and only if none of these sensors is. Each sensor is sensible to the one particular celestial body and has a conical field of view defined by an orientation axis and a guard half angle. Due to its reduced luminosity, the effect of lunar albedo was considered negligible from a thermal point of view. Orientations and exclusion angles for the fictitious sensor are given in Table 4.2:

Fictitious sensor name	Associated celestial body	Body Frame orientation	Exclusion half-angle
Baffle Sun	Sun	{0.06, 0.97, -0.22}	90°
Baffle Earth	Earth	{0.06, 0.97, -0.22}	25°
Baffle notch Earth	Earth	{0.03, 0.96, 0.28}	2°

Table 4.2: Baffle fictive sensors orientations and apertures.

A graphical representation of the sensors is given in Figure 4.3 in Nadir mode configuration. It can be observed that the baffle-sun sensor field of view corresponds to a semi plane oriented as the baffle-earth sensor, whereas the pointing axis of the baffle-notch-earth has an offset of 16° in the $-Z_{sat}$ direction.

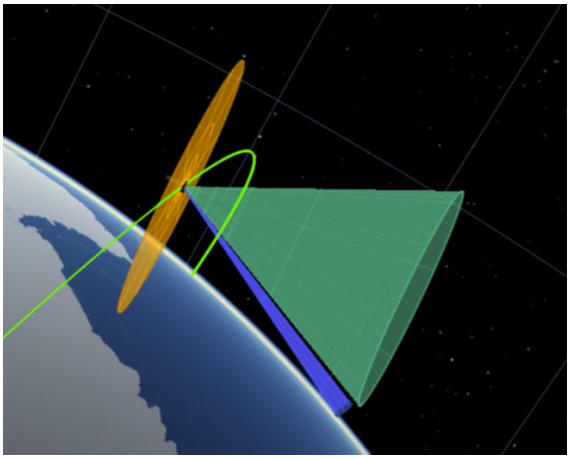

Figure 4.3: Baffle Sun (orange), Earth (Green) and notch-Earth (blue) orientation in Nadir Mode.

During the simulations, an event checker is implemented to constantly verify that, at each time step, none of these phenomena occurs:

1. The star tracker is dazzled by Sun;
2. The star tracker is dazzled by Earth;
3. The star tracker is dazzled by the Moon;
4. The baffle-earth fictitious sensor is dazzled by Earth;
5. The baffle-notch-earth fictitious sensor is dazzled by Earth;
6. The baffle-sun fictitious sensor is dazzled sun;
7. The earth port is dazzled by Sun;

This gives a total of 7 attitude constraints that must be simultaneously respected. Other attitude constrains involve the reaction wheels

4.3. Modelling the Moon motion

The Moon rotates around the Earth on a nearly circular orbit with a semi-major axis of 384'748 km and a synodic period of 29.53 days. Its orbital plane has an inclination of 5.14° with respect to the Ecliptic and the line of nodes follows a retrograde motion in west direction (as seen from the Earth), completing a full rotation in 18,6 years. Its relative position with respect to the Earth-Sun system is given by the lunar phase (φ), defined as the angle between the Earth-Moon and Earth-Sun directions projected on the ecliptic plane. The convention adopted is that the phase belongs to the interval [-180°; 180°] and it decreases in time, as illustrated in Figure 4.4. So:

1) φ >0 during the ascending phase, that is [0°, +180°];
2) φ<0 during the descending phase, that is [-180°, 0°];
3) φ=0 at full moon;
4) φ = ±180° at new Moon;

The interval is centred at full Moon so that the new Moon is at the extremity of the interval. This choice is made considering that the portion of interest for observations is the [90°; -90°] interval since the Moon has a higher luminosity.

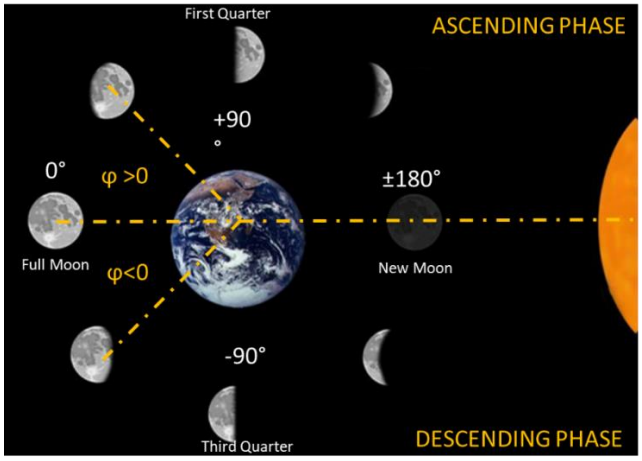

Figure 4.4: Lunar phase convention.

Two successive events of new Moon define a lunar synodic month. As it can be seen in Figure 4.5, its duration depends on the relative Sun-Moon-Earth position and it is associated to a rotating reference frame. The present analysis is conducted over 13 lunar synodic months: the average

duration being 29,5 days, the overall timespan covered corresponds to roughly one solar year. The mission planning team decided to perform analysis in between June 2022 and June 2023, when the calibration/validation phase is more likely to occur[3].

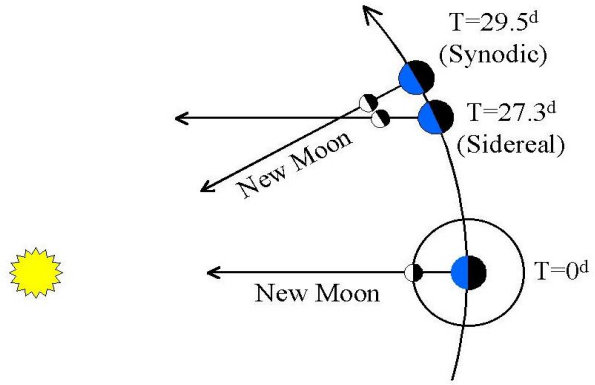

Figure 4.5: Synodic lunar period representation [11].

Month	Begin	End
1	30/05/2022	29/06/2022
2	29/06/2022	28/07/2022
3	28/07/2022	27/08/2022
4	27/08/2022	25/09/2022
5	25/09/2022	25/10/2022
6	25/10/2022	23/11/2022
7	23/11/2022	23/12/2022
8	23/12/2022	21/01/2023
9	21/01/2023	20/02/2023
10	20/02/2023	21/03/2023
11	21/03/2023	20/04/2023
12	20/04/2023	19/05/2023
13	19/05/2023	18/06/2023

Table 4.3: Lunar months selected for feasibility analysis.

Table 4.3 gives the begin and end date of each lunar month considered in the analysis. Hereinafter, each month will be referred by means of its identification number.

4.3.1. Horns line, sweep direction and approach angle

This section describes how the spacecraft orients with respect to the Moon during acquisitions. First of all, it is required [11] that the FOV can be oriented orthogonally or perpendicularly to the clear edge of the Moon. For this, the horns line is introduced and defined as:

$$\overline{HL} = \overline{MO} \times \overline{MS}$$

[3] The launch date is actually supposed to be set in 2022; however, delays in the mission development are expected and thus taken into account.

where $\overline{\mathrm{MO}}$ is the Moon-observer (in this case, the spacecraft) direction. Note that, according to this definition, the horn line is oriented in the northern hemisphere during the ascending phase and vice versa for the descending phase.

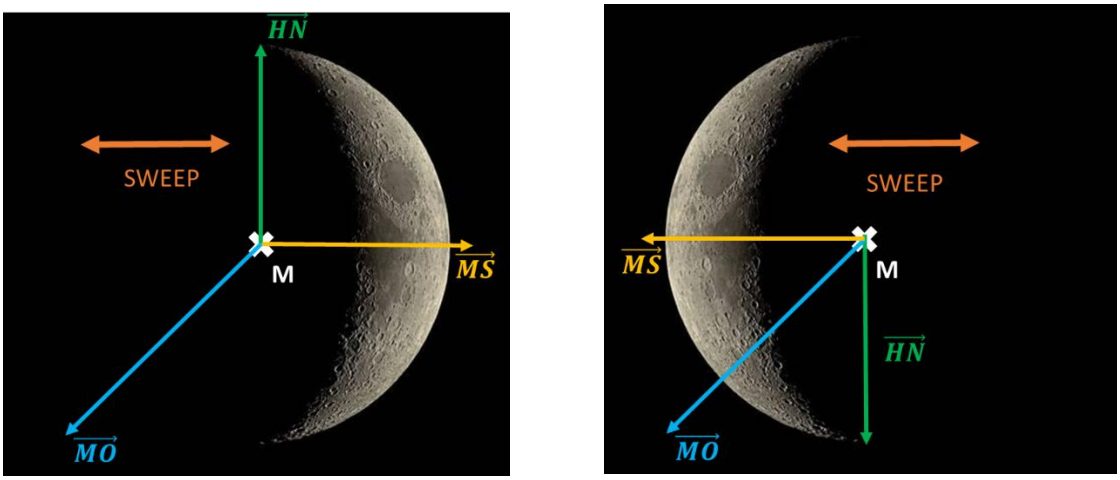

Figure 4.6: Horns line orientation for ascending (left) and descending (right) phase.

In other words, the horns line projection on the celestial north pole direction is positive for 0°<φ<180° and negative for -180°<φ<0°. At full moon, this definition may arise problems since the $\overline{\mathrm{MO}}$ and $\overline{\mathrm{MS}}$ may be aligned in case of lunar eclipse. In this case, in fact, the horns line is not defined. However, this situation is of no interest in Moon observation since the whole surface of the Moon is shadowed. In general, whenever the moon is at 0° phase, its whole perimeter is enlightened, so every orientation of the horn line around $\overline{\mathrm{MO}}$ is equivalent. To scan the lunar surface, the FOV will move back and forth along a specific sweep direction, that is always parallel to $\overline{\mathrm{MS}}$.

The orientation of the FOV with respect to the horns line is given by the approach angle α. It is defined as the angle between the horns line and the FOV pointing vector defined in section 3.7, positive if the rotation is made around $\overline{\mathrm{MO}}$. Relying on these definitions, four configurations are particularly interesting: for α=0° and α=180°, the FOV and the sweep direction are orthogonal one another. Vice versa, for α=90° and α= 270° the FOV is parallel to the sweep direction.

An important remark on this subject concerns the approach angle and the corresponding spacecraft attitude: since the horns line changes direction from ascending to descending phase though the approach angle is measured clockwise with respect to $\overline{\mathrm{MO}}$, a given angle of approach do not always correspond to the same spacecraft orientation in space. As can be seen in Figure 4.7, the FOV orientations are specular with respect to $\overline{\mathrm{HL}}$ in ascending/descending phase conditions. Though this

choice may seem confusing at first sight, it offer an advantage: as it will be seen in section 6.3, acquisitions made with a same approach angle for 10.30 am/pm and 01.30 am/pm orbits will be associated to different attitudes but will provide equivalent performances. This will therefore simplify the results discussion.

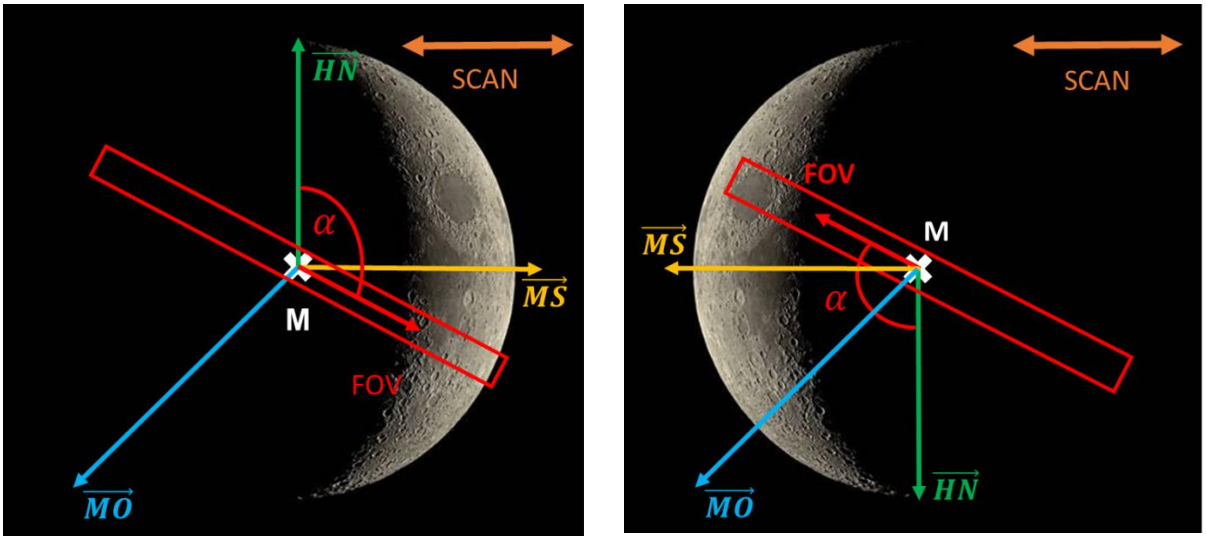

Figure 4.7: FOV orientation for a same α in ascending phase (left) and descending phase (right).

4.3.2. Moon relative elevation

The lunar phase defines the position of the Moon projection in the ecliptic plane; in particular, at isophase the Moon will be under the same enlightening conditions. However, this does not completely define its position since its orbit is inclined with respect to the Ecliptic. Furthermore, the orbit plane inclination is not constant with respect to the ecliptic plane, meaning that over different synodic months the satellite sees the Moon at different elevations in correspondence of same phase conditions. To quantify this effect, the Orbit Horizon Plane (OHP) is introduced to define a reference surface from which the elevation of the Moon can be computed. This is useful to understand how "high" or "low" the Moon is seen in the sky from the point of view of the spacecraft in orbit. The OHP is defined as the surface orthogonal to the unitary vector $\vec{n}$, resulting from the projection of the ecliptic normal direction $\vec{k}$ on the orbital plane:

$$\vec{n} = \vec{h} \times (\vec{h} \times \vec{k})$$

where $\vec{h}$ is the angular momentum of the orbit. The Moon elevation with respect to the OHP can be then computed as the angle that the Earth-Moon vector forms with respect to the plane (Figure 4.8)

.

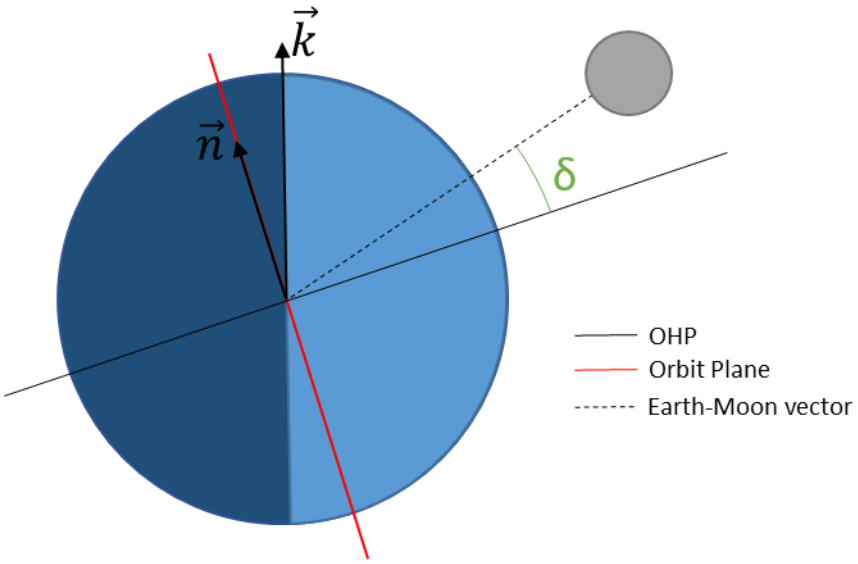

Figure 4.8: Representation of OHP and moon elevation δ.

The elevation δ is useful to compare two isophase conditions in different moments of the years; however, this measure is intrinsically dependent on the value of the chosen phase, so $\delta = \delta(\varphi)$. In order to directly compare two different synodic months on a wider phase interval, an averaged elevation δ^* on a generic interval $I_\varphi = [\varphi_b - \varphi_a]$ is defined as:

$$\delta^* = \frac{1}{\varphi_b - \varphi_a} \int_{\varphi_a}^{\varphi_b} \delta(\varphi)\, d\varphi \; ; \qquad I_\varphi = \begin{cases} [0°; 90°], \; in\ ascending\ phase \\ [-90°; 0°], \; in\ descending\ phase \end{cases}$$

As it can be seen in Figure 4.9, the evolution of δ^* over the year has a sinusoidal trend, according to the rotation of the spacecraft orbital plane around the poles axis. Furthermore, the curves for associated orbits 10.30 am/pm and 01.30 am/pm are shifted of 16°; this corresponds to the relative angle formed by the two planes due to the 8° of inclination with respect to the north pole. It is also interesting to notice that, under the same conditions of lunar phase, orbits 10.30 pm and 01.30 pm see the moon with a lower elevation. This means that observations are expected to be more critical in the proximity of the north pole. Equivalently, the same can be said for 10.30 am and 01.30 am orbits in the vicinity of the south pole.

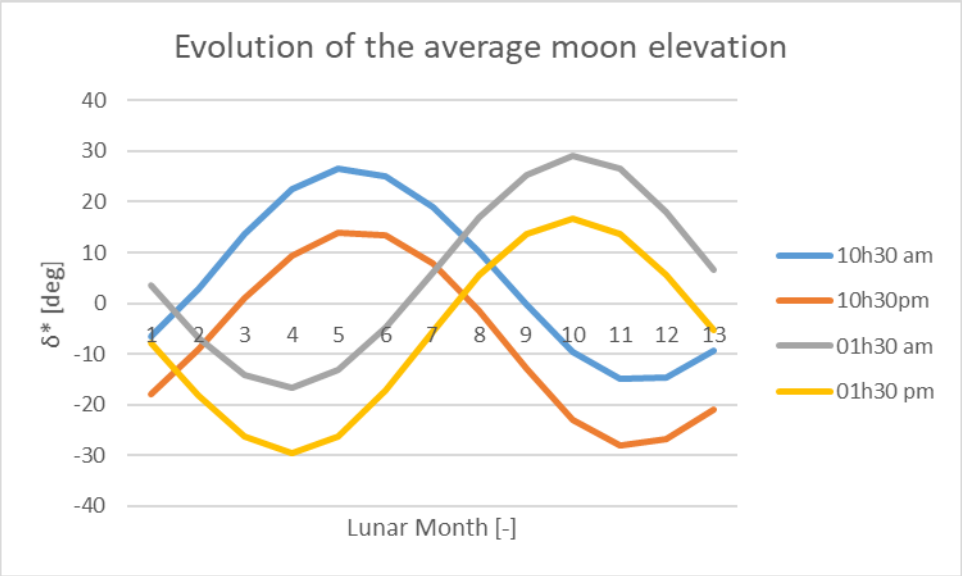

Figure 4.9: δ^* evolution over one year for the four candidate orbits.

4.4. Programs and tools

A spacecraft model, as well as its orbit and its full operational environment, were simulated in Java language under the Eclipse IDE. This work contributed to the development of the existing libraries with the introduction of new features for Moon guidance legs implementation. In particular, the already-existing algorithm for moon leg sequences generation was enriched to include a check for Moon visibility from the satellite, as well as lunar eclipses detection. Furthermore, an additional output file was generated to provide visibilities and dazzling flags: at each time step, this file tells whether any sensor is dazzled by a Celestial body and if the Moon was visible, in a format compatible with the visualisation toolkit to generate an event timetable (see Figure 4.11, section 4.4.2). Another contribution was given in the develoment of algorithms for the generation of tests for lunar guidance modes performances under several conditions. A detailed description of such algorithm is given in section 5.4.

4.4.1. Polaris and Patrius Libraries

The present internship is also intended to contribute to the development of a guidance library called POLARIS. The interest is to develop an autonomous and easy to integrate deliverable for the PLGS. Amongst others, it will have to handle guidance law computation, dazzling management or slew manoeuvres. The library is currently in its development phase; MicroCarb represent the first mission

to exploit it, though today the library is shared with other missions such as Mars Moon eXplorer (MMX).

POLARIS relies on other existing libraries:

- PATRIUS: this library is dedicated to guidance and orbital mechanics. It is an overlay of the free library OREKIT which is entirely dedicated to orbital mechanics. It has been developed by Thales Services and is coded in JAVA.
- MANIAC: this library is dedicated to optimal slew manoeuvres computation, which is the transition between two guidance laws. MANIAC is coded in C language and has been developed by CS enterprise.

In the long term, the library will be fully adapted for a multi-mission context (Figure 4.10). POLARIS will also have to be integrated to a simulation environment called ALIS, which gathers simulators for both guidance and mission planning.

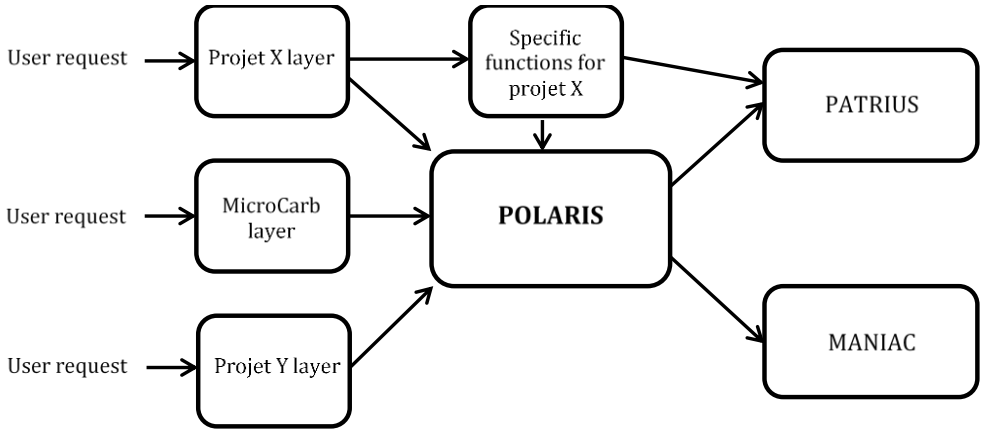

Figure 4.10: Organisation of the POLARIS library.

4.4.2. Visalisation tools

The Visualisation Toolkit for Space data (VTS) is a visualisation program which allows to import orbit and attitude data under a specific format and then visualise the evolution of the satellite along its orbit, its attitude, its ground track. For this internship, it was used as a tool to validate the results of simulations performed.

Figure 4.11 shows how guidance legs are presented in VTS: together with the spacecraft evolution along the orbit, a timeline event provides the moon visibility intervals and all the possible dazzling events occurring during the simulation.

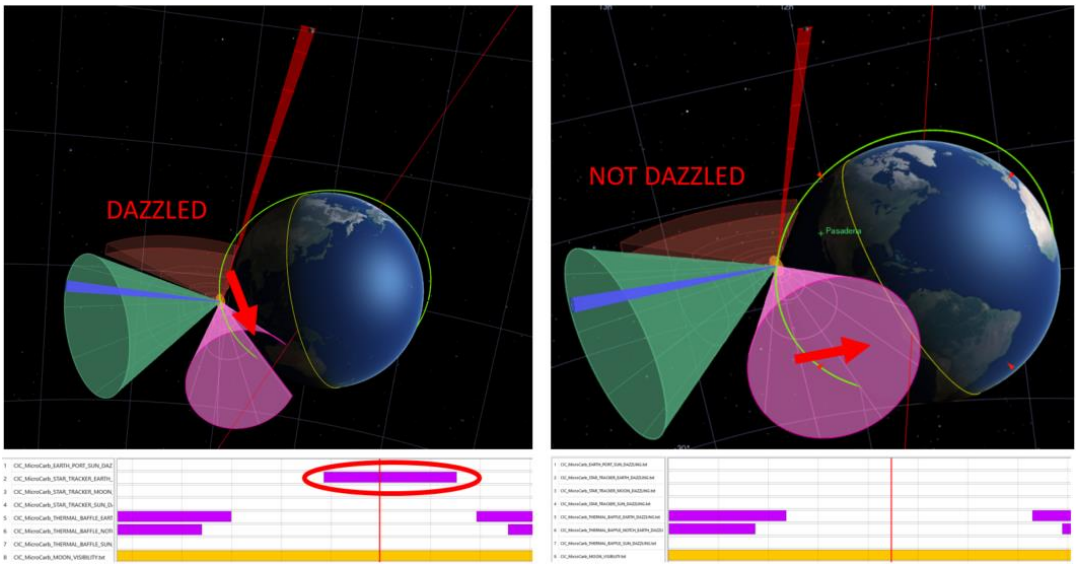

Figure 4.11: VTS interface.

The color-code used for the fields of view representation of sensors is given in Table 4.4.

Element	**Colour**
Earth port	Dark Red
MCV	Red
SST	Pink
Baffle earth	Green
Baffle notch-earth	Blue
Baffle sun	Orange

Table 4.4: Sensors colour-code.

It is important to remark that the baffle sun fictitious sensor was rescaled to have a better visual representation of scenarios; in any case its pointing axis is parallel to the baffle earth sensor, so the orientation in space can be deduced from it. Also, for the SST visualisation, the Earth guard angle was considered since Earth is generally the most critical body for this sensor.

5. Lunar guidance modes implementation

5.1. Lunar modes requirements

Lunar calibrations will be crucial during calibration and validation (cal/val) phase. However, they are scheduled in routine phase as well, though with a lower frequency. This is to consider any possible degradation of the instrument's components in time that could have an impact on measurements. Measurements performance requirements are defined by SI department and given to the Mission Planning team (MP) to develop the associated guidance legs. In particular, for each calibration the SI team should provide:

- the frequency at which it should be performed, both in routine and cal/val phase;
- The MCV roll angles to be tested;
- The FOV scan speed;
- The minimal duration required to get enough acquisitions;

At this phase of the mission, however, the instrument system team (SI – Systèmes Instrumentaux) team can only provide a preliminary study that gives a first idea of the order of magnitude of the parameters involved. Also, they do not consider the constraints imposed by mission programming as well as attitude control. The development of the requirements is thus an iterative process based on cooperation between the mission programming (MP) and SI teams.

As detailed in the following sections, the scope of this analysis will not be to provide a definitive solution but rather explore the domain of interest and search for solutions of interest. This will give an idea of what is feasible form a guidance point of view allowing the SI team to elaborate a more precise formulation of the problem.

5.1.1. Geometric calibration

A geometric calibration is required to validate the intra-spectral inter-spectral coregistration processes of the instrument. During the acquisitions in fact, photons are collected by the *MCV* and separated by the scaled network in the four spectral bands of interest; the four beams are then redirected toward the detector for the measure. Inaccuracies along the path introduce registration errors, meaning that measures correspond to different observed regions (Figure 5.1). It is of paramount importance that:

1) The four spectral bands refer to the same spatial area on ground (inter-spectral coregistration);
2) Each of the 1024 wavelengths contained in a band refer to the same region on ground (intra-spectral coregistration);

To meet this requirement, the clear side of the Moon edge will be exploited: the absence of atmosphere offers a sharp transition in the luminosity curve when the *FOV* sweep across the edge. It corresponds thus to a natural step function. The acquisitions should be performed both in *ACT* and *ALT* configuration, that is, with the *FOV* oriented both parallel and perpendicular to the sweep direction. Two guidance modes are then associated to this calibration, referred as *CAL_MOONGEAC* and *CAL_MOONGEAL*.

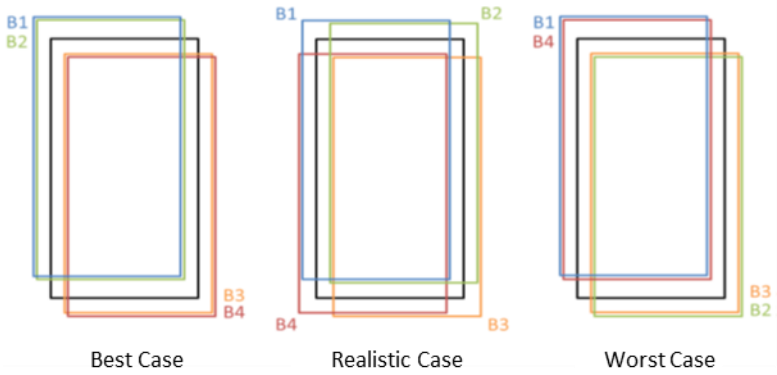

Figure 5.1: Inter-band coregistration bias for a best, realistic and worst case scenarios.

After a preliminary analysis, the *SI* team proposed to perform a single, slow scan of the clear edge of the Moon to see how a peak in luminosity is recorded in the four spectral bands. It is important that

acquisitions in the nearby of the edge are sufficiently abundant to ensure a faithful representation of the edge. Details about proposed requirements are given in Table 5.1.

MCV roll angles to test	{-35°, -18°, -9°, 0°, 9°, 18°}
Moon phase interval	[-90°; +90°]
FOV orientation	ALT and ACT
Calibrations during cal/val phase	3 (for each MCV roll of interest)
Calibrations during routine phase	1 per year (for each MCV roll of interest)
Scan speed	6.4 µrad/s
Minimal Duration	14 min
Acquired samples	100

Table 5.1: Performance requirements for the geometric calibration.

Such a model for the geometric calibration was declared not feasible [20] because the scan speed is far below the limits imposed by the AOCS. Such a value, in fact, cannot be accepted for attitude stability reasons; micro-vibrations, would have a non-negligible impact on the pointing accuracy of the instrument. Since the minimal angular speed allowed by the AOCS is of the order of 150 µrad/s [20], the idea to perform a single-slow scan is not realizable. As a solution, the MP team proposed instead to perform a sequence of scans at higher speed (160 µrad/s) and overlap the obtained data to recreate an equivalent acquisition. The feasibility of this solution is still under analysis in the SI team, though it currently seems the most likely method to adopt.

5.1.2. Radiometric calibration

This calibration concerns the radiometric gain of the spectrometer. The idea is to compare the luminosity curves obtained by measurements with available, existing data of lunar radiometry. This performance is a key element to monitor the instrument degradation over the time. The spacecraft should be oriented such that the FOV of the instrument and the sweep direction are orthogonal one another (ALT configuration): the associated guidance mode is called CAL_MOONRADI.

For the radiometric calibration, performances requirements specified by the SI department are given in Table 5.2. The underlying model is again a single scan of the lunar surface to calibrate the radiometric gain of the instrument. Differently from the geometric calibration, during routine phase, the radiometric calibration is to be performed once every lunar month at Isophase (with a tolerance of ±1°, corresponding to the displacement of the Moon during an orbit) along ALT direction only. On

the other hand, in cal/val phase the requirements are close to the ALT geometric calibration, so the two acquisitions could be performed together.

MCV roll angles to test in cal/val	{-35°, -18°, -9°, 0°, 9°, 18°}
MCV roll angles to test in routine	1 angle, arbitrary
Moon phase interval	[-90°; +90°]
FOV orientation	ALT
Calibrations during cal/val phase	3 (for each MCV roll of interest)
Calibrations during routine phase	1 per month at isophase
Scan speed	16 µrad/s
Minimal Duration	10 min
Acquired samples	80

Table 5.2: Performance requirements for the radiometric calibration.

Again, the required velocity is not sufficiently elevated to satisfy the pointing stability performances discussed in the previous paragraph. As for the geometrical calibration, the alternative solution proposed is to realise a series of scans that provide equivalent performances.

5.1.3. Polarisation calibration

This calibration aims at studying the sensitivity of the instrument to polarisation; however, requirements and performances are still to be defined, so this mode is outside the scope of this internship. It will not be considered hereinafter.

5.2. Guidance legs, guidance profiles and slews

The implementation of a guidance mode over a given timespan can be represented by a guidance leg or guidance profile (also referred as attitude leg/profiles). In both cases, an attitude law must be initially specified, defining a reference target (as a TCCON or a celestial body) or a pointing direction (as nadir direction or glint direction). Since an attitude law does not refer to any particular time instant, the target is no associated to any concrete direction in space (for example, a lunar-pointing attitude law tells the spacecraft to point the Moon, but the position of the body is not given, since it changes over time). The attitude law is indeed implemented by an attitude leg, that is defined over a time interval: at this stage the target position is computed instant by instant and the satellite's attitude is constrained. To be fully defined, an attitude leg must also contain the MCV roll orientation profile over the specified interval. A guidance leg can thus be seen as an ideal implementation of a particular mode in time; the difference with a real case scenario is that the quaternions evolution in time is

represented by generic functions that could be not physically implementable by the AOCS. A guidance profile describes a leg attitude evolution in time by means of polynomial or harmonic functions combined in a Fourier series. Finally, a profile or leg sequence is defined as the ensemble of multiple legs/profiles adjacent in time.

Slews [21] are transition manoeuvres that connect two consecutive attitude legs. They are required to ensure that the quaternions describing the attitude of the spacecraft, as well as the angular velocity vector, are continuous in time. The calculation of such manoeuvres is done in MANIAC, a C-language based library developed at CNES. When computing a slew, the user specifies the method to implement. As it can be seen in Table *5.3*, they can impose a continuous profile, both at the beginning and the end of the manoeuvres, to: quaternions, angular velocities, angular accelerations and jerks. The higher the degree of smoothness required, the longer the slew duration will be. Therefore, the method selection always represents a compromise between a good stability of the attitude profile and a reasonable slew duration in time. The duration of the slew can be fixed (if boundaries conditions are given both at the begin and the end of the manoeuvre), or be the minimal allowed (if conditions are specified for only one of the two boundaries). In the first case, the slew manoeuvre cannot be computed if the duration imposed is lower than the minimal one; this is why the second option is generally preferred when the slew calculation is made automatically.

For a minimal duration slew, the algorithm will attribute a higher priority to the guidance leg where boundary conditions are imposed. It computes then the slew manoeuvre that overlaps on the non-priority leg.

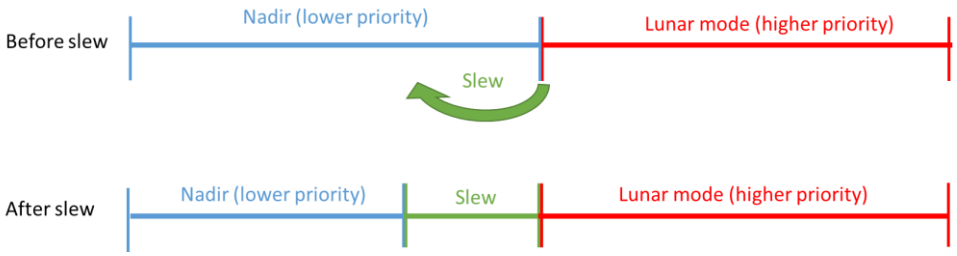

Figure 5.2: Minimal duration slew implementation.

In the example given in Figure *5.2*, a Nadir leg is followed by a Moon leg, the last one having a higher priority. The conditions are imposed for the end of the slew that is superposed to the last part of the Nadir.

Method	Continuity at manoeuvre begin	Continuity at manoeuvre end
B00	Quaternion, Velocity	Quaternion, Velocity
B01	Quaternion, Velocity	Quaternion, Velocity, acceleration
B11	Quaternion, Velocity, acceleration	Quaternion, Velocity, acceleration
B12	Quaternion, Velocity, acceleration	Quaternion, Velocity, acceleration, jerk

Table 5.3: Slew calculation methods implemented in MANIAC.

5.3. Moon observation leg sequence

The three acquisition modes defined for lunar calibrations features the same strategy from an attitude control viewpoint. As stated in section 5.1, a full acquisition is composed by several scan of the lunar surface is performed along the sweep direction. To do so, the spacecraft will:

1. Orient the FOV with the clear side of the Moon with an inclination equal to the specified α;
2. Preform a series of lunar surface full scans for the whole duration of the acquisition with an angular widespan of 1° (two times the apparent diameter of the Moon as seen from the spacecraft); this introduces a margin of 2 to compensate uncertainties about Moon position and pointing errors.
3. Between two successive scans, perform internal slews to slow down and accelerate in the opposite direction;

Before and after the sequence, slew manoeuvres are introduced to give continuity to the attitude profile. Since lunar modes are prioritary with respect to routine acquisitions (typically Nadir or Glint), slews will not overlap with the Moon sequence. Its duration will therefore not be affected by slews. Concerning internal slews, their typical duration is of 10s about, corresponding to a displacement of the FOV of 0.09° along the sweep direction. This slightly reduces the widespan of the scan, though the widespan of 1° ensures that internal sweeps always fall outside the field of view of the Moon.

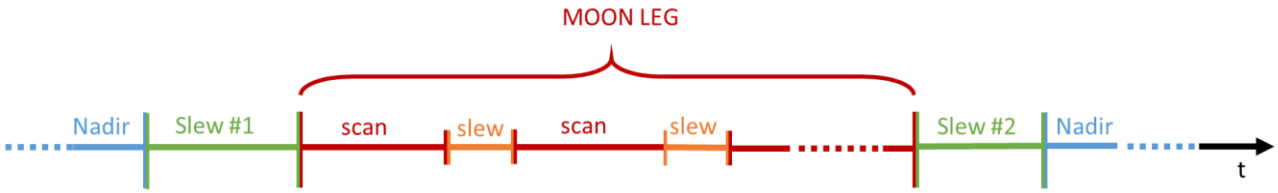

Figure 5.3: Timeline representing a moon leg sequence which take place in between two nadir legs.

Considering a single acquisition, the overall required time is 1.4s; this duration includes both the integration time and a latency and is referred as FrameSynch. The corresponding angular

displacement, considering a speed of 160 µrad/s is therefore 225 µrad. Further details about acquisitions are given in Table 5.4.

Widespan	*1°*
FrameSynch	*1.4s*
Single scan duration	*110s*
Internal slew duration	*10s*
Sample resolution	*0.013°*

Table 5.4: Moon observation performances parameters.

5.4. Guidance leg sequences simulation algorithm

This section details the structure of the algorithm implemented to simulate a set of Moon leg guidance sequences over a synodic lunar month, to compute the associated relative duration. As input parameters, the user specifies the desired approach angle α, the spacecraft's orbit and the start date of the selected lunar month. Guidance sequences are then simulated within a specific domain provided in terms of lunar phase φ and MCV orientation ρ:

- $\varphi \in [-90°, +90°]$; the interval is discretised with a 5° step;
- $\rho \in [-35°; +35°]$; the interval is discretised with a 5° step;

Each simulation gets the input parameters from a .cvs file. Then the following steps are performed:

- For each lunar phase φ, the corresponding date within the month is computed;
  - a search interval centred on the selected date with a time span of 1.5 orbital periods is generated to search for solutions; the timespan is chosen to make results independent from the position of the boundaries on the orbit;
  - For each MCV roll value on the list, the Moon sequence is generated as follows:
    - Within the search interval, the algorithm computes the intervals where the Moon is visible from the spacecraft;
    - The algorithm checks if lunar eclipses occur within the search interval;
    - The algorithm builds a moon guidance leg for each visibility interval;
    - The event checker detects if dazzling events occur during the leg;

- by subtracting dazzling event and lunar eclipse to the visibility intervals, candidate intervals for acquisitions are identified.
- For each candidate interval, the algorithm checks if slews manoeuvres before and after the leg are feasible in terms of attitude constrains; whenever one of the two manoeuvres is not possible, the algorithm reduces the duration of the Moon leg of 10s and tries to compute the slew again. This process is carried out iteratively as long as both the slews are declared feasible or the leg duration is reduced to 0;

- The results, provided in terms of feasible durations, are stored in a .cvs file.

The output of a simulation is an acquisition table where each line corresponds to a MCV roll value and each column to a specific lunar phase. Durations are provided in minutes and rounded to the third significant digit. An example is given in Figure 5.4. As it can be seen, a three-color scale is introduced to give an easier visual interpretation of the results.

Lunar phase [deg] — Ascending phase (φ>0)

MCV Roll [deg]	90	85	80	75	70	65	60	55	50	45	40	35	30	25	20	15	10	5	0
-35	12.1	13.1	14.5	15.6	16.8	18.2	19.7	21	22.4	22.8	23.4	23	22	21.4	20.7	19.8	18.8	16.2	16.7
-30	11.8	13	14.2	15.5	16.8	18.1	19.4	20.8	21.5	21.9	22.2	21.2	20.3	19.5	18.8	17.9	16.9	14.4	16.5
-25	12	13.2	14.3	15.7	17	18.1	19.3	20.6	20.8	21.2	20.2	19.4	18.4	17.6	16.9	16.1	15.1	14.1	16.2
-20	12.2	13.5	14.8	15.8	17	18.4	19.7	20.1	20.4	19.4	18.3	17.4	16.4	15.7	15.1	14.3	13.6	12.6	15.8
-15	13.2	14.2	15.1	16.3	17.7	19	19.6	19.8	18.3	17.3	16.2	15.4	14.6	14	13.4	13	12.5	11.3	15.2
-10	13.9	14.8	15.8	17	18.3	19.4	19.1	17.4	16.2	15.3	14.3	13.6	12.9	12.4	12.1	11.7	11.3	10.2	14.5
-5	14.8	15.7	16.8	18	19.6	18.3	16.6	15.4	14.2	13.4	12.6	12	11.5	11.1	10.8	10.5	10.2	0	0
0	15.9	16.8	18	19	17.6	15.9	14.7	13.5	12.6	11.9	11.2	10.8	10.4	10.1	9.83	9.62	0	0	0
5	17.2	18	18	16.9	15.3	13.9	12.8	12	11.3	10.7	10.2	9.86	9.53	9.31	9.13	0	0	0	0
10	18.2	17.1	16.4	14.9	13.6	12.5	11.6	10.8	10.2	9.8	9.34	9.06	8.97	8.81	0	0	0	0	0
15	16.6	15.7	14.7	13.5	12.4	11.5	10.8	10.1	9.63	9.28	8.94	8.72	8.52	0	0	0	0	0	0
20	15.7	14.6	13.5	12.5	11.7	11	10.3	9.82	9.39	9.1	8.81	8.64	0	0	0	0	0	0	0
25	14.7	13.8	12.9	12.1	11.4	10.8	10.2	9.79	9.42	9.18	8.92	0	0	0	0	0	0	0	0
30	14.1	13.3	12.6	12	11.4	10.8	10.4	10	8.88	0	0	0	0	0	0	0	0	0	0
35	13.9	13.3	12.7	12.1	11.6	11.2	9.65	8.67	0	0	0	0	0	0	0	0	0	0	0

Lunar phase [deg] — Descending phase (φ<0)

MCV Roll [deg]	-5	-10	-15	-20	-25	-30	-35	-40	-45	-50	-55	-60	-65	-70	-75	-80	-85	-90
-35	22.2	23.6	25.2	26.4	27.6	28.9	30.2	31.7	33	34.3	35.9	37.8	44.3	45.3	46.1	47	47.9	20.3
-30	21.2	22.6	23.9	25.2	26.6	28.1	29.6	31.4	32.8	34.3	36.1	38.2	44.1	45.1	45.8	46.7	47.1	21.2
-25	20.1	21.3	22.6	24	25.5	26.9	28.6	30.7	32.4	34.1	36.3	38.4	43.8	44.8	45.5	46.2	46.1	21.2
-20	18.9	19.8	20.9	22.2	23.8	25.5	27.4	29.8	31.8	33.8	36.1	38.4	43.4	44.6	45.3	45.4	45.1	21.4
-15	17.5	18	19	20.3	21.9	23.5	25.5	28.2	30.5	32.8	35.6	38.1	42.8	44	44.8	44.6	44.4	21.4
-10	15.8	16.2	17.1	18.1	19.5	21.3	23.3	26	28.5	31.2	34.4	37.3	41.7	43.1	44	44.9	45.6	24.6
-5	1.09	14.4	15.1	16.1	17.1	18.7	20.6	23.4	26.1	28.8	32.5	35.9	40.1	41.8	42.9	44	44.8	24.7
0	0	0.03	13.3	14.1	14.9	16.3	17.9	20.4	22.9	25.9	29.9	33.5	37.7	39.9	41.4	42.7	43.7	24.5
5	0	0	0	12.2	13.1	14.2	15.6	17.6	19.8	22.5	26.4	30.4	34.3	37.2	39.1	40.8	42.1	23.9
10	0	0	0	0	11.7	12.6	13.7	15.4	17.2	19.5	22.9	26.7	30.2	33.4	35.8	38.1	39.9	22.7
15	0	0	0	0	0	11.3	12.2	13.7	15.2	17	20.1	23	25.9	29.1	31.8	34.6	36.9	20.7
20	0	0	0	0	0	0	11.4	12.6	13.9	15.4	17.9	19.8	22.3	25.1	27.6	30.6	33.3	18
25	0	0	0	0	0	0	0	11.9	13	14.5	16.6	17.8	19.5	21.9	24.1	26.8	29.6	14.8
30	0	0	0	0	0	0	0	0.66	2.26	13.9	15.7	16.6	18.1	19.7	21.6	23.9	26.4	11.7
35	0	0	0	0	0	0	0	0.12	1.63	3.08	15.4	16.1	17.3	18.5	19.9	21.8	24.1	9.16

Duration [min]

0 25 50

Figure 5.4 : Acquisitions table for α = 270°, 10.30 orbit, 1st month of the year.

5.5. Configurations of interest and simulation scenario

In this section, the configurations of interest selected for each type of calibration are summarised to provide the overall scenario about the totality of cases that need to be simulated for the feasibility analysis.

As described in section 5.1, three different lunar calibrations need to be analysed; the radiometric and geometric ALT require that the FOV orientation and the scan direction are orthogonal one another (ALT configuration), whereas the geometric ACT needs to be done with the FOV oriented parallel to the scan direction (ACT configuration). In terms of approach angles, two possible orientations of the FOV are identified, corresponding to α=0° and α=180° for the ALT configuration and α=90° and α=270° for the ACT configuration. Each of these angles needs to be analysed individually to determine how the spacecraft behaves in correspondence of different orientations of the MCV. Nonetheless, performances must be evaluated for all the possible candidate orbits to meet the mission requirements. This means that a total of 16 cases have to be analysed all over the 13 lunar months within the cal/val phase of the mission.

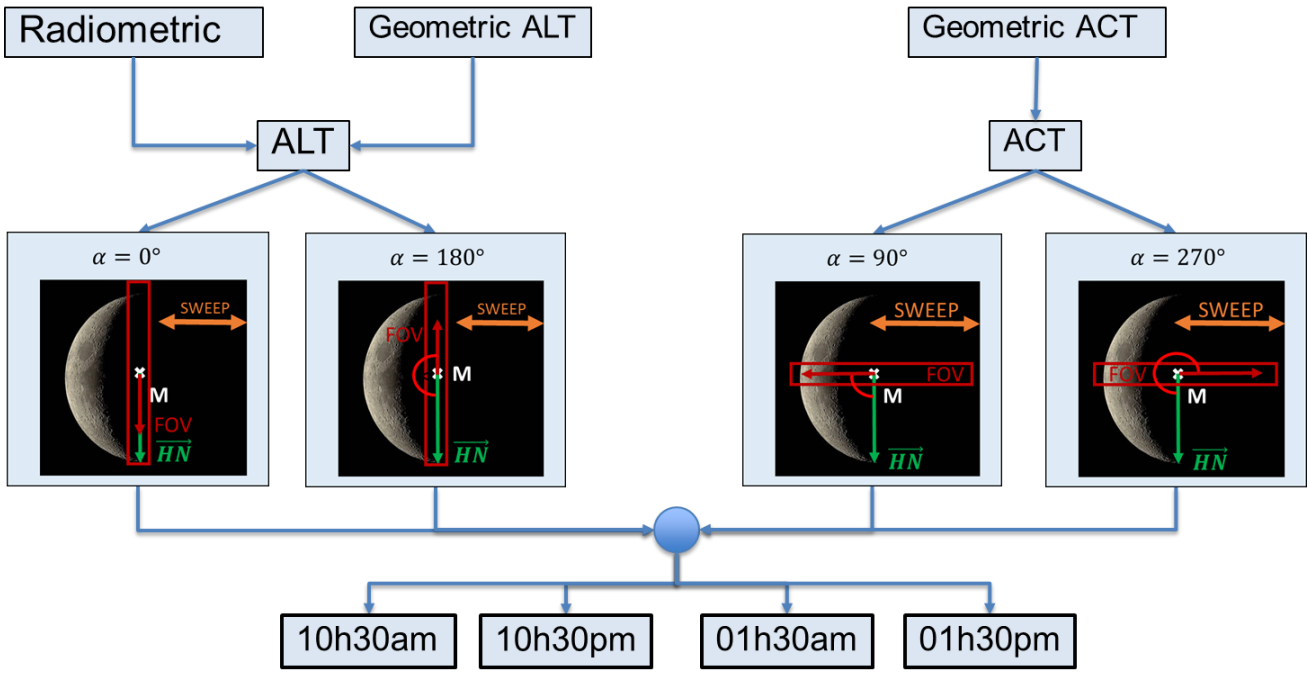

Figure 5.5: Simulation scenario for the three types of lunar calibrations.

However, a series of symmetries in the orientation of the orbits in space can be exploited to simplify the discussion of the results:

- Similar performances can be expected for opposite orbits sharing the same nodal line (10.30 am and 10.30 pm for example). In fact, if one approximates these orbits as perfectly polar (*i=90°*), their planes become coincident and the trajectories overlap one another. This means that every leg performed on a10.30 am orbit is perfectly equivalent to a leg on a 10.30 pm orbit traveled backward in time; furthermore, if one considers that the Moon displacement is

negligible during a lunar acquisition (the Moon phase varies of approximately *1°* over one orbit), two guidance legs simulated on opposite orbits at equal conditions should be equivalent.

- 10.30 pm and 13h30 pm orbits, as well as the respective spacecraft orientation in Nadir mode, are symmetric with respect to the plane orthogonal to the Earth/Sun direction. This means that performances on 10.30 pm orbits in the ascending phase of the Moon should be equivalent for a 01.30 pm orbit in the descending phase and vice versa. The same can be said for 10.30 am and 01.30 pm orbits.

For this reason, a more detailed analysis will be performed on the 10.30 pm orbit, currently selected as the design case. Results will be then extended to the three backup orbits exploiting the above mentioned symmetries.

5.6. Guidance legs preliminary analysis

Before to simulate the acquisition legs for all the possible case mentioned in the previous section, it is useful to build a simplified model to represent them in a 2D scenario. This step provides useful insights about the most suitable location on orbit where acquisitions can take place avoiding dazzling phenomena. Furthermore, a preliminary analysis can also show which is the orientation of the spacecraft in space resulting from a given approach angle.

The model is build considering an equatorial inertial reference frame centred on Earth. The X axis is oriented in the Earth-Sun direction, the Z axis is parallel to the north pole and the Y axis completes the frame. The following simplifications are considered:

1) The spacecraft orbit is perfectly polar (*i=90°*) with a MLTAN=00h00 (the nodal line lies along the X direction);
2) The Moon is fixed at third quadrant (*φ=-90°*);
3) The Moon orbit plane, the ecliptic and the equator are coincident;
4) The horn line is parallel to the Celestial South Pole;
5) The presence of the fictitious baffle notch earth sensor is neglected;
6) The earth port, thermal baffle and the star tracker are oriented along the $+Z_{sat}$, $+Y_{sat}$ and $-Z_{sat}$ spacecraft body axis, respectively;

A graphical representation of this model is given in Figure 5.6. At third quarter, the Moon lies along the Y direction of the inertial reference frame. It can be seen that, for an approach angle for α=270°,

the earth port field of view is oriented along the X direction, the star tracker is pointed in the –Y direction whereas the thermal baffles points in –X direction.

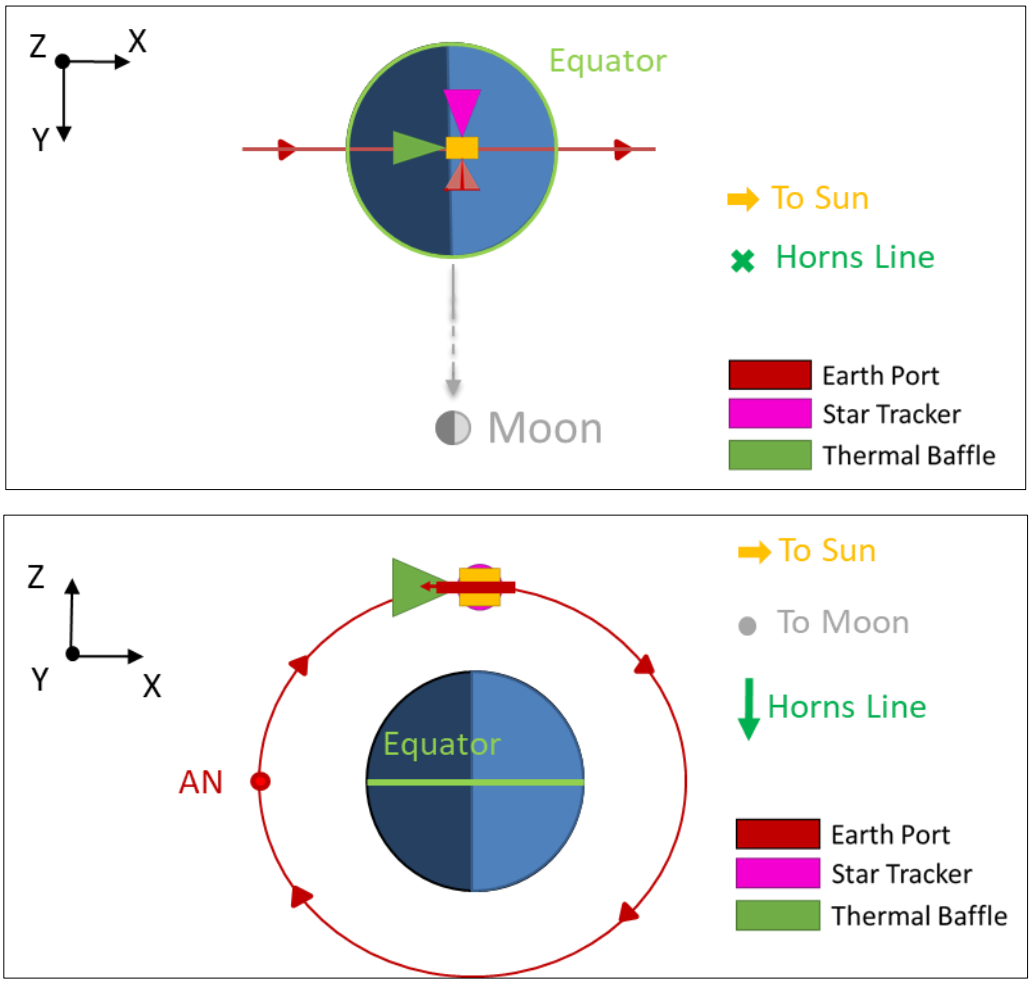

Figure 5.6: Polar (top) and equatorial (bottom) views of the spacecraft configuration for α=270°.

An acquisition leg implementation over one complete orbit is given in Figure 5.7. Starting from the descending node position (1), the baffled is initially oriented toward the Earth and remains dazzled until its field of view become tangent to the planet's surface (2), in proximity of the south pole. From this condition on, the acquisition leg can take place all over the night side of the orbit, passing through the ascending node (3) toward the north hemisphere. After the passage of the spacecraft on the north pole, the baffle is again dazzled by the Earth once its field of view becomes tangent to its surface (4).

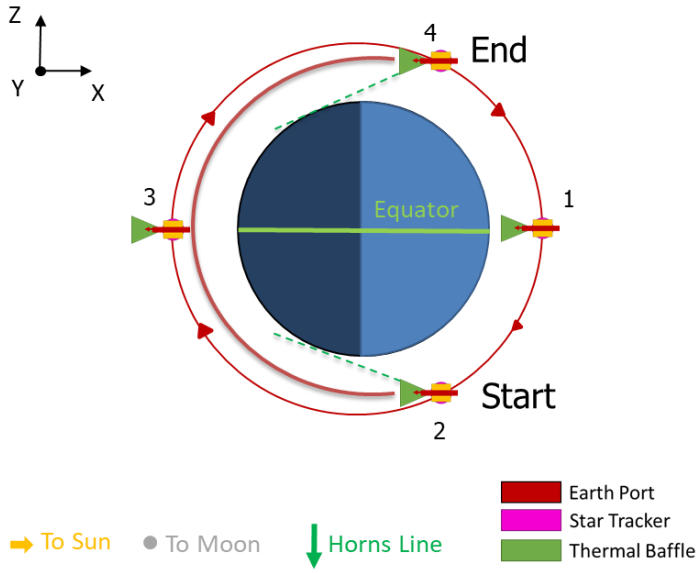

Figure 5.7: Acquisition leg for α=270° in a simplified model.

In such a scenario, the feasible interval for an ACT acquisition corresponds to the whole night side of the orbit, and has a duration of approximately 50 minutes (half of the orbital period). This case can be identified as optimal, providing the highest duration expectable for a lunar guidance leg. In a more realistic scenario, in fact, the presence of the star tracker must be also taken into account, as well as the fact that the Moon could not always be in visibility.

For the other three approach angles, analogous discussions can be done; their orientations are illustrated in Figure 5.8. In particular, α=90°, it can be immediately observed in that this configuration is not suitable for acquisitions. In fact, all over the day side of the orbit, the baffle oriented toward the Sun, whereas in the night side it is dazzled by the Earth. For α=0°, acquisitions take place over the southern hemisphere, for α=180°, acquisitions take place over the northern hemisphere;

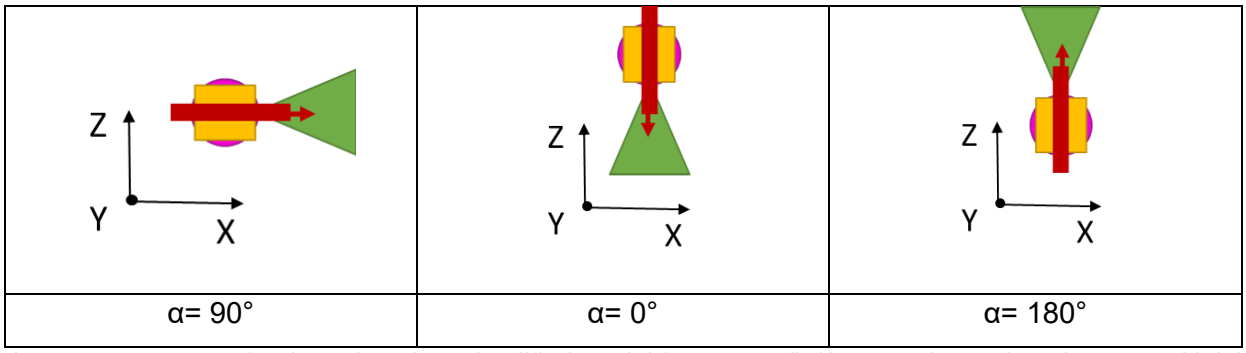

Figure 5.8: Spacecraft orientations in a simplified model for α= 90° (left), α= 0° (centre) and α= 180° (right).

6. Results

In this section, the results of the simulations generated by the algorithm described in section will be presented and discussed. At first place, a detailed analysis for the four approach angles of interest is carried out for the current design orbit 10.30 pm. The performances will be studied a short term within a lunar month, analyzing how the acquisition durations varies as a function of the lunar phase and MCV orientation. The most relevant phenomena constraining the acquisitions will be highlighted and analysed as well. Then, a long term analysis will be conducted over one year to study how the solutions evolves in time: same configurations in terms of φ and ρ will be compared for different lunar months to find out which are the most favorable periods to perform calibrations. In a second step, the analysis will be extended to the 10.30 am backup orbit, opposite to the design one. Eventually, results on 01.30 am and 01.30 pm will be presented in comparison with the two cases previously presented.

6.1. 10.30 pm orbit, short term analysis

6.1.1. ACT configuration, α=270°

In such a configuration the thermal baffled is oriented away from the Sun. Preliminary analyses showed that observations can be done along the night side of the orbit, from southern to northern latitudes, with acquisition durations up to approximately 50 minutes in the best case scenario.

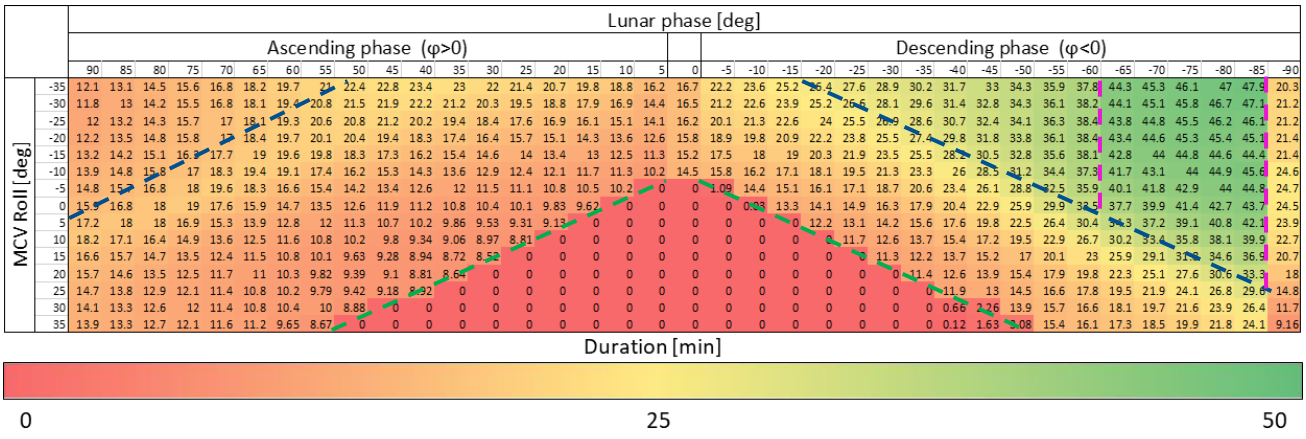

Figure 6.1: Acquisition table for α = 270°, 10.30 pm orbit, 3rd month of the year. Dashed lines highlight limit conditions for star tracker dazzling (blue), Moon visibility (pink) and baffle-sun dazzling (green).

Simulation results are shown in Figure 6.1; it can be observed that the best case scenario is obtained over the descending phase for lunar phases between -85° and -65°. Also, it appears that performances over the descending phase are better compared to the ones in the ascending phase. This is due to two phenomena in particular:

1) The *MLTAN* of the real orbit introduces an angle of *22.5*° between the orbit plane and the Earth-Sun direction; this means that the orientation of the spacecraft is not symmetrical with respect to full Moon condition. In particular, the angle is beneficial for observations over the descending phase;

2) Slews introduce significant losses over the ascending phase. As explained in section 5.4, for an acquisition leg to be feasible it must be ensured that slews manoeuvers before and after the leg do not cause any dazzling. When this happens, the leg is progressively reduced at the boundaries until both slews can be performed respecting all the attitude constrains. This phenomenon can be appreciated in Figure 6.2, which tells how much of the actual leg was removed due to problems in slews;

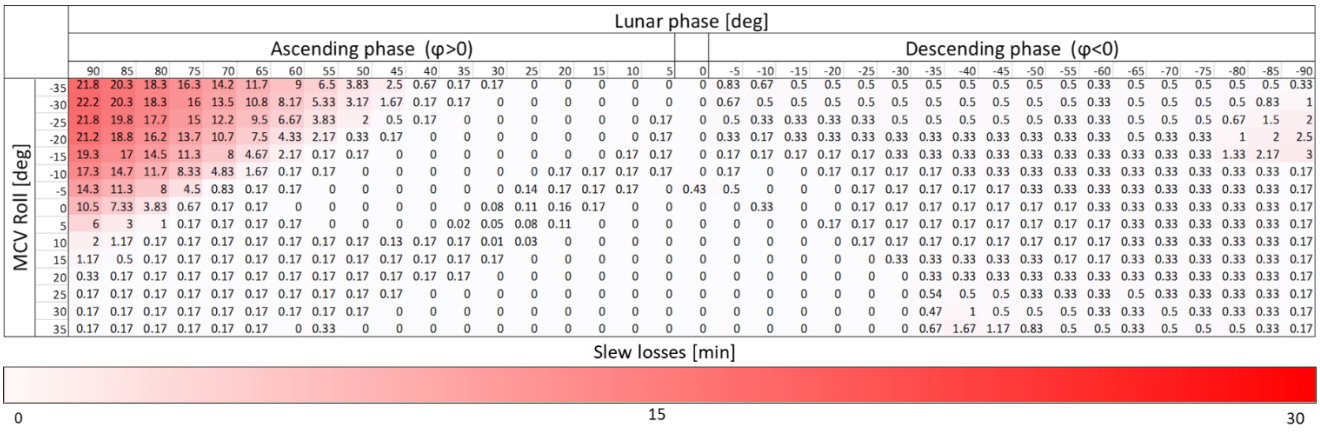

MCV Roll [deg]	Ascending phase (φ>0)																		Descending phase (φ<0)																	
	90	85	80	75	70	65	60	55	50	45	40	35	30	25	20	15	10	5	0	-5	-10	-15	-20	-25	-30	-35	-40	-45	-50	-55	-60	-65	-70	-75	-80	-85	-90
-35	21.8	20.3	18.3	16.3	14.2	11.7	9	6.5	3.83	2.5	0.67	0.17	0.17	0	0	0	0	0	0	0.83	0.67	0.5	0.5	0.5	0.5	0.5	0.5	0.5	0.5	0.5	0.33	0.5	0.5	0.5	0.5	0.5	0.33
-30	22.2	20.3	18.3	16	13.5	10.8	8.17	5.33	3.17	1.67	0.17	0.17	0	0	0	0	0	0	0	0.67	0.5	0.5	0.5	0.5	0.5	0.5	0.5	0.5	0.5	0.5	0.33	0.5	0.5	0.5	0.5	0.83	1
-25	21.8	19.8	17.7	15	12.2	9.5	6.67	3.83	2	0.5	0.17	0	0	0	0	0	0	0.17	0	0.5	0.33	0.33	0.33	0.33	0.5	0.5	0.5	0.5	0.5	0.33	0.33	0.5	0.5	0.5	0.67	1.5	2
-20	21.2	18.8	16.2	13.7	10.7	7.5	4.33	2.17	0.33	0.17	0	0	0	0	0	0	0	0.17	0	0.33	0.17	0.33	0.33	0.33	0.33	0.33	0.33	0.33	0.33	0.33	0.33	0.5	0.33	0.33	1	2	2.5
-15	19.3	17	14.5	11.3	8	4.67	2.17	0.17	0.17	0	0	0	0	0	0	0	0.17	0.17	0	0.17	0.17	0.17	0.17	0.17	0.33	0.33	0.33	0.33	0.33	0.33	0.33	0.33	0.33	0.33	1.33	2.17	3
-10	17.3	14.7	11.7	8.33	4.83	1.67	0.17	0.17	0	0	0	0	0	0	0.17	0.17	0.17	0.17	0	0.17	0	0	0.17	0.17	0.17	0.17	0.33	0.33	0.33	0.33	0.33	0.33	0.33	0.33	0.33	0.33	0.17
-5	14.3	11.3	8	4.5	0.83	0.17	0.17	0	0	0	0	0	0	0.14	0.17	0.17	0.17	0	0.43	0.5	0	0	0	0.17	0.17	0.17	0.17	0.17	0.33	0.33	0.33	0.33	0.33	0.33	0.33	0.33	0.17
0	10.5	7.33	3.83	0.67	0.17	0.17	0	0	0	0	0	0	0.08	0.11	0.16	0.17	0	0	0	0	0.33	0	0	0.17	0.17	0.17	0.17	0.17	0.17	0.33	0.33	0.33	0.33	0.33	0.33	0.33	0.17
5	6	3	1	0.17	0.17	0.17	0.17	0	0	0	0	0.02	0.05	0.08	0.11	0	0	0	0	0	0	0	0.17	0.17	0.17	0.17	0.17	0.17	0.17	0.17	0.17	0.33	0.33	0.33	0.33	0.33	0.17
10	2	1.17	0.17	0.17	0.17	0.17	0.17	0.17	0.17	0.13	0.17	0.17	0.01	0.03	0	0	0	0	0	0	0	0	0	0.17	0.17	0.17	0.17	0.17	0.17	0.17	0.17	0.33	0.33	0.33	0.33	0.33	0.17
15	1.17	0.5	0.17	0.17	0.17	0.17	0.17	0.17	0.17	0.17	0.17	0.17	0.17	0	0	0	0	0	0	0	0	0	0	0	0.33	0.33	0.33	0.33	0.33	0.17	0.17	0.33	0.33	0.33	0.33	0.33	0.17
20	0.33	0.17	0.17	0.17	0.17	0.17	0.17	0.17	0.17	0.17	0.17	0.17	0	0	0	0	0	0	0	0	0	0	0	0	0	0.33	0.33	0.33	0.33	0.33	0.33	0.33	0.33	0.33	0.33	0.33	0.17
25	0.17	0.17	0.17	0.17	0.17	0.17	0.17	0.17	0.17	0.17	0	0	0	0	0	0	0	0	0	0	0	0	0	0	0	0.54	0.5	0.5	0.33	0.33	0.33	0.5	0.33	0.33	0.33	0.33	0.17
30	0.17	0.17	0.17	0.17	0.17	0.17	0.17	0.17	0.17	0	0	0	0	0	0	0	0	0	0	0	0	0	0	0	0	0.47	1	0.5	0.5	0.5	0.33	0.33	0.5	0.33	0.33	0.33	0.17
35	0.17	0.17	0.17	0.17	0.17	0.17	0	0.33	0	0	0	0	0	0	0	0	0	0	0	0	0	0	0	0	0	0.67	1.67	1.17	0.83	0.5	0.5	0.33	0.5	0.5	0.5	0.33	0.17

Figure 6.2: Slew losses table for α = 270°, 10.30 pm orbit, 3rd month of the year.

Concerning the descending phase, it can be useful to analyse the variations observed at constant *MCV* roll. Considering, for example, *ρ=-5°*, *φ<0°* and referring to Figure 6.1 :

- Optimal performances are found for *-85°<φ<-65°*; in this case the acquisition are limited both at the beginning and at the end by thermal baffle dazzled by Earth;
- For φ> -65° and φ = 90°, a reduction of the acquisition durations is caused by a lack of visibility of the Moon in the proximity of the south pole, highlighted by brown dashed lines. It can be seen that these lines are verticals, meaning that this phenomenon does not depend on the MCV orientation. Indeed, Moon visibility is related to the spacecraft position only, regardless of its orientation;
- For φ>-55°, intervals are furtherly reduced because the Earth enters the field of view of the star tracker at equatorial latitudes. The dashed blue line, corresponding to the limit condition where the star tracker field of view becomes tangent to the Earth surface, has an obliquus slope indicating that such condition depends both on φ and ρ. Referring to the simplified model, Figure 6.3 show that, from a geometrical point of view, this is due to the fact that both variations in φ and ρ results in a tilt of the satellite's attitude around the Z axis.
- For φ>-5°, the thermal baffle gets dazzled by Sun in the vicinity of the poles (green dashed line). In such conditions no feasible interval can be found. Similarly to what discussed for the star tracker, the baffle sun dazzling limit condition appears as a diagonal line as well and correspond to a rotation of the spacecraft around the Z axis.

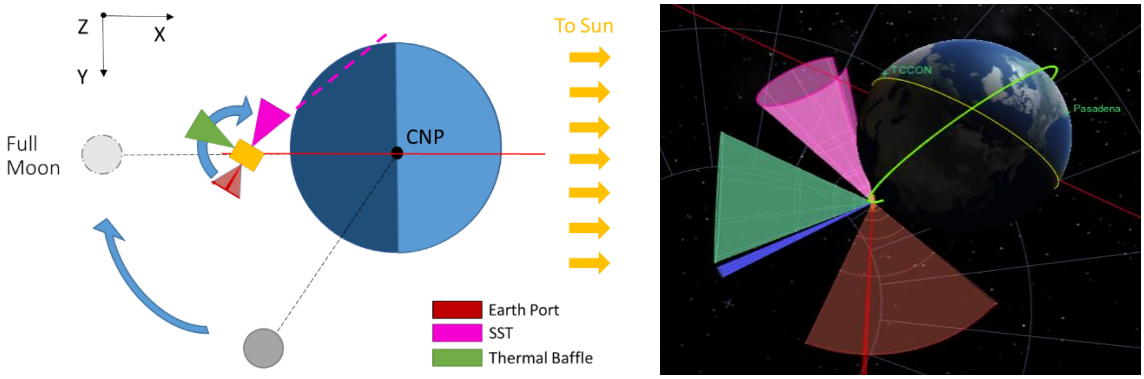

Figure 6.3: Top view of star tracker dazzling caused by spacecraft rotation around his $-X_{Sat}$ axis represented in a simplified model (left) and in a VST simulation (right).

6.1.2. ACT configuration, α = 90°

The preliminary analysis discussed in section 5.6 showed that this configuration was critical since the thermal baffle is dazzled by Sun over the day side of the orbit and by Earth over the night side. Performances in Figure 6.4 confirm this prevision and shows that, in the vast majority of cases, no feasible interval can be found. However, solutions are available in proximity of full Moon conditions, for -25°<φ<25° and -35°<ρ<20°. Physically, they correspond to acquisitions performed in proximity of the south pole and are restricted by the limiting conditions of star tracker dazzling by Earth (highlighted by dashed blue lines).

Due to its general poor performances, this configuration is not of interest for ACT acquisitions and will therefore be not considered hereinafter.

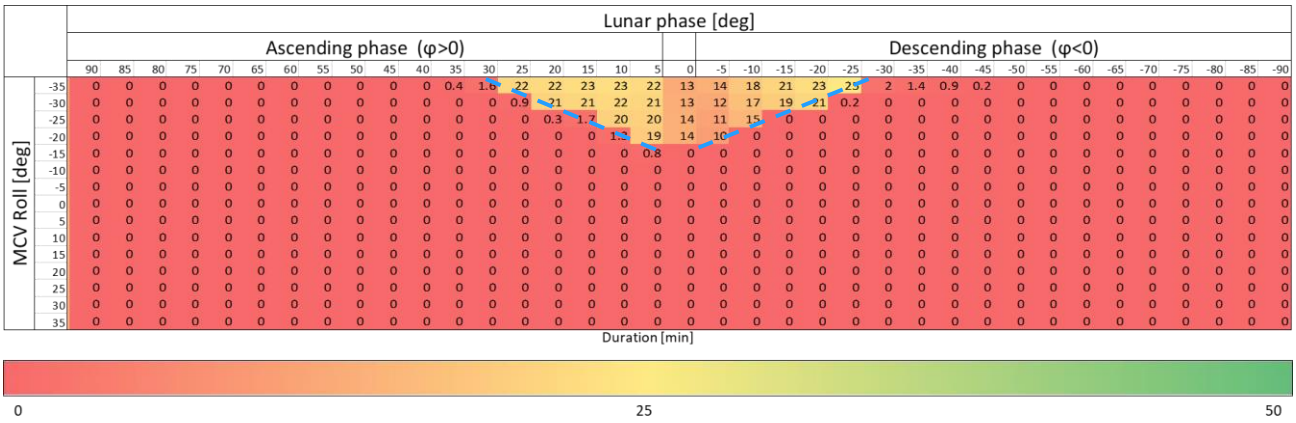

Figure 6.4: Acquisition table for α = 90°, 10.30 pm orbit, 3rd month of the year. The dashed line highlight limit conditions for star tracker dazzling.

6.1.3. ALT configuration, α=0°

In such a configuration the thermal baffled is oriented in the south pole direction. Preliminary analyses showed that observations take place along the southern hemisphere, from descending to ascending node, with acquisition durations up to approximately 50 minutes in the best case scenario.

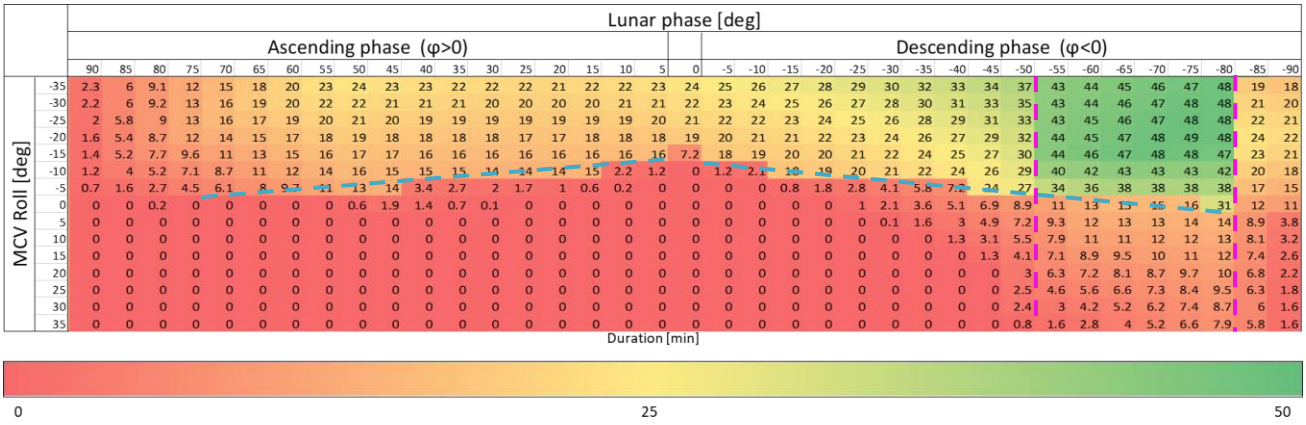

Figure 6.5: Acquisition table for α = 0°, 10.30 pm orbit, 3rd month of the year. The dashed line highlights limit conditions for baffle-sun dazzling (blue) and Moon visibility (pink).

Results are shown in Figure 6.5. As for the case α=270°, better performances are found over the descending phase. However, this time it can be observed that acquisitions performed for positive values of ρ feature short durations that do not exceed 10 minutes. This is caused by the thermal baffle

which is dazzled by the Sun. This phenomenon –highlighted by the blue dashed line - is due to the fact that a change in the MCV roll orientation corresponds to a rotation of the plane representing the field of view of the baffle-sun sensor; therefore, if the sun crosses this plane, the sensor gets dazzled. Figure 6.6 and Figure 6.7 represent the two limits conditions as seen from an observed placed across the baffle-sun plane (in orange).

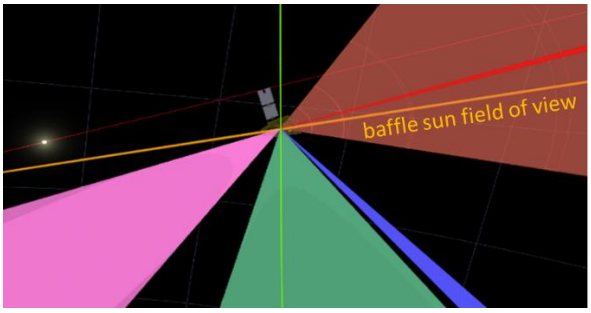

Figure 6.6: Acquisitions at α =0°,φ=-60°, ρ = −5°.

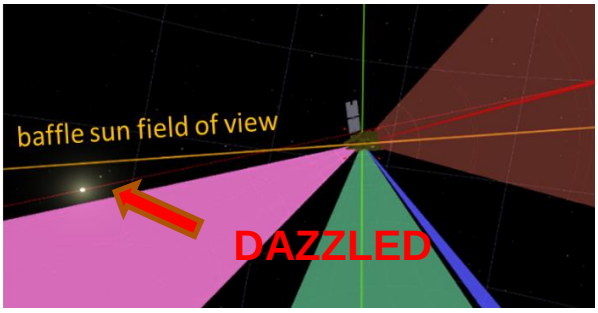

Figure 6.7: Acquisitions for α = 0° φ= -60°, ρ = 0°

For negative *MCV* rolls, solutions can be divided in two groups. Referring to Figure 6.5:

1) For φ ϵ [-80°; -55°], the system configuration is such that neither the star tracker and the thermal baffle are dazzled in the southern hemisphere. This gives feasible durations up to *49* minutes, corresponding to the best case scenario performance;
2) For φ= 90° and φ<55° the Moon is hidden by Earth when the satellite flies in between the south pole and the equator (pink dashed lines); this drastically reduce the feasible interval durations;

In conclusion, a *ALT 0°* configuration offers interesting performances and can be exploited to test negative *MCV* roll angle for calibration measurements.

6.1.4. ALT configuration, α=180°

In this configuration the thermal baffled is oriented in the north pole direction. Preliminary analyses showed that observations take place along the northern hemisphere, from ascending to descending node, with acquisition durations up to approximately 50 minutes in the best case scenario.

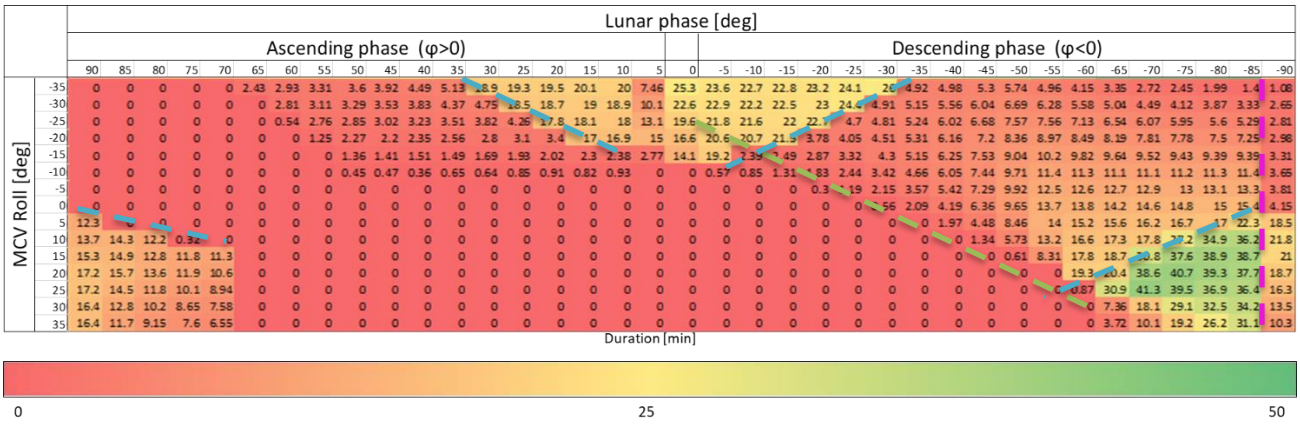

Figure 6.8: Acquisition table for α = 180°, 10.30 pm orbit, 8th month of the year. The dashed line highlights limit conditions for baffle-sun dazzling (blue), star tracker (green) and Moon visibility (pink).

Results shown in Figure 6.8 shows that this configuration is more critical than the one for α=0° previously analysed. In fact, two phenomena play a significant role as limiting factor:

- the thermal baffle sun dazzling condition (highlighted with blue lines) limits observations during the day part of the orbit. This condition is not represented as an horizontal line on the table since in a real model the baffle-sun pointing axis is tilted of *13*° in the $-Z_{Sat}$ direction (see section 4.2) meaning that the moon position as well as the MCV roll have an influence on the semi plane orientation.
- The star tracker become constraining when it intersects the Earth (green line): also in this case, both the moon position and the *MCV* roll both have an impact. Figure 6.9 gives a representation of this phenomenon. It can be seen that the SST can be pointed away from Earth both rotating northward (decreasing the value of *ρ*) and/or eastward (decreasing the value of *φ*).

It is interesting to notice that for *-30°<φ<0°* and *-35°<ρ<-15°* acquisitions can be done at polar latitudes. In such conditions, the baffle is no longer dazzled by Sun, so acquisitions can be done as long as the Moon is in visibility. However, in equivalent conditions, the *α=0°* configuration offers better performances, so this group of solutions is not of practical interest.

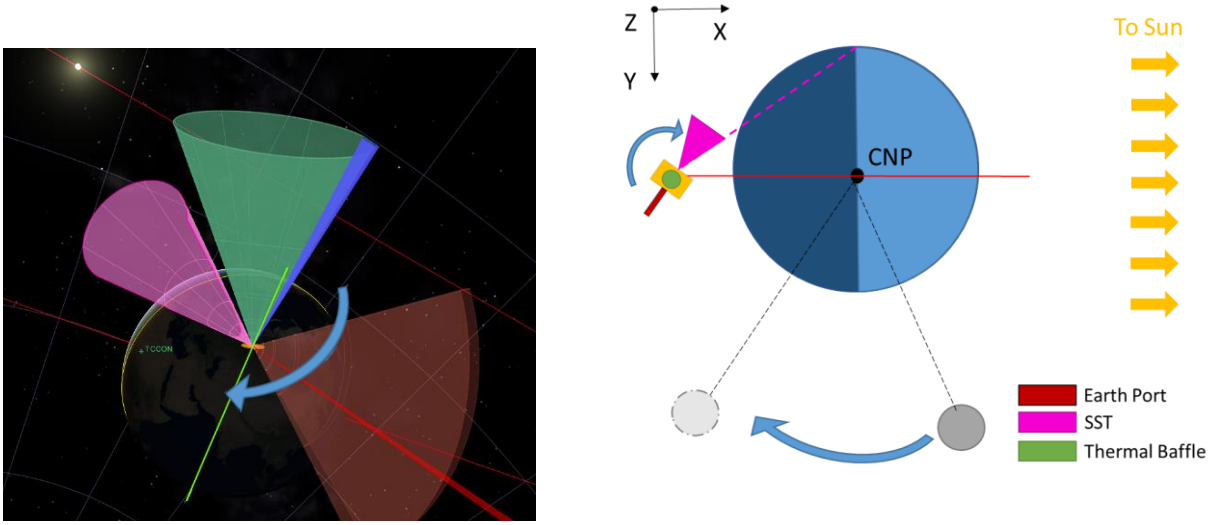

Figure 6.9: SST dazzling, simulated in VTS (left) and illustrated in the simplified model (right) for a 180° acquisition.

6.2. 10.30 pm orbit, long term analysis

According to the discussion in section 4.3.2, over one year the Moon relative elevation with respect to the OHP changes periodically. In this section, it will be observed that this phenomenon has a relevant impact for acquisitions at polar latitudes, reducing their overall acquisition durations. The δ^* evolution for a 10.30 pm orbit is given in Figure 6.10: its average elevation corresponds to approximately to *-8*°.

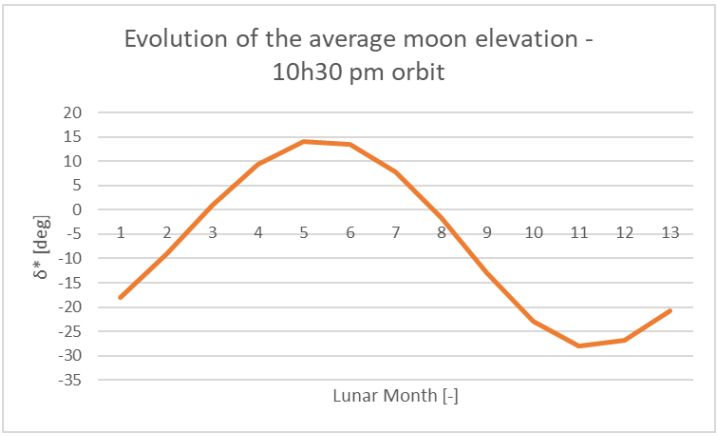

Figure 6.10: One year evolution for δ^* parameter on 10.30 pm orbit

The evolution of acquisition tables over one year will be analysed by selecting *5* configurations of interest that are associated with typical durations[4] of *45* minutes, corresponding to the ideal case scenario. These configurations are then plotted over the *13* lunar months to see which are the most critical periods of the year. The results will be supported by means of geometrical analysis that show

[4] « typical » refers to conditions that are not affected by moon-elevation related visibility problems

which phenomena cause a reduction of acquisition durations. Finally, to visualise the impact directly on the acquisition tables, the best and worst cases scenario for each α are reported in Annex 1.

6.2.1. ACT configuration, α=270°

Acquisitions in this configuration take place over the night side of the orbit. As it can be observed in Figure 6.11, performances are significally affected in correspondence of the months featuring the lowest value of δ*.
Geometrically, this can be explained considering that:

- In proximity of the north pole, the low elevation of the moon affects its visibility at high latitudes;
- In proximity of the south pole, the rotation required for the spacecraft to point at the moon causes the SST to tilt toward the Earth; it follows that for low elevations of the moon, this sensor is easily dazzled at low latitudes.

These two phenomena are schematically illustrated in Figure 6.12

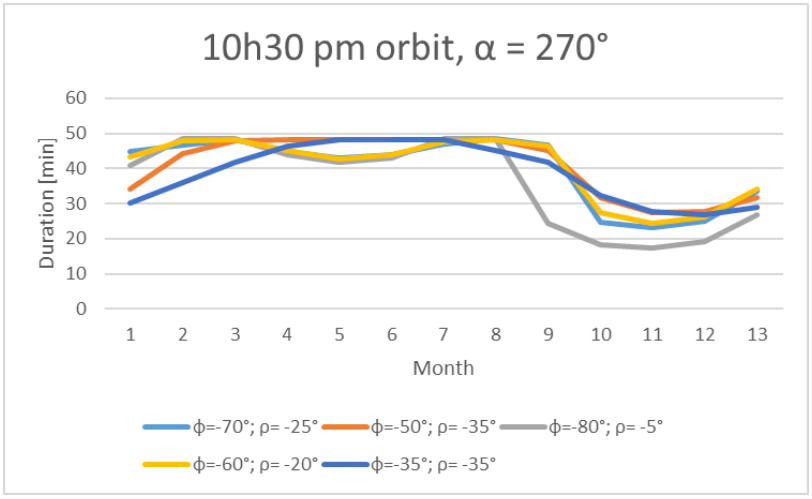

Figure 6.11: One-year evolution of acquisitions for α =270° on 10.30 pm orbit.

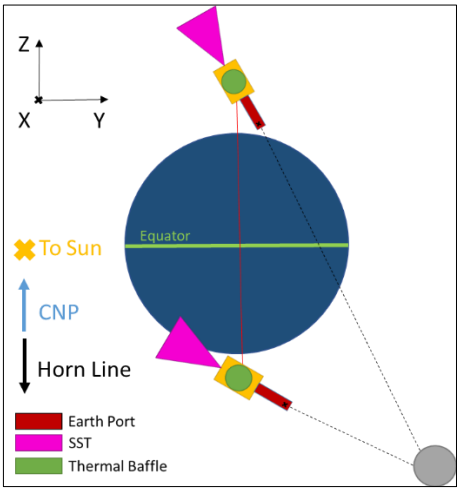

Figure 6.12: Effects of low moon elevation for α =270°.

The duration of the acquisitions is reduced from their boundaries near the Earth poles: if in ideal conditions the whole night side of the orbit can be exploited for observations, the low elevation of the

Moon shrinks the intervals moving their boundaries toward lower latitudes. Table *8.2* and Table *8.3*, provided in Annex1, show a best/worst case scenario for this configuration.

6.2.2. ALT configuration, α=0°

Since this configuration is associated with observation legs taking place in the southern hemisphere, performances in low elevation conditions are generally less affected by low elevations. However, it can be observed (Figure 6.13) that feasible durations are nonetheless influenced from 10th to 12th months. As seen for ACT configuration at α=270°, the main responsible phenomenon is the star tracker getting dazzled by Earth, this time in the proximity of the equator. By comparing Table *8.4* and Table *8.5* in Annex 1, it can be observed that the SST dazzling curve is much more evident for lower elevation conditions.

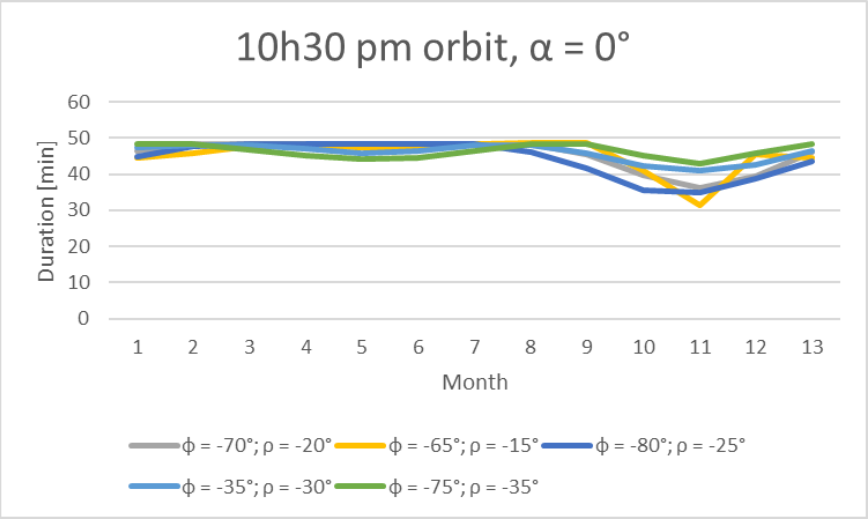

Figure 6.13: One-year evolution of acquisitions for α= 0° on 10.30 pm orbit.

6.2.3. ALT configuration, α =180°

Acquisitions in this configuration are the most affected by Moon elevation-related effects. For such a case, in fact, performances are degraded both for high and low values of δ*. Durations are significally reduced during 4th to 7th months (highest elevations), and 10th to 12th months (lowest elevation).

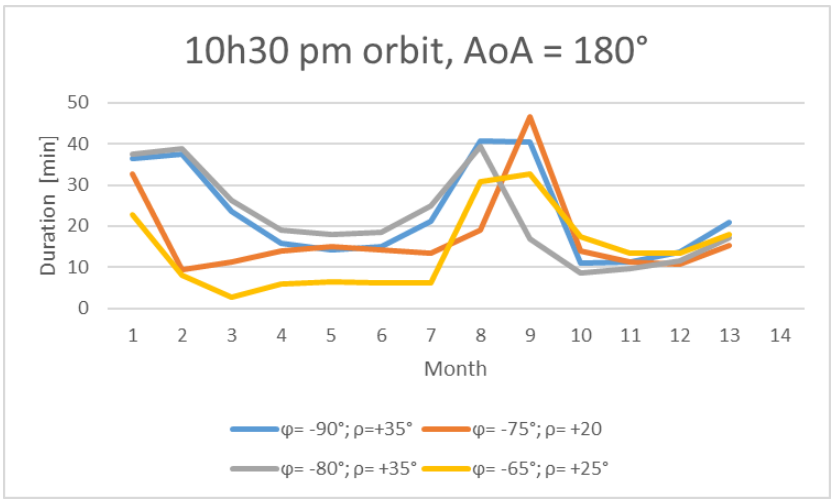

Figure 6.14: One-year evolution of acquisitions for α = 180° on 10.30 pm orbit.

In the first case, for high Moon elevations, the spacecraft has to rotate around its X_{body} axis to point at the Moon, thus rotating the star tracker toward the Earth. (Figure 6.15, left). On the other hand, for low elevations, the Moon is no longer visible when the satellite flies over the north pole (Figure 6.15, right). In between this two extreme cases, a third scenario with *δ* ~0°* shows that the spacecraft can point at the Moon without dazzling the *SST* all over its passage over the north pole (Figure 6.15, centre). This last situation corresponds to months 1-2 and 8-9. Table *8.6* and Table *8.7* in Annex 1 provide a best/worst case scenario, respectively.

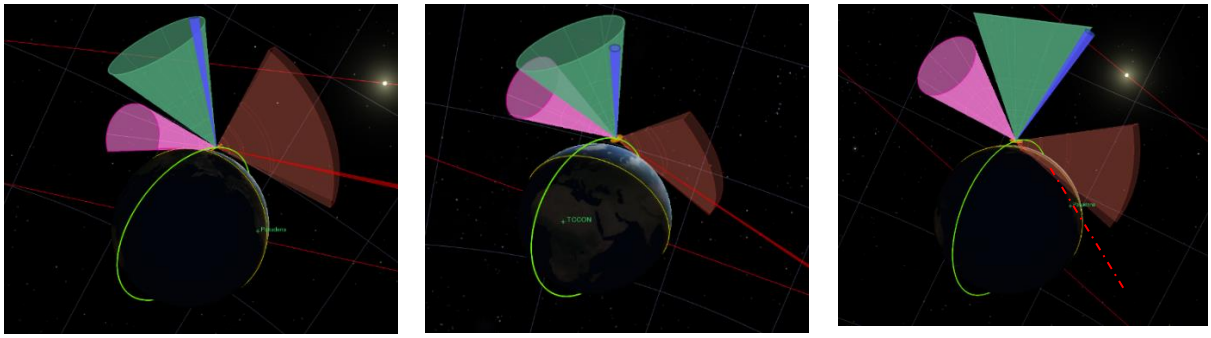

Figure 6.15: Acquisitions with α=180°, ρ=20°, φ -75, months 4 (left) , 8 (centre) and 12 (right).

6.3. Acquisitions on 10.30 am orbit

Relying on the analysis conducted in previous sections, performances for a *10.30 am* orbit will be now discussed to point out the main differences with respect to the previous case. As stated in section 5.5, if one considers that 10.30 am and 10.30 pm orbits as perfectly polar, they overlap on the same plane, resulting in the same exact trajectory travelled in forward and backward directions. Considering an ACT configuration made at α=270°, for example, it was seen that the associated guidance leg takes

place over the night part of the orbit. Particularly, on a *10.30 pm* orbit, acquisitions start at the south pole and end at the north pole.

The equivalent scenario on a 10.30 pm orbit is similar, though the satellite travels from north to south pole in this case.

Indeed, it can be observed in Figure 6.16that an *ACT 270°* acquisition table on a *10.30 am* is perfectly equivalent to the one analysed for a *10.30 pm* solution (Figure 6.1). The same considerations about *SST* dazzling and Moon visibility curves, as well as slews performances applies in this case. The same can be said for the two *ALT* configurations, whose acquisition tables are given in Annex 1(Table *8.10* and Table *8.11*).

Lunar phase [deg] — Ascending phase (φ>0)

MCV Roll [deg]	90	85	80	75	70	65	60	55	50	45	40	35	30	25	20	15	10	5
-35	4.6	6.4	8.7	11	13	15	17	19	21	22	22	21	20	19	18	17	16	13
-30	8.4	10	12	14	16	18	19	19	21	21	20	19	18	17	16	15	14	13
-25	12	14	16	18	20	20	18	20	21	19	18	17	16	15	14	14	13	11
-20	15	17	19	22	19	17	19	20	18	17	16	15	14	13	13	12	12	10
-15	18	21	22	17	16	18	19	18	16	15	14	13	12	12	11	11	11	10
-10	22	22	16	15	17	17	17	15	14	13	12	11	11	11	10	10	9.7	10
-5	21	14	14	15	15	14	14	13	12	11	11	10	9.9	9.7	9.4	9.2	8.9	0
0	12	14	13	12	12	13	13	12	11	10	9.7	9.3	9	8.8	8.8	8.6	0	0
5	13	11	10	10	11	12	11	11	9.9	9.4	9.1	8.8	8.6	8.4	8.3	0	0	0
10	9.8	9	8.8	9.2	9.4	9.8	10	10	9.5	9.1	8.8	8.5	8.3	7.5	0	0	0	0
15	8.1	7.7	7.6	7.3	7.1	6.6	7.1	9.3	9.2	8.8	8.6	8.4	8.2	0	0	0	0	0
20	7.2	6.6	5.8	4.9	3.6	4.6	10	9.4	8.9	8.5	8.3	8.1	0	0	0	0	0	0
25	6.3	5	3.5	3.3	8.1	10	9.5	8.9	8.4	8	7.7	0	0	0	0	0	0	0
30	5	3	4.5	11	11	9.5	8.8	8.2	7.7	0	0	0	0	0	0	0	0	0
35	3	5.3	12	11	9.6	8.6	7.9	7.3	0	0	0	0	0	0	0	0	0	0

Lunar phase [deg] — 0 and Descending phase (φ<0)

MCV Roll [deg]	0	-5	-10	-15	-20	-25	-30	-35	-40	-45	-50	-55	-60	-65	-70	-75	-80	-85	-90
-35	18	24	26	29	31	33	36	38	42	44	45	46	47	48	48	48	48	48	24
-30	18	23	25	27	29	32	35	38	42	44	45	46	47	48	48	48	48	48	23
-25	17	22	23	26	28	31	34	38	42	43	45	46	47	47	47	47	47	47	22
-20	17	20	22	24	26	29	33	37	41	43	44	46	47	48	48	48	46	46	20
-15	16	19	20	21	24	26	30	35	39	42	44	46	47	48	48	48	48	48	18
-10	15	17	17	19	21	23	27	31	36	39	43	45	47	48	48	48	48	48	21
-5	0	1	15	16	18	20	23	26	31	36	40	44	46	48	48	48	48	48	23
0	0	0	0	14	15	17	20	21	25	29	35	42	45	47	48	48	49	49	24
5	0	0	0	0	13	15	16	17	19	22	28	36	42	46	47	48	48	48	25
10	0	0	0	0	0	13	13	13	15	16	20	27	35	42	45	46	47	47	25
15	0	0	0	0	0	0	11	11	11	12	15	19	25	34	40	43	45	45	24
20	0	0	0	0	0	0	0	8.4	9	9.8	12	14	18	24	31	37	41	43	23
25	0	0	0	0	0	0	0	0	6.9	7.7	9.5	12	14	18	23	30	34	38	20
30	0	0	0	0	0	0	0	0	0	1.7	7.9	9.7	12	15	18	23	28	32	16
35	0	0	0	0	0	0	0	0	0	1	2.7	8.4	10	13	15	19	23	27	11

Duration [min]

0 — 25 — 50

Figure 6.16: ACT acquisitions results for α=270°, orbit 10.30 am, 13th month of the lunar year.

Differences in performances between the two orbits, for a given date, are caused by the relative elevation of the Moon. In fact, the angle between the two orbital planes causes the Moon to have a higher elevation for an observer placed on a *10.30 am* orbit (Figure 4.9). As a consequence, the most critical period of the year to perform acquisitions corresponds to months 4 to 6. In particular, it is interesting to remark that acquisitions at α=0° are more affected on 10.30 am orbit with respect to what observed for 10.30 pm case, since they take place over the southern hemisphere. For α=180°, acquisitions are affected by high elevations over a wider period (2nd to 8th month).

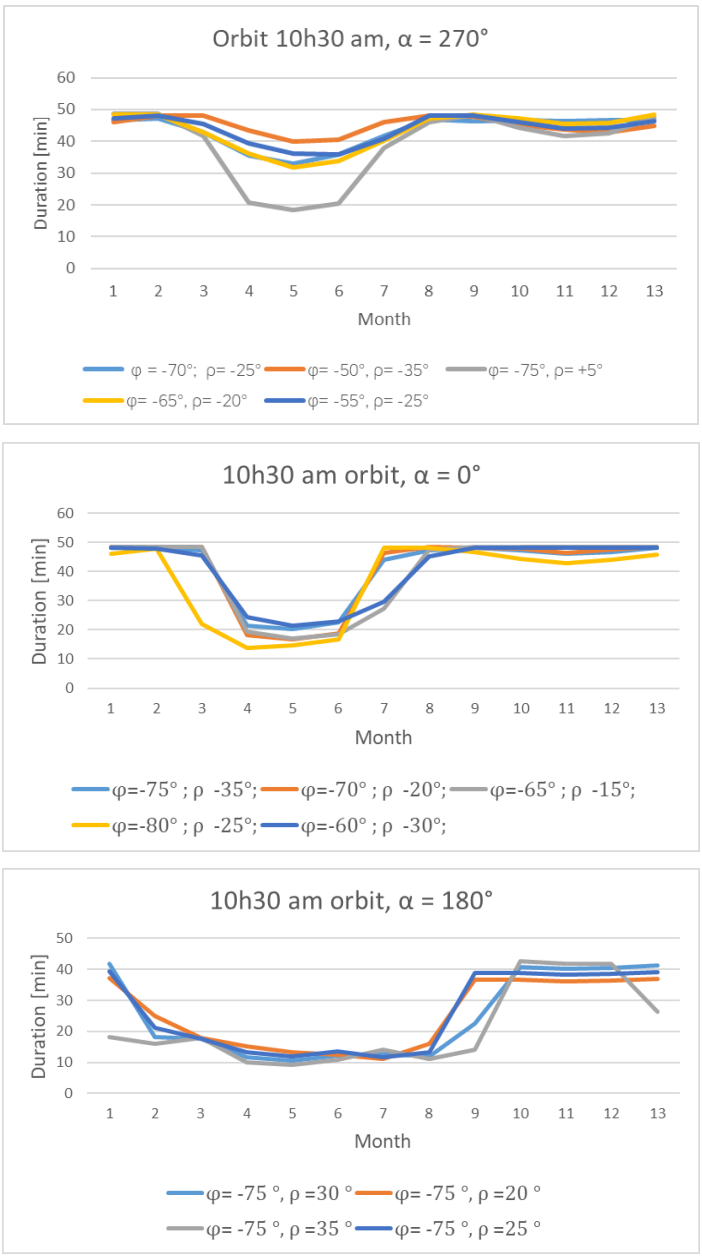

Figure 6.17: One-year evolution of acquisitions for α= 270° (top), α=0° (centre) and α= 180° (bottom) configurations on 10.30 am orbit.

6.4. Acquisitions on 01.30 am and 01.30 pm orbits

The analysis is now extended to 01.30 am/pm backup orbits. According to statements made in section 5.5, it exists a high degree of symmetry in their the geometrical disposition with respect to *10.30 am/pm* orbits. This symmetry is directly reflected on the acquisition tables. Results provided in this section refer to *01.30 pm* orbit, whereas performances on *01.30 am* orbit are given in Annex 1.

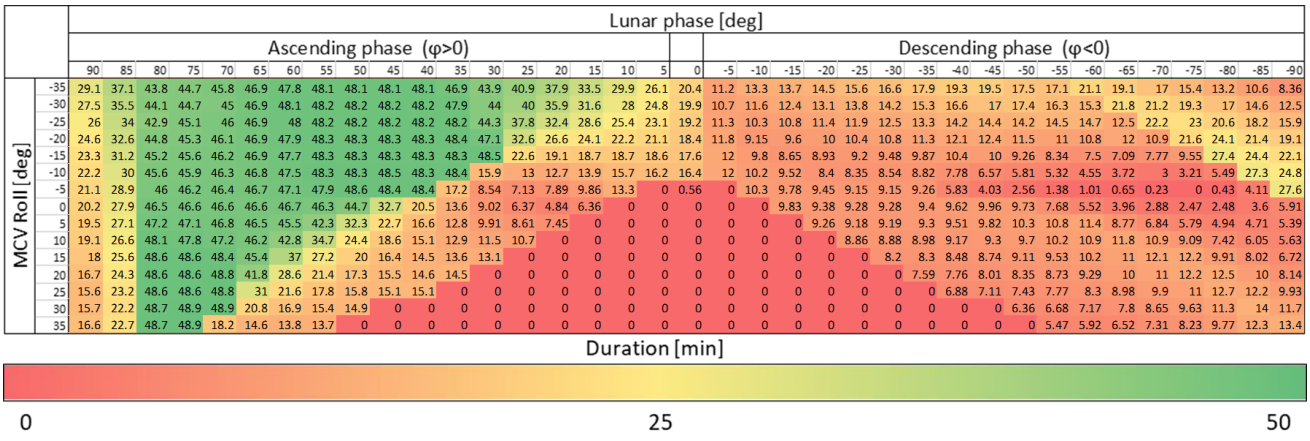

MCV Roll [deg]	Ascending phase (φ>0)																		Descending phase (φ<0)																	
	90	85	80	75	70	65	60	55	50	45	40	35	30	25	20	15	10	5	0	-5	-10	-15	-20	-25	-30	-35	-40	-45	-50	-55	-60	-65	-70	-75	-80	-85	-90
-35	29.1	37.1	43.8	44.7	45.8	46.9	47.8	48.1	48.1	48.1	48.1	46.9	43.9	40.9	37.9	33.5	29.9	26.1	20.4	11.2	13.3	13.7	14.5	15.6	16.6	17.9	19.3	19.5	17.5	17.1	21.1	19.1	17	15.4	13.2	10.6	8.36
-30	27.5	35.5	44.1	44.7	45	46.9	48.1	48.2	48.2	48.2	48.2	47.9	44	40	35.9	31.6	28	24.8	19.9	10.7	11.6	12.4	13.1	13.8	14.2	15.3	16.6	17	17.4	16.3	15.3	21.8	21.2	19.3	17	14.6	12.5
-25	26	34	42.9	45.1	46	46.9	48	48.2	48.2	48.2	48.2	48.2	44.3	37.8	32.4	28.6	25.4	23.1	19.2	11.3	10.3	10.8	11.4	11.9	12.5	13.3	14.2	14.4	14.2	14.5	14.7	12.5	22.2	23	20.6	18.2	15.9
-20	24.6	32.6	44.8	45.3	46.1	46.9	47.9	48.3	48.3	48.3	48.3	48.4	47.1	32.6	26.6	24.1	22.2	21.1	18.4	11.8	9.15	9.6	10	10.4	10.8	11.3	12.1	12.4	11.5	11	10.8	12	10.9	21.6	24.1	21.4	19.1
-15	23.3	31.2	45.2	45.6	46.2	46.9	47.7	48.3	48.3	48.3	48.3	48.3	48.5	22.6	19.1	18.7	18.7	18.6	17.6	12	9.8	8.65	8.93	9.2	9.48	9.87	10.4	10	9.26	8.34	7.5	7.09	7.77	9.55	27.4	24.4	22.1
-10	22.2	30	45.6	45.9	46.3	46.8	47.5	48.3	48.3	48.5	48.3	48.4	15.9	13	12.7	13.9	15.7	16.2	16.4	12	10.2	9.52	8.4	8.35	8.54	8.82	7.78	6.57	5.81	5.32	4.55	3.72	3	3.21	5.49	27.3	24.8
-5	21.1	28.9	46	46.2	46.4	46.7	47.1	47.9	48.6	48.4	48.4	17.2	8.54	7.13	7.89	9.86	13.3	0	0.56	0	10.3	9.78	9.45	9.15	9.15	9.26	5.83	4.03	2.56	1.38	1.01	0.65	0.23	0	0.43	4.11	27.6
0	20.2	27.9	46.5	46.6	46.6	46.6	46.7	46.3	44.7	32.7	20.5	13.6	9.02	6.37	4.84	6.36	0	0	0	0	0	9.83	9.38	9.28	9.28	9.4	9.62	9.96	9.73	7.68	5.52	3.96	2.88	2.47	2.48	3.6	5.91
5	19.5	27.1	47.2	47.1	46.8	46.5	45.5	42.3	32.3	22.7	16.6	12.8	9.91	8.61	7.45	0	0	0	0	0	0	0	9.26	9.18	9.19	9.3	9.51	9.82	10.3	10.8	11.4	8.77	6.84	5.79	4.94	4.71	5.39
10	19.1	26.6	48.1	47.8	47.2	46.2	42.8	34.7	24.4	18.6	15.1	12.9	11.5	10.7	0	0	0	0	0	0	0	0	0	8.86	8.88	8.98	9.17	9.3	9.7	10.2	10.9	11.8	10.9	9.09	7.42	6.05	5.63
15	18	25.6	48.6	48.6	48.4	45.4	37	27.2	20	16.4	14.5	13.6	13.1	0	0	0	0	0	0	0	0	0	0	0	8.2	8.3	8.48	8.74	9.11	9.53	10.2	11	12.1	12.2	9.91	8.02	6.72
20	16.7	24.3	48.6	48.6	48.8	41.8	28.6	21.4	17.3	15.5	14.6	14.5	0	0	0	0	0	0	0	0	0	0	0	0	0	7.59	7.76	8.01	8.35	8.73	9.29	10	11	12.2	12.5	10	8.14
25	15.6	23.2	48.6	48.6	48.8	31	21.6	17.8	15.8	15.1	15.1	0	0	0	0	0	0	0	0	0	0	0	0	0	0	0	6.88	7.11	7.43	7.77	8.3	8.98	9.9	11	12.7	12.2	9.93
30	15.7	22.2	48.7	48.9	48.9	20.8	16.9	15.4	14.9	0	0	0	0	0	0	0	0	0	0	0	0	0	0	0	0	0	0	0	6.36	6.68	7.17	7.8	8.65	9.63	11.3	14	11.7
35	16.6	22.7	48.7	48.9	18.2	14.6	13.8	13.7	0	0	0	0	0	0	0	0	0	0	0	0	0	0	0	0	0	0	0	0	0	5.47	5.92	6.52	7.31	8.23	9.77	12.3	13.4

Figure 6.18: ACT acquisitions results for α =270°, orbit 01.30 pm, 11th month of the cycle.

Considering for example a α =270° configuration, it can be observed in Figure 6.18 that acquisition tables give equivalent but specular performances with respect to what observed in section 6.2.1 for the 10.30 pm case. Equivalent considerations can be made for ACT configurations, whose acquisition tables are given in Annex 1.

This specularity can be explained considering that:

- The *β* angle introduces a rotation of the orbital plane that is now beneficial for moon observations in its ascending phase; on the other hand, it penalises the descending phase.
- Slews are easier to perform on one side of the orbit; in this case the ascending phase is favorited;

It follows that analysis conducted for *10.30 am/pm* orbits can be fully extended to *01.30 am/pm* orbits. However, it is important to remark that, for Moon observations in its ascending phase, the horn line is oriented in the northern hemisphere, according to the definition provided in section 4.3.1; this means that the relative orientation of the satellite with respect to the Moon is different in this case, as illustrated in Figure 6.19.

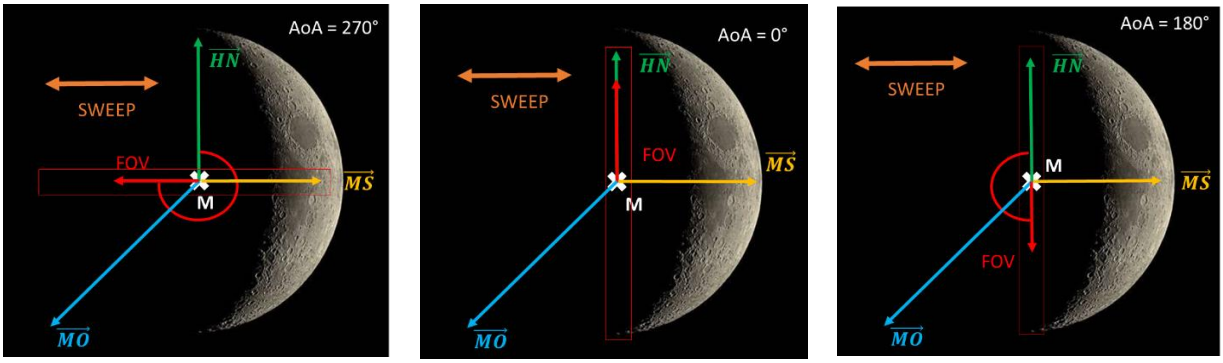

Figure 6.19: FOV orientation for observations of the Moon in ascending phase.

Therefore, for observations made during ascending phase of the Moon, the following considerations can be done:

- For α =*270°,* acquisitions still take place over the night side of the orbit, since the thermal baffle is oriented away from the Sun;
- For α = *0°*, acquisitions take place over the northern hemisphere;
- For α =*180°*, acquisitions take place over the southern hemisphere;

It can be observed that, with respect to previous cases, the location in orbit of α =0°/180° are inverted. Nonetheless, performances are equivalent to the associated configurations on 10.30 am/pm orbits with the same approach angle.

Concerning the long-term analysis, it can be observed (section 4.3.2, Figure 4.9) that lowest elevations for a 01.30 pm orbit occur from 3rd to 5th months. Equivalently to what observed for 10.30 am orbit, acquisitions performed at α=270° and α=0° shows a degradation of their performances over months 3-5, whereas acquisitions at α=180° are affected over a longer period (months 1-7).

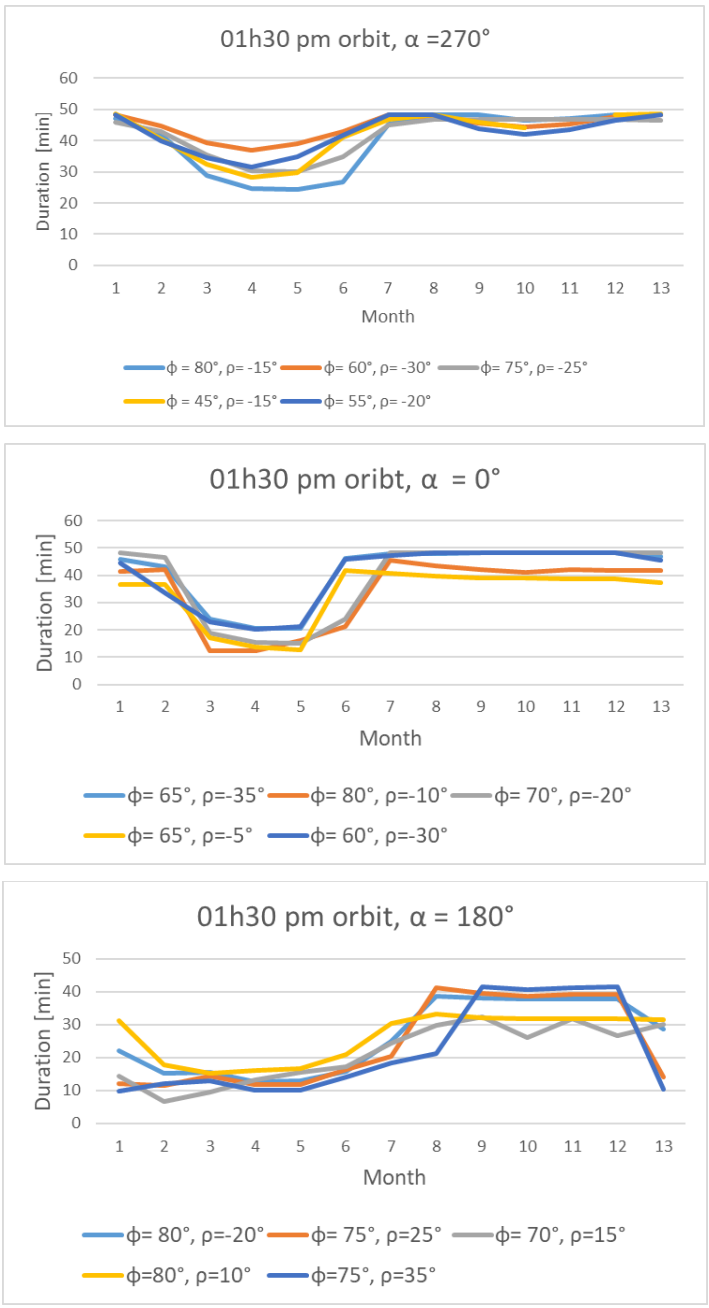

Figure 6.20: One-year evolution of acquisitions for α = 270° configuration 13h30 orbit.

6.5. Overall considerations

It was observed that performances of acquisitions along the four candidate orbits are not uncorrelated one another. In particular, lunar calibration legs on opposite orbits 10.30 am/pm share the same behaviour in terms of lunar phases: it was observed that for such cases the descending phase of the Moon allows for longer observations due to the angle that the MLTAN introduces between the orbit plane and the Earth-Sun direction. Similarly, orbits 01.30 am/pm offer better performances over the ascending phase. Concerning the temporal evolution of performances over different lunar months, it

was observed that acquisitions over orbits 10.30 pm and 01.30 pm are sensible to low relative elevations of the Moon, in correspondence of which visibility problems arise in proximity of the south pole. In a similar fashion acquisitions over orbits 10.30 am and 01.30 am are affected by high elevations of the Moon.

7. Conclusions

The aim of this work was to investigate the feasibility of guidance modes defined to perform lunar calibrations for MicroCarb mission. The four approach angle identified to satisfy mission requirements were identified and tested over a timespan of one year to analyse their performances over the calibration and validation phase of the mission. All the four candidate orbits were considered to ensure that feasibility could be granted for all cases.

7.1. Summary of the work done

Both radiometric and geometric calibration measurements are deemed to be feasible for the four candidate orbits considered. In particular:

- ACT acquisitions with an angle of approach of 270° allow to perform the geometric ACT calibration testing all the 6 values of MCV roll required;
- ALT acquisitions allow to perform both radiometric and geometric ALT calibrations; in particular, MCV positive values will be tested with an angle of approach of 180°, whereas negative values will be associated to an angle of approach of 0°;

FOV orientation	α	MCV roll angles to test	Calibration	Guidance Mode
ACT	90°	-	Geometric (ACT)	CAL_MOONGEAC
	270°	{-35°, -18°, -9°, 0°, 9°, 18°}		
ALT	0°	{-35°, -18°, -9°}	Radiometric Geometric (ALT)	CAL_MOONRADI CAL_MOONGEAL
	180°	{0°, 9°, 18°}		

Table 7.1: Summary of the configurations selected to perform geometric and radiometric calibrations.

It was observed that acquisitions along 10.30 am/pm orbits offer better performances the descending phase of the Moon, whereas the ascending phase is more suitable for 01.30 am/pm orbits. This is both due to the nodal lines orientations and slew feasibility. Particularly, optimal performances are limited to a specific portion of a lunar synodic month: the third quarter ($\varphi \epsilon$ [-90°, 0°]) for 10.30 am/pm orbits and the second quarter ($\varphi \epsilon$ [0°,90°]) for 01.30 am/pm orbits. These intervals correspond to one week, referred as “Moon Week”, that will be exploited for lunar calibrations.

Acquisitions performed along 10.30 am/pm and 01.30 am/pm orbits offer specular performances, due to the symmetrical orientation of the orbital planes as well as of the spacecraft attitude in Nadir mode. More specifically:

- Observations made on 10.30 am and 01.30 am orbits are degraded during periods of high relative elevation with respect to the orbit plane;
- Observations made on 10.30 pm and 01.30 pm are degraded during periods of low elevation with respect to the orbit plane;

It was also observed that the α =180° is the most critical configuration, since it is harder to avoid sensor dazzling phenomena. Also it appears to be the particularly sensible to variation in Moon relative elevation. This is why guidance legs corresponding to this case can only be performed at specific periods of the year.

7.2. Limitations

The main drawback of the obtained results is related to difficulties in the definition of simple criteria able to make reliable predictions on when optimal performances can be expected. This is due to the non-periodic evolution of the Earth-Sun-Moon system as well as the high sensibility of the sensors to dazzling. It must be considered in fact that the non-uniform rotation of the Earth around the Sun causes variations in the beta angle which in turn shift the actual projection of the Moon on the Ecliptic plane, for a given phase angle; also, the orbital plane of the Moon rotates with respect to the Ecliptic due to nodal regression. On the other hand, orbital plane of the spacecraft rotates with respect to the Ecliptic to be sun-synchronous. These three phenomena overlap and interact in a complex way, making hard to isolate the effect of a single phenomenon. For this reason, lunar guidance modes can be inserted in the mission planning by using the acquisition tables as ephemerides and manually select the optimal periods to perform lunar calibrations.

Other major limitations in the development of these analyses were due to temporal constraints imposed by academic deadlines for thesis submission, set more than one month before the end of the internship. This imposed an interruption of the scheduled activities to prepare the final report before the end of the internship. For this reason, part of the activities will be carried out at a later time and will not be included in this report.

7.3. Further developments

Thanks to the feasibility analysis conducted, lunar guidance modes can be inserted into the mission planning. In the context of MicroCarb Mission, this process relies on SIMONE, a software developed

by CNES to generate optimised schedules, in terms of guidance sequences, over a specified timespan – generally from 24h to one week.
Within this time window, for each guidance mode defined for the mission, the program generates a list of all the feasible legs that can be performed and sort them according to a priority code. Polaris algorithms are used to implement the legs. The priority level depends both on the type of guidance mode considered (calibration modes have in general a higher priority with respect to routine modes) and the performances related to the specific leg.

For lunar modes to be fully integrated in the mission planning, it is then necessary to provide criteria to determine their priority level with respect to the other guidance sequences, based on their performances. In particular, these criteria should take into account:

- the overall feasible duration provided by the leg concerned;
- the date: as it was seen, optimal performances are contained within one specific week for each lunar month, and in correspondence of specific periods of the year;
- the level of criticality of the associated configuration. For example, ALT acquisitions at 180° angle of approach can only be performed in a restricted window, so they have to be considered prioritary with respect to the other two configurations;
- the number of times the acquisition has already been done. For example, in routine phase, geometric ACT calibration has to be done once per year for each of the six selected MCV orientations: if one of this configuration have already been tested, there is no need to perform the same measurement again, so the corresponding leg will not be considered;

These task will be partially addressed in the last period of the internship, where further studies will be carried out outside the context of the present report.

8. Annexes

This section provides the acquisition tables of interest for the four candidate orbits.

8.1. 10.30 pm orbit

8.1.1. 10.30 pm, ACT 270° configuration

Table *8.1* and Table *8.2*shows the impact of slews over the overall feasibility of acquisition leg: in the first table the feasible duration do not take into account slew manoeuvres; in the second one, losses caused by slews are given. It can be observed that significant reductions of the acquisition intervals appear in proximity of the third quarter (φ=90°) for negative MCV rolls.

A best/worst case scenario for ACT acquisitions made at α =270° is given in Table *8.2* and Table *8.3*, respectively.

MCV/MOON	90	85	80	75	70	65	60	55	50	45	40	35	30	25	20	15	10	5	0	-5	-10	-15	-20	-25	-30	-35	-40	-45	-50	-55	-60	-65	-70	-75	-80	-85	-90
-35	34	33	33	32	31	30	29	27	26	25	24	23	22	21	21	20	19	16	17	23	24	26	27	28	29	31	32	34	35	36	38	45	46	47	47	48	21
-30	34	33	33	31	30	29	28	26	25	24	22	21	20	20	19	18	17	14	17	22	23	24	26	27	29	30	32	33	35	37	38	45	46	46	47	48	22
-25	34	33	32	31	29	28	26	24	23	22	20	19	18	18	17	16	15	14	16	21	22	23	24	26	27	29	31	33	35	37	39	44	45	46	47	48	23
-20	33	32	31	29	28	26	24	22	21	20	18	17	16	16	15	14	14	13	16	19	20	21	23	24	26	28	30	32	34	36	39	44	45	46	46	47	24
-15	33	31	30	28	26	24	22	20	18	17	16	15	15	14	13	13	13	11	15	18	18	19	20	22	24	26	29	31	33	36	38	43	44	45	46	47	24
-10	31	29	27	25	23	21	19	18	16	15	14	14	13	12	12	12	11	10	14	16	16	17	18	20	21	23	26	29	32	35	38	42	43	44	45	46	25
-5	29	27	25	23	20	18	17	15	14	13	13	12	11	11	11	11	10	0	0.4	1.6	14	15	16	17	19	21	24	26	29	33	36	40	42	43	44	45	25
0	26	24	22	20	18	16	15	14	13	12	11	11	10	10	10	9.8	0	0	0	0	0.4	13	14	15	16	18	21	23	26	30	34	38	40	42	43	44	25
5	23	21	19	17	15	14	13	12	11	11	10	9.9	9.6	9.4	9.2	0	0	0	0	0	0	0	12	13	14	16	18	20	23	27	31	35	37	39	41	42	24
10	20	18	17	15	14	13	12	11	10	9.9	9.5	9.2	9	8.8	0	0	0	0	0	0	0	0	0	12	13	14	16	17	20	23	27	30	34	36	38	40	23
15	18	16	15	14	13	12	11	10	9.8	9.4	9.1	8.9	8.7	0	0	0	0	0	0	0	0	0	0	0	12	13	14	15	17	20	23	26	29	32	35	37	21
20	16	15	14	13	12	11	11	10	9.6	9.3	9	8.8	0	0	0	0	0	0	0	0	0	0	0	0	0	12	13	14	16	18	20	23	25	28	31	34	18
25	15	14	13	12	12	11	10	10	9.6	9.3	8.9	0	0	0	0	0	0	0	0	0	0	0	0	0	0	0.5	12	13	15	17	18	20	22	24	27	30	15
30	14	14	13	12	12	11	11	10	9	0	0	0	0	0	0	0	0	0	0	0	0	0	0	0	0	0.5	1.7	2.8	14	16	17	18	20	22	24	27	12
35	14	13	13	12	12	11	9.6	9	0	0	0	0	0	0	0	0	0	0	0	0	0	0	0	0	0	0.7	1.8	2.8	3.9	16	17	18	19	20	22	24	9.3

Table 8.1: ACT acquisition table without accounting for slew feasibility for α = 270°, 10.30 pm orbit, , 1st month of the year.

MCV/MOON	90	85	80	75	70	65	60	55	50	45	40	35	30	25	20	15	10	5	0	-5	-10	-15	-20	-25	-30	-35	-40	-45	-50	-55	-60	-65	-70	-75	-80	-85	-90
-35	7.3	9	11	13	15	16	17	18	16	18	19	19	19	18	17	17	18	20	24	11	23	32	39	44	48	48	48	48	48	48	48	48	47	46	45	44	43
-30	11	13	15	17	18	20	16	14	16	16	17	17	16	16	15	15	16	18	23	13	12	22	33	48	48	48	48	48	48	48	48	48	46	46	45	45	44
-25	14	16	18	20	22	10	13	13	13	13	14	14	14	14	13	14	14	16	21	14	7.2	11	18	48	48	48	48	48	48	48	48	48	47	46	44	44	44
-20	18	20	22	24	8.7	8.3	7.6	8.1	9.3	11	12	12	12	12	12	12	13	15	19	17	8.9	7.3	8.4	14	48	48	48	48	48	48	48	48	47	47	46	43	43
-15	21	23	25	2.7	1.5	2.1	3.4	4.9	6.6	8.7	11	11	11	10	10	11	11	13	18	16	11	9.4	9.8	12	19	48	48	48	48	48	48	47	47	47	46	46	46
-10	23	22	3.6	3.7	0.9	0	0.3	1.8	3.5	5.3	7.2	9.6	9.4	9.4	9.5	9.7	10	12	16	15	14	12	11	13	16	22	34	45	47	47	47	47	47	47	47	47	46
-5	19	5.7	7.2	5.6	4.6	3.7	3.4	3.5	4	4.3	4.5	4.6	8.7	8.7	8.8	9	9.6	0	0.3	0	14	14	13	14	15	18	24	32	41	45	46	47	47	47	47	47	47
0	9.8	8.9	9	8.1	8	8.1	8.6	9.6	10	10	9.6	9.2	8.9	8.7	8.5	8.5	0	0	0	0	0	14	15	15	16	17	20	25	33	40	44	46	47	47	48	48	48
5	10	11	10	10	11	12	12	11	10	9.9	9.5	9.1	8.9	8.8	8.6	0	0	0	0	0	0	0	14	15	17	17	19	21	27	34	41	45	47	48	48	49	49
10	13	12	12	13	13	12	11	10	9.9	9.5	9.1	8.9	8.7	8.6	0	0	0	0	0	0	0	0	0	14	16	18	18	20	23	28	36	43	47	49	49	49	49
15	13	13	14	14	12	11	10	9.7	9.2	8.8	8.5	8.3	8.1	0	0	0	0	0	0	0	0	0	0	0	14	16	18	19	21	24	30	38	47	49	49	49	49
20	14	15	14	12	11	10	9.4	8.8	8.4	8	7.8	7.6	0	0	0	0	0	0	0	0	0	0	0	0	0	14	17	18	19	20	24	30	47	49	49	49	49
25	15	14	12	11	9.7	8.9	8.2	7.7	7.4	7.1	6.9	0	0	0	0	0	0	0	0	0	0	0	0	0	0	0	15	18	18	18	20	23	34	49	49	49	49
30	15	13	11	9.2	8.2	7.5	7	6.6	6.2	5.5	0	0	0	0	0	0	0	0	0	0	0	0	0	0	0	0	0	0	18	17	17	18	22	49	49	49	49
35	14	11	8.8	7.6	6.7	6.1	5.6	5.3	0	0	0	0	0	0	0	0	0	0	0	0	0	0	0	0	0	0	0	0	0	15	15	14	14	17	49	49	49

Table 8.2: ACT acquisition table for α = 270°, 10.30 pm orbit, , 7st month of the year.

MCV/MOON	90	85	80	75	70	65	60	55	50	45	40	35	30	25	20	15	10	5	0	-5	-10	-15	-20	-25	-30	-35	-40	-45	-50	-55	-60	-65	-70	-75	-80	-85	-90
-35	17.83	18.74	19.8	20.95	21.77	22.34	22.96	23.47	23.97	23.42	22.81	22.33	21.91	21.54	21.36	21.12	20.89	20.39	0	22.7	23.53	24.43	25.15	25.84	26.36	26.9	27.25	27.49	27.66	27.43	26.8	25.96	24.58	23.15	21.24	19.6	17.84
-30	17.22	18.31	19.55	19.9	20.57	21.16	21.5	22.05	22.44	21.98	21.3	20.78	20.32	20.1	19.72	19.47	19.23	18.7	0	21.67	22.52	23.33	24.17	24.99	25.64	26.35	26.83	27.4	27.55	27.43	26.93	26.18	24.9	23.55	21.72	20.13	18.27
-25	17.22	17.99	18.56	19.11	19.62	20.07	20.3	20.91	21.06	20.38	19.67	19.12	18.65	18.43	18.06	17.81	17.57	17.04	0	20.47	21.13	22.17	23.11	23.9	24.68	25.71	26.34	26.92	27.24	27.25	26.89	26.25	25.07	23.8	22.05	20.52	18.88
-20	16.62	17.21	17.94	18.34	18.7	19.2	19.68	20.06	19.34	18.64	17.93	17.4	17.11	16.74	16.4	16.17	15.96	15.45	0	19.09	19.72	20.61	21.61	22.68	23.58	24.61	25.4	26.17	26.67	26.83	26.63	26.11	25.06	23.88	22.22	20.75	19.01
-15	16.18	16.75	17.31	17.75	18.32	18.74	19.18	18.37	17.5	16.83	16.15	15.83	15.42	15.09	14.8	14.61	14.43	13.97	0	17.58	18.14	19.01	19.87	20.99	21.98	23.16	24.09	25.07	25.78	26.11	26.11	25.73	24.82	23.74	22.18	20.79	19.28
-10	15.85	16.58	16.99	17.51	18.03	18.26	17.38	16.45	15.64	15.03	14.59	14.16	13.81	13.54	13.3	13.15	13.02	12.63	0	16	16.3	17.1	18.09	19.22	20.07	21.35	22.4	23.56	24.49	25.01	25.23	25.02	24.29	23.34	21.91	20.6	19.18
-5	15.96	16.55	17.06	17.56	17.26	16.22	15.42	14.58	13.86	13.33	12.99	12.63	12.34	12.12	11.95	11.85	11.76	0	0	0.951	14.64	15.18	16.07	17.13	18.12	19.4	20.51	21.63	22.75	23.46	23.92	23.9	23.39	22.77	21.5	20.29	18.81
0	16.08	16.81	17.17	16.23	15.21	14.28	13.58	12.87	12.26	11.83	11.57	11.29	11.06	10.9	10.77	10.71	0	0	0	0	0.236	13.36	14.13	15.07	15.96	17.15	18.22	19.53	20.76	21.61	22.29	22.48	22.22	21.61	20.54	19.48	18.13
5	16.43	16.06	15.04	14.22	13.35	12.57	11.99	11.41	10.92	10.56	10.23	10	10	9.88	9.801	0	0	0	0	0	0	0	12.41	13.19	13.95	14.99	15.94	17.15	18.34	19.24	20.06	20.42	20.39	19.99	19.15	18.25	17.09
10	14.9	14.03	13.18	12.51	11.8	11.18	10.71	10.24	9.85	9.57	9.308	9.134	9.007	8.924	0	0	0	0	0	0	0	0	0	11.62	12.24	13.09	13.88	14.9	15.95	16.77	17.58	18.01	18.14	17.91	17.3	16.59	15.63
15	13.04	12.36	11.7	11.17	10.62	10.13	9.757	9.385	9.073	8.853	8.648	8.516	8.423	0	0	0	0	0	0	0	0	0	0	0	10.74	11.41	12.03	12.84	13.67	14.5	15.16	15.53	15.68	15.54	15.09	14.54	13.78
20	11.6	11.1	10.61	10.22	9.789	9.407	9.118	8.825	8.579	8.407	8.248	8.149	0	0	0	0	0	0	0	0	0	0	0	0	0	10.3	10.78	11.38	11.99	12.45	12.9	13.12	13.31	13.14	12.72	12.27	11.65
25	10.58	10.25	9.902	9.612	9.291	8.998	8.774	8.545	8.354	8.22	8.101	0	0	0	0	0	0	0	0	0	0	0	0	0	0	0.543	9.931	10.36	10.76	11.04	11.25	11.28	11.11	10.81	10.48	10	9.429
30	9.946	9.753	9.526	9.323	9.09	8.871	8.701	8.527	8.383	4.398	0	0	0	0	0	0	0	0	0	0	0	0	0	0	0	0	1.27	5.999	9.969	10.09	10.08	9.921	9.526	9.051	8.383	7.813	7.347
35	9.646	9.569	9.442	9.313	9.154	9	8.878	8.754	1.613	0.381	0	0	0	0	0	0	0	0	0	0	0	0	0	0	0	0	0.597	2.261	4.201	9.355	9.333	9.004	8.395	7.742	6.875	6.163	5.399

Table 8.3: ACT acquisition table for α = 270°, 10.30 pm orbit, , 12th month of the year.

8.1.2. 10.30 pm, ALT 0° configuration

A best/worst case scenario for ALT acquisitions made at α =0° is given in Table *8.4* Table *8.5*, respectively.

MCV/MOON	90	85	80	75	70	65	60	55	50	45	40	35	30	25	20	15	10	5	0	-5	-10	-15	-20	-25	-30	-35	-40	-45	-50	-55	-60	-65	-70	-75	-80	-85	-90
-35	1.1	3.9	7.11	10.3	13.4	16.1	18.6	20.9	23	24	23.2	22.2	21.5	21.1	20.4	20	19.1	16.8	15.6	22.3	24.6	26.4	27.9	29.8	32	34.6	38	41.8	43.3	44.7	46	47.2	48.1	48.1	48.1	48.1	46.3
-30	1.67	4.53	8.15	11.3	14.4	17.3	19.7	21.3	22.2	22.2	21.6	20.8	20.2	19.7	19.4	19.2	18.5	16.6	13.9	20.6	22.8	24.5	25.9	27.7	29.9	32.5	36.1	41.3	43.3	44.9	46.4	47.5	48.2	48.2	48.2	47.8	46.1
-25	2.25	5.36	8.73	12.1	15.1	17.9	19	20.1	21.2	20.7	20	19.4	18.9	18.6	18.4	18.1	17.8	16.3	12.4	19	21.1	22.7	24	25.7	28	30.6	34.1	39.4	43.3	45	46.6	47.9	48.3	48.3	48.2	47.5	45.8
-20	3.53	5.72	9.03	12.5	15.4	16.6	17.6	18.7	19.7	19.1	18.5	18	17.6	17.4	17.3	17.1	17	15.9	11.2	17.4	19.4	20.9	22.1	24	26	28.6	32.1	37.4	43.4	45.1	46.9	48.5	48.3	48.3	48.3	47.2	45.5
-15	3.18	5.94	9.54	12.2	13.4	14.8	16	17.2	18	17.4	17	16.6	16.3	16.1	16	16.1	16.1	15.3	10	15.8	17.9	19.2	20.5	22.1	24.1	26.6	30.2	35.5	43.4	45.3	47.2	48.4	48.4	47.7	46.9	45.9	45
-10	3.52	6.21	9.27	10.3	11.5	12.8	14.1	15.5	16.4	15.8	15.5	15.2	14.9	14.8	14.7	14.7	0.39	0	0	0.1	2.16	17.7	18.8	20.3	22.2	24.7	28.3	33.8	40.2	41.9	43.7	44.3	43.8	43.3	42.8	42.2	41.5
-5	3.73	6.35	7.22	8.22	9.39	10.7	12.2	13.5	14.8	14.3	1.1	0.48	0.09	0	0	0	0	0	0	0	0	1.08	2.05	3.07	4.41	5.94	7.58	26.5	33.3	35.7	38.1	38.7	38.7	38.5	38.5	38.1	37.8
0	3.99	4.73	5.05	0	0	0	0	0	0	0	0	0	0	0	0	0	0	0	0	0	0	0	0	1.23	2.33	3.63	5.36	6.84	9.12	12	15.1	15.8	16.2	16.9	31.6	32.4	32.8
5	0	0	0	0	0	0	0	0	0	0	0	0	0	0	0	0	0	0	0	0	0	0	0	0	0.14	1.38	2.89	4.7	6.95	9.95	13.4	13.8	14.5	15	15.6	16.2	16.9
10	0	0	0	0	0	0	0	0	0	0	0	0	0	0	0	0	0	0	0	0	0	0	0	0	0	0	0.79	2.4	4.82	8.23	11.5	12.1	12.7	13.5	14	14.8	15.7
15	0	0	0	0	0	0	0	0	0	0	0	0	0	0	0	0	0	0	0	0	0	0	0	0	0	0	0	0.1	2.69	6.74	9.71	10.3	11	12	12.7	13.7	14.7
20	0	0	0	0	0	0	0	0	0	0	0	0	0	0	0	0	0	0	0	0	0	0	0	0	0	0	0	0	0.9	6.11	7.93	8.63	9.66	10.6	11.6	12.6	13.8
25	0	0	0	0	0	0	0	0	0	0	0	0	0	0	0	0	0	0	0	0	0	0	0	0	0	0	0	0	0	5.35	6.37	7.16	8.16	9.39	10.4	11.7	13.1
30	0	0	0	0	0	0	0	0	0	0	0	0	0	0	0	0	0	0	0	0	0	0	0	0	0	0	0	0	0	3.77	4.72	5.77	6.9	8.13	9.44	11	12.5
35	0	0	0	0	0	0	0	0	0	0	0	0	0	0	0	0	0	0	0	0	0	0	0	0	0	0	0	0	0	2.1	3.14	4.29	5.57	7.15	8.65	10.3	12.3

Table 8.4: ALT acquisition table for α = 0°, 10.30 pm orbit, 7th month of the year.

MCV/MOON	90	85	80	75	70	65	60	55	50	45	40	35	30	25	20	15	10	5	0	-5	-10	-15	-20	-25	-30	-35	-40	-45	-50	-55	-60	-65	-70	-75	-80	-85	-90
-35	21	23	25	21	6.4	8.6	11	11	11	12	12	13	14	14	13	12	11	10	20	26	26	27	31	42	48	48	48	48	47	45	42	41	41	39	36	34	32
-30	25	26	17	8	11	13	13	14	14	15	16	15	15	14	13	13	12	8.9	18	24	25	25	26	30	39	48	48	48	48	46	43	41	40	38	36	33	31
-25	23	13	9.2	12	14	15	15	16	17	16	15	15	14	14	13	13	12	9.8	16	22	23	24	25	26	28	32	48	48	48	48	43	41	39	37	35	32	30
-20	7.7	10	13	15	16	17	18	17	16	15	15	14	14	14	13	13	12	10	15	20	21	22	23	24	24	25	27	48	48	48	42	38	36	35	33	30	28
-15	11	14	15	16	18	17	16	16	15	15	14	14	14	13	13	13	12	11	13	19	19	20	21	22	22	22	21	21	22	48	32	31	31	31	30	28	26
-10	14	15	17	18	17	16	15	15	14	14	14	13	13	13	13	13	0	0	0	1	0.4	18	19	20	20	19	17	15	12	9.1	16	21	24	25	26	25	23
-5	15	17	17	16	15	15	14	14	13	13	0	0	0	0	0	0	0	0	0	0	0	0	0	0	0	0	0	7.4	6	2.8	8.3	12	17	20	21	21	20
0	16	16	15	0	0	0	0	0	0	0	0	0	0	0	0	0	0	0	0	0	0	0	0	0	0	0	0	0	0	0	3.5	7.2	11	15	17	18	17
5	0	0	0	0	0	0	0	0	0	0	0	0	0	0	0	0	0	0	0	0	0	0	0	0	0	0	0	0	0	0	0.1	3.5	7.3	11	13	15	15
10	0	0	0	0	0	0	0	0	0	0	0	0	0	0	0	0	0	0	0	0	0	0	0	0	0	0	0	0	0	0	0	0.5	4.3	7.9	11	14	13
15	0	0	0	0	0	0	0	0	0	0	0	0	0	0	0	0	0	0	0	0	0	0	0	0	0	0	0	0	0	0	0	1.4	5.2	8.3	12	12	
20	0	0	0	0	0	0	0	0	0	0	0	0	0	0	0	0	0	0	0	0	0	0	0	0	0	0	0	0	0	0	0	0	2.4	5.9	10	12	
25	0	0	0	0	0	0	0	0	0	0	0	0	0	0	0	0	0	0	0	0	0	0	0	0	0	0	0	0	0	0	0	0	0	2.5	8.2	11	
30	0	0	0	0	0	0	0	0	0	0	0	0	0	0	0	0	0	0	0	0	0	0	0	0	0	0	0	0	0	0	0	0	0	0	4	10	
35	0	0	0	0	0	0	0	0	0	0	0	0	0	0	0	0	0	0	0	0	0	0	0	0	0	0	0	0	0	0	0	0	0	0	0	0	

Table 8.5: ALT acquisition table for α = 0°, 10.30 pm orbit, 11th month of the year.

8.1.3. 10.30 pm, ALT 180° configuration

A best/worst case scenario for ALT acquisitions made at α =180° is given in Table *8.6* and Table *8.7*, respectively.

MCV/MOON	90	85	80	75	70	65	60	55	50	45	40	35	30	25	20	15	10	5	0	-5	-10	-15	-20	-25	-30	-35	-40	-45	-50	-55	-60	-65	-70	-75	-80	-85	-90
-35	0	0	0	0.391	4.459	4.419	4.454	4.683	4.801	5.126	5.335	5.759	17.22	17.53	18.04	17.22	11.59	8.24	25.97	22.35	20.74	20.1	20.1	20.55	21.15	3.941	3.877	2.69	1.399	0.902	0.201	0	0	0	0	0	0
-30	0	0	0	0	2.239	4.604	4.559	4.696	4.736	4.8	4.91	5.229	5.411	17.11	17.33	17.58	13.92	1.663	24.21	21.9	20.52	20.27	20.31	20.94	4.097	4.468	4.875	4.284	3.305	2.731	2.092	1.496	1.224	1.034	0	0	0
-25	0	0	0	0	0	3.633	4.677	4.561	4.527	4.506	4.529	4.591	4.693	4.796	16.75	16.78	16.24	4.806	22.29	21.27	20.31	20.12	20.53	4.008	4.323	4.869	5.594	5.727	5.073	4.438	4.05	3.528	3.135	3.144	0	0	0
-20	0	0	0	0	0	1.331	3.968	4.27	4.004	3.907	3.856	3.843	3.879	3.905	3.907	16.12	15.56	7.998	19.95	20.43	19.76	19.96	3.509	3.914	4.389	5.291	6.016	7.137	6.555	6.204	5.747	5.318	5.155	5.215	0	0	0
-15	0	0	0	0	0	0	1.919	3.817	3.66	3.333	3.22	2.979	2.963	2.93	2.714	2.551	1.732	0	17.53	17.2	2.249	2.474	3.015	3.617	4.428	5.536	6.448	7.968	7.933	7.703	7.521	7.2	7.114	7.238	0	0	0
-10	0	0	0	0	0	0	0.516	2.857	2.988	2.612	2.45	2.163	1.941	1.864	1.611	1.44	0.73	0	0	1.008	1.07	1.52	2.272	3.073	4.061	5.393	6.681	8.467	9.384	9.112	9.043	9.005	9.174	9.206	1.267	0	0
-5	0	0	0	0	0	0	0	1.546	2.148	1.738	1.378	1.226	0.976	0.87	0.427	0.09	0	0	0	0	0	0.291	1.236	2.56	3.726	5.294	6.816	8.747	10.58	10.6	10.65	10.73	11	11.11	3.078	0	0
0	0	0	0	0	0	0	0	0.548	1.138	0.881	0.506	0.17	0	0	0	0	0	0	0	0	0	0	0.038	1.354	2.68	4.482	6.256	8.718	11.26	11.85	12.01	12.22	12.58	12.95	4.827	0.234	0
5	6.456	0	0	0	0	0	0	0	0.134	0	0	0	0	0	0	0	0	0	0	0	0	0	0	0	1.18	3.344	5.364	8.068	11.29	13.01	13.29	13.96	14.26	14.71	6.505	1.984	8.539
10	7.307	6.522	6.559	6.949	0	0	0	0	0	0	0	0	0	0	0	0	0	0	0	0	0	0	0	0	0	1.608	3.636	7.069	10.91	14.19	14.66	15.46	16.02	24.46	12.89	12.4	12.42
15	7.73	6.796	6.643	6.989	7.518	0	0	0	0	0	0	0	0	0	0	0	0	0	0	0	0	0	0	0	0	0	1.452	4.934	9.233	13.93	15.95	16.88	34.01	37.58	15.43	14.66	14.43
20	8.384	7.462	7.2	7.387	7.74	0	0	0	0	0	0	0	0	0	0	0	0	0	0	0	0	0	0	0	0	0	0	1.52	6.184	11.84	17.16	18.21	38.39	40.55	16.98	16.17	14.61
25	9.292	8.11	7.762	7.801	7.651	0	0	0	0	0	0	0	0	0	0	0	0	0	0	0	0	0	0	0	0	0	0	0	1.51	7.259	15.8	32.55	40.93	42.93	18.02	16.85	13.83
30	10.16	8.659	7.519	6.714	6.032	0.865	0	0	0	0	0	0	0	0	0	0	0	0	0	0	0	0	0	0	0	0	0	0	0	0.223	7.548	37.98	42.8	44.97	19.02	16.99	13.39
35	8.876	6.929	5.926	5.225	4.634	0	0	0	0	0	0	0	0	0	0	0	0	0	0	0	0	0	0	0	0	0	0	0	0	0	0	20.28	44.18	46.51	19.62	17.78	13.61

Table 8.6: ALT acquisition table for α =180°, 10.30 pm orbit, 8th month of the year.

MCV/MOON	90	85	80	75	70	65	60	55	50	45	40	35	30	25	20	15	10	5	0	-5	-10	-15	-20	-25	-30	-35	-40	-45	-50	-55	-60	-65	-70	-75	-80	-85	-90
-35	0	0	0	0	0	0	0	0.36	0.94	1.46	1.98	3.13	21.5	21.7	21.8	22.1	22.4	22	11.5	17.3	20.2	21.7	23	24.6	26.3	5.29	5.04	5.02	5.12	5.41	5.79	6.35	7	6.55	5.9	5.28	4.8
-30	0	0	0	0	0	0	0	0	0.02	0.45	1.22	1.77	9.08	20.5	20.5	20.7	20.9	20.4	10.2	17.2	19.9	21.3	22.8	24.3	14.5	4.99	5.02	5.13	5.41	5.91	6.57	7.52	8.32	7.72	7.16	6.64	6.4
-25	0	0	0	0	0	0	0	0	0	0	0.01	0.48	1.19	2.85	19.2	19.2	19.4	18.8	9.06	16.9	19.3	20.7	22.2	12.8	4.42	4.49	4.62	4.87	5.53	6.27	7.32	8.81	9.45	8.96	8.51	8.09	7.95
-20	0	0	0	0	0	0	0	0	0	0	0	0	0	0.04	0.77	17.9	17.9	17.2	4.81	16.6	18.7	20.1	3.43	3.55	3.56	3.71	4.11	4.48	5.36	6.22	7.79	10.3	10.6	10.3	9.94	9.81	9.59
-15	0	0	0	0	0	0	0	0	0	0	0	0	0	0	0	0	0.08	15.7	3.38	16	2.23	2.17	2.25	2.37	2.39	2.74	3.03	3.67	4.75	5.93	8.22	12.2	11.9	11.7	11.6	11.5	11.5
-10	0	0	0	0	0	0	0	0	0	0	0	0	0	0	0	0	0	0	0	0.15	0.77	0.96	0.81	0.88	1.02	1.16	1.59	2.23	3.4	4.85	8.28	13.4	13.4	13.3	13.4	13.4	13.5
-5	0	0	0	0	0	0	0	0	0	0	0	0	0	0	0	0	0	0	0	0	0	0	0	0	0	0	0	0	0.92	2.23	6.43	14.8	15	15.2	15.3	15.6	15.8
0	0	0	0	0	0	0	0	0	0	0	0	0	0	0	0	0	0	0	0	0	0	0	0	0	0	0	0	0	0	0	0	16.4	16.7	17.1	17.6	18	18.5
5	14.7	0	0	0	0	0	0	0	0	0	0	0	0	0	0	0	0	0	0	0	0	0	0	0	0	0	0	0	0	0	0	7.72	15.4	19.4	20.1	23.2	25.2
10	14.9	17.2	17.1	0	0	0	0	0	0	0	0	0	0	0	0	0	0	0	0	0	0	0	0	0	0	0	0	0	0	0	0	6.07	11.7	16.5	20	22.5	22.4
15	13	15.8	15	13.3	9.04	0	0	0	0	0	0	0	0	0	0	0	0	0	0	0	0	0	0	0	0	0	0	0	0	0	0.53	5.92	10.2	14.9	18.6	21.5	19.5
20	11.9	14.8	13.4	11.9	10.8	0	0	0	0	0	0	0	0	0	0	0	0	0	0	0	0	0	0	0	0	0	0	0	0	0	0	1.35	6.08	9.89	14.2	17.9	20.5	16.8
25	11.5	14.3	12.4	10.9	9.88	0	0	0	0	0	0	0	0	0	0	0	0	0	0	0	0	0	0	0	0	0	0	0	0	0	0	2.18	6.56	10.2	14	17.6	17.9	14.3
30	11.9	13.8	11.9	10.3	9.27	0	0	0	0	0	0	0	0	0	0	0	0	0	0	0	0	0	0	0	0	0	0	0	0	0	0	3.15	7.35	10.8	14.4	17.6	15.4	11.9
35	12.7	13.7	11.7	10	8.97	0	0	0	0	0	0	0	0	0	0	0	0	0	0	0	0	0	0	0	0	0	0	0	0	0	0	4.43	8.5	11.6	15	17.9	13.1	9.51

Table 8.7: ALT acquisition table for α = 180°, 10.30 pm orbit, 12th month of the year.

8.2. 10.30 am orbit

8.2.1. 10.30 am orbit, ACT 270° configuration

A best/worst case scenario for ACT acquisitions made at α =270° is given in Table *8.8* and Table *8.9*, respectively.

MCV/MOON	90	85	80	75	70	65	60	55	50	45	40	35	30	25	20	15	10	5	0	-5	-10	-15	-20	-25	-30	-35	-40	-45	-50	-55	-60	-65	-70	-75	-80	-85	-90
-35	8.44	10.9	13.5	15.5	17.5	19.4	21.6	20	15.1	15.4	17.8	19.3	19.7	18.9	18.4	18.3	18.9	20.7	23.2	19.4	11.4	20.8	48.2	48.2	48.1	48.1	48.1	48.1	48.1	48.1	47.7	47.9	47.1	46.3	45.4	44.4	43.5
-30	10.6	13.2	16	18.2	20.3	22.5	19.9	11.1	13.4	15.7	16.4	17.5	17	16.4	16.2	16.3	17	19.1	21.7	20.2	12.5	10.6	18.9	48.1	48.1	48.1	48.1	48.1	48.1	48.1	48.1	46.5	46.1	46	45.5	44.7	44
-25	12.6	15.4	18.4	21	23.2	25.7	9.05	11.5	11.5	12.5	13.7	15.2	14.5	14.2	14.2	14.5	15.3	17.4	20.2	19	14.1	10.7	11.2	17.9	48.2	48.2	48.2	48.2	48.2	48.2	48	47.3	46.8	44.5	44.4	44.2	44.1
-20	14.7	17.6	20.7	23.4	25.9	5.97	5.13	5.99	7.48	9.52	11.4	12.9	12.5	12.3	12.4	12.8	13.7	15.8	18.7	17.8	16.1	12.4	11.9	14.2	21.7	48.2	48.2	48.2	48.2	48.2	47.5	47.1	46.6	46.3	45.9	42.9	43
-15	16.5	19.6	23.1	17.5	5.68	0.56	0	2.3	4.63	7.39	9.73	11.1	10.9	10.8	11	11.4	12.2	14.3	17.2	16.7	16	14.4	13.2	14.1	17.2	22.8	34	44.8	46.1	46.5	46.7	46.5	46.4	46.3	46.1	45.8	45.5
-10	18.3	21.4	15.6	7.85	5.96	3.25	1.12	0	1.24	3.77	6.25	9.05	9.68	9.69	9.85	10.3	11	12.9	15.7	15.6	15.1	15.4	14.9	14.9	16.4	19.1	24.7	32.9	40.5	43.7	45.1	45.7	46.1	46.3	46.3	46.2	46.1
-5	20.1	17.7	9.73	9.73	7.33	5.93	4.92	4.32	3.96	3.8	3.63	3.3	8.87	8.89	9.04	9.4	10	0	0.8	3.01	14.2	14.5	15.5	16.2	16.7	18.1	21.3	26.4	33.4	38.9	42.8	44.6	45.7	46.2	46.6	46.6	46.7
0	18.9	10.8	12.1	10.1	9.09	8.77	8.82	9.14	9.91	10.7	10.2	9.61	9.17	8.8	8.51	8.8	0	0	0	0	0	13.6	14.4	15.8	17.6	18.2	19.7	22.9	28.2	33.5	39.5	42.9	45.1	46.2	46.9	47.2	47.5
5	13.7	12.7	12.3	11.4	11.1	11.3	12.2	12	11.2	10.5	10	9.54	9.18	8.93	8.69	0	0	0	0	0	0	0	13.2	14.3	15.9	17.8	19.4	21.2	24.7	28.9	35.1	40.2	44.2	46.1	47.3	48	48.3
10	13.1	14.3	13.1	12.9	13.3	13.3	12	11.2	10.5	9.87	9.45	9.08	8.97	8.79	0	0	0	0	0	0	0	0	0	13	14.4	16	18.7	20.3	22.5	25.3	30.5	36.3	42.5	45.9	48	48.5	48.5
15	14.7	14.3	14.1	14.6	13.3	12.1	11	10.3	9.73	9.22	8.88	8.58	8.38	0	0	0	0	0	0	0	0	0	0	0	12.7	14.1	16.4	20.1	21.1	22.8	26.4	31.4	39.5	45.6	48.6	48.6	48.6
20	14.8	14.7	15	13.2	11.8	10.8	9.89	9.3	8.83	8.41	8.13	7.9	0	0	0	0	0	0	0	0	0	0	0	0	0	12.4	14.4	17.7	20.3	21	23.1	26.6	34.2	44.7	48.6	48.6	48.6
25	14.7	15.3	13	11.4	10.3	9.44	8.68	8.18	7.79	7.44	7.23	0	0	0	0	0	0	0	0	0	0	0	0	0	0	0	12.5	15.4	19.7	19.8	20.5	22.3	27.4	39.6	48.7	48.7	48.7
30	14.9	13.7	11.1	9.7	8.73	8.01	7.37	6.96	6.63	0	0	0	0	0	0	0	0	0	0	0	0	0	0	0	0	0	1.92	19.5	18.8	18.6	19	21	26.5	48.7	48.7	48.7	48.7
35	15.3	11.4	9.12	7.95	7.13	6.51	5.98	5.63	0	0	0	0	0	0	0	0	0	0	0	0	0	0	0	0	0	0	0	0	0	0	0	18.1	17	16.3	16.3	17.1	48.8	48.8	48.8

Table 8.8: ACT acquisition table for α = 270°, 10.30 am orbit, , 8st month of the year.

MCV/MOON	90	85	80	75	70	65	60	55	50	45	40	35	30	25	20	15	10	5	0	-5	-10	-15	-20	-25	-30	-35	-40	-45	-50	-55	-60	-65	-70	-75	-80	-85	-90
-35	16.6	19.5	22.1	24	20.5	7.93	8.67	5.5	3.19	1.89	1.33	1.42	2.07	3.67	6.02	9.83	12.7	15.7	21	23.2	18.8	17.1	48	48	43.4	41	40.4	40	40	39.7	39.3	39.1	37.6	36	34.1	31.9	29.9
-30	17.9	20.7	22.4	18.5	10.8	11.3	9.83	8.11	6.89	6.46	6.38	7.09	8.21	10.4	11.8	12.2	13.1	15.7	20.1	19.5	11.5	8.25	16.1	24.9	30	33.3	35.3	36.6	37.4	37.8	38.1	37.3	35.5	33.6	31.8	29.8	27.9
-25	18.9	21.5	17.7	13.5	14	13.5	11.9	10.8	10.4	10.5	11.3	12.5	12.5	12.2	12.2	12.5	13.3	15.5	19.3	16	6.07	10.2	15.5	21.2	25.4	28.9	31.6	33.8	35.1	36.1	35.4	34.5	33	31.2	29.6	27.7	26
-20	19.1	18.4	15.4	16.2	16.1	15	14	13.8	13.8	14.3	13.5	12.9	12.6	12.4	12.4	12.6	13.3	15.2	18.2	12.6	6.53	12.2	16.2	20.3	23.7	26.6	29.1	31.5	32.4	32.7	32.5	31.8	30.5	29	27.5	25.7	24.1
-15	19.4	16.8	17.6	18.3	17.1	16.8	16.4	15.6	14.6	13.9	13.2	12.7	12.5	12.3	12.3	12.5	13.1	14.7	17.1	9.96	9.65	14.4	17.5	20.3	22.5	24.4	26.3	27.9	29	29.6	29.6	29.1	28.1	26.8	25.4	23.8	22.3
-10	17.6	18.5	19.5	19.2	17.9	16.7	15.6	14.8	13.9	13.3	12.8	12.4	12.2	12.1	12.1	12.3	12.8	14.1	15.8	9.64	13.1	15	16.6	18.6	20.1	21.8	23.4	24.9	26	26.7	26.9	26.6	25.8	24.6	23.4	21.9	20.5
-5	18.6	19.2	18.9	17.6	16.3	15.3	14.3	13.8	13.1	12.6	12.2	11.9	11.7	11.6	11.7	11.8	12.3	0.08	0.16	0	12.8	14.2	15.5	17	18.2	19.6	20.9	22.4	23.2	24.1	24.4	24.2	23.6	22.5	21.5	20.1	18.8
0	17.5	18.2	16.9	15.9	14.8	14	13.2	12.6	12.1	11.8	11.5	11.2	11.1	11	11.1	11.2	0	0	0	0	0	13.3	14.1	15.3	16.4	17.5	18.7	19.9	20.7	21.5	21.9	21.8	21.4	20.5	19.6	18.4	17.2
5	16.1	16.1	15	14.2	13.3	12.6	12	11.5	11.1	10.8	10.5	10.3	10.2	10.3	10.3	0	0	0	0	0	0	0	12.9	13.8	14.7	15.6	16.6	17.7	18.5	19.1	19.5	19.6	19.2	18.5	17.7	16.7	15.6
10	14.6	14.1	13.2	12.5	11.8	11.3	10.7	10.3	9.97	9.72	9.49	9.34	9.26	9.22	0	0	0	0	0	0	0	0	0	12.2	12.9	13.6	14.4	15.3	16.2	16.8	17.2	17.3	17.1	16.6	15.9	15.1	14.2
15	13	12.2	11.4	10.8	10.3	9.82	9.39	9.08	8.78	8.58	8.4	8.27	8.2	0	0	0	0	0	0	0	0	0	0	0	11.2	11.8	12.5	13.2	13.9	14.6	15.1	15.2	15.2	14.6	14.2	13.5	12.8
20	10.9	10.3	9.64	9.18	8.7	8.35	8	7.75	7.51	7.35	7.2	7.09	0	0	0	0	0	0	0	0	0	0	0	0	0	10	10.5	11.2	11.7	12.4	12.8	13	13	12.9	12.6	12	11.5
25	8.9	8.34	7.85	7.49	7.11	6.83	6.55	6.36	6.16	6.03	5.9	0	0	0	0	0	0	0	0	0	0	0	0	0	0	0	8.63	9.11	9.52	10.1	10.5	10.7	10.9	10.9	10.8	10.7	10.3
30	6.83	6.42	6.05	5.77	5.48	5.27	5.06	4.9	4.75	4.64	0	0	0	0	0	0	0	0	0	0	0	0	0	0	0	0	0	7.05	7.35	7.86	8.17	8.4	8.64	8.86	9.04	9.22	9.33
35	4.74	4.47	4.21	4.03	3.82	3.67	3.52	3.4	0	0	0	0	0	0	0	0	0	0	0	0	0	0	0	0	0	0	0	0	0	5.36	5.74	5.95	6.26	6.69	7.17	7.8	8.39

Table 8.9: ACT acquisition table for α = 270°, 10.30 am orbit, , 5st month of the year.

8.2.2. 10.30 am, ALT 0° configuration

A best/worst case scenario for ALT acquisitions made at α =0° is given in Table *8.10* and Table *8.11*, respectively.

MCV/MOON	90	85	80	75	70	65	60	55	50	45	40	35	30	25	20	15	10	5	0	-5	-10	-15	-20	-25	-30	-35	-40	-45	-50	-55	-60	-65	-70	-75	-80	-85	-90
-35	5.067	7.577	9.847	12.99	15.87	18.82	20.76	22.8	24.36	23.58	22.7	21.99	21.38	21.23	21.13	21.3	21.9	23.75	23.53	26.21	30.38	32.25	34.28	37.21	39.33	40.8	42.61	43.73	45.31	46.4	47.64	48.21	48.21	48.21	48.37	47.18	27.38
-30	5.985	8.406	10.51	14.51	16.64	19.89	21.8	23.02	23.07	21.96	21.22	20.64	20.16	20.11	20.08	20.3	20.88	22.22	17.83	25.15	27.68	29.48	31.55	34.4	37.22	40.03	42.04	43.34	45.15	46.42	47.84	48.27	48.27	48.27	48.15	46.87	28.03
-25	6.727	9.125	11.39	15.28	17.52	20.75	21.29	22.01	21.36	20.4	19.77	19.3	18.92	18.77	18.97	19.2	19.74	20.67	12.49	22.91	25.27	27	29.03	31.7	34.57	38.26	41.46	42.93	44.96	46.43	48.06	48.32	48.33	48.33	47.86	46.53	28.57
-20	7.63	9.857	12.66	15.81	18.68	19.39	19.89	20.58	19.7	18.87	18.33	17.94	17.64	17.55	17.61	17.84	18.31	18.96	7.869	20.94	23	24.6	26.52	29.28	32.14	35.88	40.86	42.47	44.75	46.42	48.3	48.37	48.38	48.38	47.52	46.12	28.96
-15	8.361	10.45	13.49	16.26	17.26	17.94	18.55	18.87	18.09	17.35	16.89	16.56	16.32	16.26	16.34	16.56	16.94	17.13	3.652	19.21	20.94	22.54	24.17	26.8	29.61	33.36	40.25	42.14	44.49	46.41	48.41	48.42	48.42	48.42	47.1	45.6	29.17
-10	8.899	11.06	14.22	14.62	15.59	16.24	16.95	17.21	16.51	15.85	15.45	15.16	14.96	14.92	14.99	15.18	2.47	1.501	0	0.635	1.856	20.46	22.11	24.44	27.16	30.87	39.29	41.26	43.68	45.55	47.29	46.96	46.46	46.1	45.72	44.92	29.13
-5	9.271	11.54	13.33	12.72	13.66	14.43	15.07	15.59	14.95	14.36	0.834	0.536	0.44	0.239	0.245	0.282	0.3	0	0	0	0	0.293	1.15	2.555	3.815	5.492	7.731	29.14	36.47	39.35	41.66	41.66	41.5	41.48	41.29	41.31	27.28
0	9.779	12.2	11.33	0	0	0	0	0	0	0	0	0	0	0	0	0	0	0	0	0	0	0	0	0	0.985	2.548	4.661	7.096	10.35	13.51	15.96	16.17	16.54	17	34.52	35.49	23
5	0	0	0	0	0	0	0	0	0	0	0	0	0	0	0	0	0	0	0	0	0	0	0	0	0	0	1.595	3.838	7.548	11.38	13.9	14.41	14.74	15.41	15.73	16.21	4.168
10	0	0	0	0	0	0	0	0	0	0	0	0	0	0	0	0	0	0	0	0	0	0	0	0	0	0	0.563	4.306	9.208	12.04	12.67	13.14	13.95	14.59	15.06	3.668
15	0	0	0	0	0	0	0	0	0	0	0	0	0	0	0	0	0	0	0	0	0	0	0	0	0	0	0	1.071	7.093	10.2	10.96	11.59	12.55	13.35	13.98	3.168
20	0	0	0	0	0	0	0	0	0	0	0	0	0	0	0	0	0	0	0	0	0	0	0	0	0	0	0	0	4.589	8.559	9.301	10.24	11.21	12.18	13.15	2.835
25	0	0	0	0	0	0	0	0	0	0	0	0	0	0	0	0	0	0	0	0	0	0	0	0	0	0	0	0	0	6.791	7.849	9.124	10.1	11.27	12.43	2.335
30	0	0	0	0	0	0	0	0	0	0	0	0	0	0	0	0	0	0	0	0	0	0	0	0	0	0	0	0	0	1.164	5.236	6.451	7.743	9.091	10.47	11.86	2.002
35	0	0	0	0	0	0	0	0	0	0	0	0	0	0	0	0	0	0	0	0	0	0	0	0	0	0	0	0	0	1.688	3.735	4.957	6.621	8.203	9.672	11.32	1.502

Table 8.10: ALT acquisition table for α = 0°, 10.30 am orbit, 2nd month of the year.

MCV/MOON	90	85	80	75	70	65	60	55	50	45	40	35	30	25	20	15	10	5	0	-5	-10	-15	-20	-25	-30	-35	-40	-45	-50	-55	-60	-65	-70	-75	-80	-85	-90
-35	16	18	20	21	22	23	23	23	23	22	22	22	22	22	22	22	22	22	0	22	22	23	23	24	24	24	25	25	25	25	24	24	23	21	19	17	15
-30	13	15	17	18	20	21	22	21	21	21	21	21	20	20	20	20	20	21	0	20	21	21	21	22	22	23	23	23	23	23	23	22	21	20	18	16	14
-25	9.1	12	14	16	17	19	20	20	19	19	19	19	19	19	19	19	19	19	0	19	19	19	20	20	21	21	21	21	22	22	21	21	20	18	17	15	12
-20	4.9	7.9	10	12	14	16	18	18	18	18	17	17	17	17	17	17	18	18	0	17	18	18	18	19	19	19	20	20	20	20	20	20	19	17	16	13	13
-15	0	3.7	6.2	8.8	11	13	15	17	16	16	16	16	16	16	16	16	16	16	0	15	16	16	17	17	17	18	18	18	19	19	19	18	18	16	14	12	13
-10	0	0	2.1	5.1	7.6	9.7	12	14	15	15	14	14	14	14	14	14	2	1	0	0.3	1.9	15	15	16	16	16	17	17	18	18	18	17	17	15	13	9.9	10
-5	0	0	0	0.8	3.6	5.8	8.3	11	13	13	5.2	4.2	3.2	2.3	1.6	0.9	0	0	0	0	0	0.9	2	3.1	4.5	5.9	7.2	16	16	17	17	17	16	14	11	8.6	7.4
0	0	0	0	0	0	0	0	0.7	2.1	3.5	3.1	2.2	1.4	0.4	0	0	0	0	0	0	0	0	0.2	1.3	2.9	4.1	5.6	6.9	8.5	10	12	14	15	12	10	7.4	5.1
5	0	0	0	0	0	0	0	0	0	0	0.3	0.5	0	0	0	0	0	0	0	0	0	0	0	0	1.3	2.5	4	5.5	7.1	9.1	11	12	13	11	8.9	6.3	4.2
10	0	0	0	0	0	0	0	0	0	0	0	0	0	0	0	0	0	0	0	0	0	0	0	0	0	1.1	2.6	4.2	6	7.9	9.7	10	11	10	7.9	5.4	3.4
15	0	0	0	0	0	0	0	0	0	0	0	0	0	0	0	0	0	0	0	0	0	0	0	0	0	0	1.4	3	5.1	7.1	7.9	8.5	9.2	9	7	4.7	2.7
20	0	0	0	0	0	0	0	0	0	0	0	0	0	0	0	0	0	0	0	0	0	0	0	0	0	0	0.7	2.4	4.6	5.4	6.3	6.9	7.9	8.1	6.2	4	2.2
25	0	0	0	0	0	0	0	0	0	0	0	0	0	0	0	0	0	0	0	0	0	0	0	0	0	0	0.1	2.2	3	3.9	4.7	5.6	6.5	7.4	5.6	3.6	1.8
30	0	0	0	0	0	0	0	0	0	0	0	0	0	0	0	0	0	0	0	0	0	0	0	0	0	0	0	0.5	1.6	2.5	3.5	4.3	5.5	6.6	5.1	3.2	1.6
35	0	0	0	0	0	0	0	0	0	0	0	0	0	0	0	0	0	0	0	0	0	0	0	0	0	0	0	0	0.2	1.3	2.5	3.3	4.6	6	4.8	3	1.5

Table 8.11: ALT acquisition table for α = 0°, 10.30 am orbit, 5th month of the year.

8.2.3. 10.30 am, ALT 180° configuration

A best/worst case scenario for ALT acquisitions made at α =180° is given in Table *8.12* and Table *8.13*, respectively.

MCV/MOON	90	85	80	75	70	65	60	55	50	45	40	35	30	25	20	15	10	5	0	-5	-10	-15	-20	-25	-30	-35	-40	-45	-50	-55	-60	-65	-70	-75	-80	-85	-90
-35	0	0	0	0	0	3	4.1	4.1	4.3	4.4	4.7	5.1	19	20	20	21	22	23	17	0.7	13	15	16	17	18	3.6	4.1	4.4	3.5	3	2.7	2.3	1.9	1.6	1.4	1.2	1.1
-30	0	0	0	0	0	0	3.3	4	4.1	4.1	4.2	4.4	4.7	19	19	20	21	22	16	11	14	15	16	18	3.8	4.1	4.9	5.3	5	4.8	4.4	4	3.7	3.5	3.3	3.2	3.1
-25	0	0	0	0	0	0	0.4	3.5	3.7	3.6	3.5	3.6	3.7	4.1	18	19	19	20	14	11	14	16	17	3.2	3.8	4.7	5.5	6.1	6.6	6.3	5.9	5.8	5.5	5.3	5.3	5.2	3.7
-20	0	0	0	0	0	0	0	1.2	3.2	3	2.9	2.8	2.7	2.8	3	18	18	19	14	12	14	16	2.7	3.1	4.2	4.9	6	6.9	7.9	7.7	7.6	7.3	7.3	7.2	7.2	7.1	3.9
-15	0	0	0	0	0	0	0	0	2.1	2.3	1.9	1.8	1.6	1.6	1.6	1.6	1.8	17	14	3.5	0.2	1.5	2.3	3.1	4.1	5.1	6.3	7.4	8.6	9	9	9	8.9	9	9.1	9.1	4.2
-10	0	0	0	0	0	0	0	0	0.4	1.3	1	0.6	0.3	0.2	0.2	0.3	0.1	0	0	0	0	1	2	2.8	3.9	5	6.4	7.7	9.2	10	11	10	11	11	11	11	4.4
-5	0	0	0	0	0	0	0	0	0	0.3	0	0	0	0	0	0	0	0	0	0	0	0.4	1.2	2.1	3.3	4.5	6.1	7.7	9.5	12	12	12	12	13	13	13	4.5
0	0	0	0	0	0	0	0	0	0	0	0	0	0	0	0	0	0	0	0	0	0	0	0.2	1.3	2.6	4	5.7	7.4	9.5	12	13	13	14	14	15	15	4.9
5	5.9	0.2	0	0	0	0	0	0	0	0	0	0	0	0	0	0	0	0	0	0	0	0	0	0.1	1.4	2.7	4.6	6.5	9	12	14	15	16	16	17	19	16
10	6.8	5.9	5.9	1.2	0	0	0	0	0	0	0	0	0	0	0	0	0	0	0	0	0	0	0	0	0	0.9	2.9	5	7.7	12	16	16	17	28	32	33	19
15	7.8	6.8	6.7	7	7.3	0	0	0	0	0	0	0	0	0	0	0	0	0	0	0	0	0	0	0	0	0	0.6	2.5	5.5	10	17	18	30	34	35	36	21
20	15	7.6	7.3	7.6	7.9	0	0	0	0	0	0	0	0	0	0	0	0	0	0	0	0	0	0	0	0	0	0	0	1.6	6.3	14	19	35	37	38	39	22
25	9.6	8.6	8	8.2	8.3	3.1	0	0	0	0	0	0	0	0	0	0	0	0	0	0	0	0	0	0	0	0	0	0	0	0.2	5.1	31	37	39	40	40	19
30	10	9.3	8.5	7.4	6.7	6	0	0	0	0	0	0	0	0	0	0	0	0	0	0	0	0	0	0	0	0	0	0	0	0	0	14	39	41	43	38	16
35	10	8.2	6.8	5.8	5.3	0	0	0	0	0	0	0	0	0	0	0	0	0	0	0	0	0	0	0	0	0	0	0	0	0	1.5	9.5	26	34	34	13	

Table 8.12: ALT acquisition table for α = 180°, 10.30 am orbit, 13th month of the year.

MCV/MOON	90	85	80	75	70	65	60	55	50	45	40	35	30	25	20	15	10	5	0	-5	-10	-15	-20	-25	-30	-35	-40	-45	-50	-55	-60	-65	-70	-75	-80	-85	-90
-35	0	0	0	0	0	0	0	0	0	0	0.54	1.55	21.7	21.6	21.6	21.6	21.6	20.3	5.1	19.1	21.9	23.4	24.5	26.1	27.4	4.77	4.16	3.72	3.21	2.9	2.7	2.45	2.55	3.09	3.76	5.35	5.36
-30	0	0	0	0	0	0	0	0	0	0	0	0	0.89	20.2	20.1	20.1	20	18.6	5.1	18.6	21.3	22.6	23.7	25.3	11.5	3.72	3.33	2.95	2.67	2.3	2.25	2.53	2.83	3.9	5.78	7.05	6.43
-25	0	0	0	0	0	0	0	0	0	0	0	0	0	18.7	18.6	18.6	18.4	16.9	5.1	18.1	20.4	21.6	22.9	3.77	3.14	2.71	2.32	1.79	1.54	1.39	1.45	1.74	2.7	5.21	8.86	8.34	7.84
-20	0	0	0	0	0	0	0	0	0	0	0	0	0	0	0	17	16.8	15.3	8.8	17.5	19.5	20.6	2.74	2.14	1.63	1.14	0.69	0.26	0	0	0	0	1.21	10.6	10.2	9.8	9.46
-15	0	0	0	0	0	0	0	0	0	0	0	0	0	0	0	0	0	13.9	8.8	16.6	2	1.55	0.91	0.36	0	0	0	0	0	0	0	0	0	9.44	11.9	11.6	11.5	
-10	0	0	0	0	0	0	0	0	0	0	0	0	0	0	0	0	0	0	0	0.46	0.37	0	0	0	0	0	0	0	0	0	0	0	1.29	7.6	11.6	13.7	13.7	
-5	0	0	0	0	0	0	0	0	0	0	0	0	0	0	0	0	0	0	0	0	0	0	0	0	0	0	0	0	0	0	0	0	3.47	8.15	11.2	14.1	16.4
0	0	0	0	0	0	0	0	0	0	0	0	0	0	0	0	0	0	0	0	0	0	0	0	0	0	0	0	0	0	0	0	0.67	5.03	8.98	11.7	14.7	17.1
5	14.7	0	0	0	0	0	0	0	0	0	0	0	0	0	0	0	0	0	0	0	0	0	0	0	0	0	0	0	0	0	0	2.55	6.49	10.1	12.8	15.7	15.9
10	13.7	13.2	12.5	0	0	0	0	0	0	0	0	0	0	0	0	0	0	0	0	0	0	0	0	0	0	0	0	0	0	0	0.83	4.34	8.12	11.6	14.2	15	14.3
15	12.8	12.1	11.4	10.8	0	0	0	0	0	0	0	0	0	0	0	0	0	0	0	0	0	0	0	0	0	0	0	0	0	0	2.82	6.18	9.89	13.3	14.2	13.5	12.8
20	12.2	11.5	10.7	10.1	9.48	0	0	0	0	0	0	0	0	0	0	0	0	0	0	0	0	0	0	0	0	0	0	0	0	0.93	5.23	8.64	12.2	13.3	12.7	12	11.2
25	11.2	11.2	10.3	9.69	9.04	0	0	0	0	0	0	0	0	0	0	0	0	0	0	0	0	0	0	0	0	0	0	0	0	3.92	8.48	11.8	12.7	12	11.3	10.4	9.59
30	10.2	11.3	10.3	9.6	8.9	2.39	0	0	0	0	0	0	0	0	0	0	0	0	0	0	0	0	0	0	0	0	0	0	2.35	7.89	9.8	12.1	11.4	10.6	9.76	8.83	7.96
35	11.6	11.6	10.5	9.78	9.02	0	0	0	0	0	0	0	0	0	0	0	0	0	0	0	0	0	0	0	0	0	1.99	5.12	6.8	8.71	10.6	10.1	9.08	8.2	7.2	6.29	

Table 8.13: ALT acquisition table for α = 180°, 10.30 am orbit, 5th month of the year.

8.3. 01.30 pm orbit

8.3.1. 01.30 pm, ACT 270° configuration

A best/worst case scenario for ACT acquisitions made at α =270° is given in Table *8.14* and Table *8.15*, respectively.

MCV/MOON	90	85	80	75	70	65	60	55	50	45	40	35	30	25	20	15	10	5	0	-5	-10	-15	-20	-25	-30	-35	-40	-45	-50	-55	-60	-65	-70	-75	-80	-85	-90
-35	47.81	48.1	48.13	48.15	48.33	48.18	47.57	46.35	45.33	43.96	42.61	40.79	37.52	34.81	32.16	29.75	27.44	25.17	0	19.42	18.84	18.98	19.37	20.09	21.1	22.17	21.59	20.02	17.8	15.64	14.15	11.78	9.896	7.233	5.061	3.005	1.646
-30	48.17	48.19	48.2	48.05	47.9	47.74	47.66	46.43	45.34	43.81	42.21	40.15	36.72	33.43	30.4	27.54	25.04	21.99	0	17.68	17.01	17.07	17.37	17.98	18.87	19.85	21.18	20.59	18.26	16.81	15.82	14.36	13.05	10.94	9.165	7.1	5.223
-25	47.41	47.09	46.94	46.78	46.62	48.3	47.71	46.45	45.26	43.45	41.45	38.81	35.32	31.32	27.75	24.77	21.83	18.68	0	16.02	15.28	15.24	15.44	15.92	16.65	17.48	18.79	20.21	18.73	16.77	19.61	18.36	16.76	14.94	13.33	10.97	8.828
-20	45.98	45.82	45.83	48.34	48.34	48.51	47.74	46.41	45.04	42.76	39.87	36.58	32.07	28.19	24.43	21.23	18.53	15.67	0	14.46	13.68	13.56	13.68	14.02	14.58	15.24	16.3	17.47	18.49	17.2	15.2	18.74	20.53	18.38	16.66	14.62	12.52
-15	44.7	48.37	48.38	48.38	48.39	48.39	47.73	46.45	44.58	41.39	37.28	32.32	27.21	23.78	20.51	17.82	15.61	13.23	0	13.04	12.26	12.09	12.13	12.36	12.77	13.26	14.07	14.98	16.26	15.78	15.93	13.6	16.49	21.92	19.86	17.53	15.65
-10	48.42	48.42	48.43	48.43	48.43	48.36	47.67	46.16	43.57	38.28	31.97	26.11	21.34	18.62	16.82	15.01	13.31	12.88	0	11.79	11.05	10.84	10.84	10.98	11.26	11.63	12.24	12.92	14.01	13.36	12.72	12.79	12.25	14.18	23.26	20.6	18.57
-5	48.47	48.47	48.47	48.47	48.47	48.22	47.5	45.23	40.71	31.19	24.08	19.27	15.93	14.2	13.09	13.19	12.29	0	0	0	10.06	9.848	9.811	9.891	10.1	10.37	10.83	11.35	12.19	11.33	10.27	9.47	9.304	10.67	9.266	23.74	21.46
0	48.51	48.51	48.51	48.45	48.43	47.91	46.97	42.17	31.67	21.64	16.68	13.73	11.67	10.88	11.28	11.52	0	0	0	0	0	9.104	9.055	9.101	9.255	9.469	9.839	10.26	10.93	10.14	8.522	7.047	6.22	5.96	6.968	7.89	24.36
5	47.86	47.88	47.88	47.81	47.61	47.1	43.85	29.88	20.43	14.44	11.55	9.534	8.7	8.479	8.363	0	0	0	0	0	0	0	8.562	8.594	8.721	8.902	9.217	9.577	9.073	7.606	6.431	5.329	4.258	3.206	3.089	4.025	7.17
10	46.62	46.58	46.44	46.12	45.2	41.89	29.13	18.4	13.28	9.767	7.823	6.526	6.07	5.501	0	0	0	0	0	0	0	0	0	8.203	8.456	8.635	8.915	7.898	3.876	3.402	3.087	2.344	1.89	1.581	0.776	0.558	1.626
15	44.75	44.42	43.69	41.97	36.84	27.88	18.24	12.39	9.22	6.528	4.891	4.328	3.951	0	0	0	0	0	0	0	0	0	0	0	8.344	8.51	8.797	9.12	9.631	10.18	6.746	3.581	1.531	0	0	0	0
20	41.83	40.75	38.36	33.38	25.39	18.57	12.65	8.795	6.377	4.135	4.027	5.233	0	0	0	0	0	0	0	0	0	0	0	0	0	8.173	8.43	8.725	9.197	9.83	10.52	10.18	7	3.769	1.636	0	0
25	37.53	35.19	30.8	24.6	18.35	13.66	9.632	6.556	4.345	4.436	6.039	0	0	0	0	0	0	0	0	0	0	0	0	0	0	0	7.861	8.132	8.568	9.157	9.8	10.82	11.98	8.451	5.391	2.14	0
30	32.33	29.08	24.29	19.28	14.41	11.03	7.735	4.719	3.891	0	0	0	0	0	0	0	0	0	0	0	0	0	0	0	0	0	0	0	7.763	8.315	8.921	9.888	10.99	12.71	9.586	5.437	2.406
35	27.59	24.31	20.15	16.05	12.32	9.472	6.259	3.291	0.565	0	0	0	0	0	0	0	0	0	0	0	0	0	0	0	0	0	0	0	0	7.321	7.896	8.818	9.869	11.69	13.49	9.093	5.216

Table 8.14: ACT acquisition table for α = 270°, 01.30 pm orbit, , 12th month of the year.

MCV/MOON	90	85	80	75	70	65	60	55	50	45	40	35	30	25	20	15	10	5	0	-5	-10	-15	-20	-25	-30	-35	-40	-45	-50	-55	-60	-65	-70	-75	-80	-85	-90
-35	29.1	30.7	32.8	34.9	36.6	38.4	39	38.9	38.7	38.3	37.5	36.2	34.5	31.4	28.6	26	25.5	24.8	22.9	17.7	14.3	12.9	12.5	12.3	10.8	8.84	7.1	5.45	3.99	2.68	1.41	4.65	27	25.4	23.6	22	20.2
-30	27.2	28.7	30.7	32.7	34.2	35.8	36.9	37.6	36.9	36.1	34.7	33.2	31.1	28.4	26.4	24.9	23.5	22.9	21.3	16	12.5	11.1	10.6	9.96	7.72	5.77	3.72	2.04	0.07	0.36	3.17	6.15	8.15	7.79	20.2	22.9	22
-25	25.3	26.8	28.6	30.5	31.9	33.3	34.1	34.5	34.5	33.7	32.4	31	29	26.4	24.5	22.6	21.5	21.2	19.7	14.4	11	9.7	9.15	5.46	3.1	1.77	2.28	3.06	3.78	5.08	6.62	8.15	10.9	11.2	10.8	17.3	21.1
-20	23.5	24.9	26.6	28.3	29.6	30.8	31.4	31.6	31.3	30.5	29.1	27.5	25.7	23.8	22.2	20.6	19.8	19.6	18.1	12.9	9.79	8.59	6.63	6.93	8.24	8.95	8.94	8.9	9.03	9.08	9.69	10.7	12.3	14.1	13.7	13.3	17.1
-15	21.8	23.1	24.7	26.2	27.4	28.4	28.8	28.8	28.3	27.5	26	24.6	23.2	21.4	20.1	18.9	18.3	18	16.6	11.6	8.85	9.42	9.9	10.4	10.8	11.3	11.7	12.4	13.2	12.8	12.9	13.2	14.1	15.1	16.4	15.6	15.1
-10	20.1	21.3	22.8	24.2	25.2	26	26.3	26.2	25.6	24.7	23.3	22	20.9	19.4	18.3	17.3	16.8	16.6	15.1	10.6	8.41	9.83	10.2	10.6	10.9	11.2	11.6	12.2	12.9	13.7	14.7	15.8	16	16.6	17.5	17.8	17.1
-5	18.5	19.6	21	22.2	23.1	23.7	23.9	23.6	23	22.2	20.9	19.8	18.8	17.6	16.7	15.8	15.3	14.9	0	0	9.4	10	10.3	10.4	10.7	11	11.4	11.8	12.4	13	13.9	14.7	15.8	16.9	18.3	19.1	18.7
0	17	18	19.2	20.3	21	21.5	21.6	21.2	20.6	19.8	18.6	17.6	16.7	15.8	15.1	14.3	1.57	0.13	0	0	0	9.97	9.99	10.2	10.4	10.6	10.9	11.3	11.7	12.2	12.8	13.5	14.4	15.3	16.5	17.6	18.7
5	15.6	16.5	17.5	18.4	19	19.4	19.3	18.9	18.3	17.5	16.5	15.6	14.8	13.9	13.3	1.02	0	0	0	0	0	0	9.65	9.75	9.89	10.1	10.3	10.4	10.7	11.2	11.7	12.3	13	13.8	14.7	15.6	16.7
10	14.3	15	15.9	16.6	17	17.2	17.1	16.6	16	15.3	14.4	13.7	13	12.3	0.93	0	0	0	0	0	0	0	0	9.15	9.05	9.17	9.33	9.55	9.82	10.1	10.6	11	11.7	12.3	13	13.8	14.7
15	13	13.6	14.3	14.8	15	15.1	14.9	14.4	13.8	13.2	12.4	11.8	11.2	0.38	0	0	0	0	0	0	0	0	0	0	8.22	8.29	8.4	8.56	8.77	9.02	9.38	9.74	10.2	10.7	11.3	11.9	12.7
20	11.9	12.3	12.7	13	13.1	12.9	12.7	12.2	11.6	11.1	10.4	9.91	0.21	0	0	0	0	0	0	0	0	0	0	0	0	7.26	7.34	7.45	7.61	7.81	8.09	8.38	8.76	9.15	9.65	10.1	10.7
25	11	11.2	11.2	11.2	11.1	10.8	10.4	9.92	9.46	9	8.45	0	0	0	0	0	0	0	0	0	0	0	0	0	0	0	6.15	6.23	6.35	6.5	6.72	6.94	7.24	7.54	7.93	8.3	8.77
30	10.3	10.1	9.78	9.51	9.13	8.66	8.27	7.64	7.25	6.88	0	0	0	0	0	0	0	0	0	0	0	0	0	0	0	0	0	2.58	5	5.12	5.28	5.45	5.68	5.9	6.19	6.46	6.81
35	9.89	9.25	8.48	7.54	6.87	6.24	5.84	5.28	0.45	0	0	0	0	0	0	0	0	0	0	0	0	0	0	0	0	0	0	0	0	3.66	3.78	3.9	4.06	4.22	4.42	4.6	4.83

Table 8.15: ACT acquisition table for α = 270°, 01.30 pm orbit, , 4th month of the year.

8.3.2. 01.30 pm, ALT 0° configuration

A best/worst case scenario for ACT acquisitions made at α =0° is given in Table *8.16* and Table *8.17*, respectively.

MCV/MOON	90	85	80	75	70	65	60	55	50	45	40	35	30	25	20	15	10	5	0	-5	-10	-15	-20	-25	-30	-35	-40	-45	-50	-55	-60	-65	-70	-75	-80	-85	-90
-35	37.7	46.1	47.5	48.1	48.1	48.1	48.1	47.7	46.3	44.7	43.1	40.8	38.7	36.7	34	31	27.5	15.3	24.1	22.5	21.5	20.8	20.8	21.1	21.5	22.2	23.3	23.2	20.7	18.6	15.9	13.5	10.5	9.22	7.98	6.81	5.43
-30	38.2	45.9	47.4	48.2	48.2	48.2	48.2	47.4	45.8	43.8	41.8	39.2	36.9	34.6	31.4	28.4	26	15.6	21.7	21.3	20.3	19.8	19.8	20	20.3	20.9	21.7	22.9	22.3	20	17.5	15.1	12.4	10.3	9.34	8.26	7.14
-25	38.6	45.6	47.3	48.2	48.2	48.2	48.2	47.1	45.1	42.6	40.4	38	34.6	31.4	28.3	25.7	23.5	16.8	19	20.1	19.3	18.8	18.7	18.7	19	19.5	20.2	21.2	22.4	21.4	19	16.7	13.7	11.2	10.4	9.64	8.87
-20	38.9	45.3	47.1	48.2	48.2	48.2	48.2	46.6	44.2	41.4	39	35.9	31.4	28.4	25.7	23.3	21.4	17.4	16.4	18.5	18.1	17.7	17.4	17.5	17.8	18.1	18.8	19.6	20.7	21	20.2	17.9	14.9	12.5	11.4	11.2	10.6
-15	38.9	44.7	46.8	47.5	48.1	48.3	48.3	46	43.1	39.9	37.5	32.7	28.6	25.8	23.2	21.1	19.5	16.4	14.1	17	16.7	16.3	16.2	16.3	16.5	16.8	17.3	18	19	19.8	19.3	18.8	16	13.5	12.5	12.3	12.3
-10	38.7	42.9	43.4	43.8	44.2	44.7	45.1	41.9	38.7	35.5	33.5	29.8	25.8	23.3	21	19.3	0.68	0	0	1.72	1.82	15.1	14.9	15	15.1	15.4	15.9	16.5	17.3	18.2	17.9	17.6	17	14.4	11.6	8.84	13.9
-5	35.9	39.1	39.3	39.4	39.5	39.7	39.7	35.2	31	24.1	4.93	2.93	1.42	0.38	0	0	0	0	0	0	0	0	0	0	0	0	0	15	15.7	16.5	16.4	16.1	16.1	15.3	12.5	9.9	6.84
0	31.4	33.3	32.4	18.2	17.7	17.4	16.4	10.3	5.95	2.96	0.94	0	0	0	0	0	0	0	0	0	0	0	0	0	0	0	0	0	0	0	0	0	0	0	13.1	11	8.07
5	16.1	17.3	16.7	16.3	15.7	15.3	12.9	5.3	1.43	0	0	0	0	0	0	0	0	0	0	0	0	0	0	0	0	0	0	0	0	0	0	0	0	0	0	0	0
10	15.5	15.9	15.3	14.6	13.7	13.2	6.68	0	0	0	0	0	0	0	0	0	0	0	0	0	0	0	0	0	0	0	0	0	0	0	0	0	0	0	0	0	0
15	15	14.7	13.7	13	12	11.3	0	0	0	0	0	0	0	0	0	0	0	0	0	0	0	0	0	0	0	0	0	0	0	0	0	0	0	0	0	0	0
20	14.5	13.5	12.3	11.4	10.2	8.25	0	0	0	0	0	0	0	0	0	0	0	0	0	0	0	0	0	0	0	0	0	0	0	0	0	0	0	0	0	0	0
25	13.8	12.5	10.9	9.81	8.65	4.51	0	0	0	0	0	0	0	0	0	0	0	0	0	0	0	0	0	0	0	0	0	0	0	0	0	0	0	0	0	0	0
30	13.4	11.7	9.81	8.3	6.92	3.01	0	0	0	0	0	0	0	0	0	0	0	0	0	0	0	0	0	0	0	0	0	0	0	0	0	0	0	0	0	0	0
35	13.1	11.1	8.78	6.98	5.32	2.16	0	0	0	0	0	0	0	0	0	0	0	0	0	0	0	0	0	0	0	0	0	0	0	0	0	0	0	0	0	0	0

Table 8.16: ALT acquisition table for α = 0°, 01.30 pm orbit, , 8th month of the year.

MCV/MOON	90	85	80	75	70	65	60	55	50	45	40	35	30	25	20	15	10	5	0	-5	-10	-15	-20	-25	-30	-35	-40	-45	-50	-55	-60	-65	-70	-75	-80	-85	-90
-35	12.3	13.8	15.6	17.4	18.9	20.5	21.5	22.3	22.7	23	23.1	23	22.8	22.3	21.9	21.2	20.2	18.4	9.47	18.8	21	21.4	21.6	21.6	21.7	21.9	22.2	22.5	22.6	23	23.4	23.7	23.1	21.6	19.7	18.2	16.3
-30	10	12.7	14.5	16.2	17.6	19.1	20.1	20.8	21.2	21.4	21.5	21.4	21.2	20.6	20.2	19.5	18.5	16.7	10.3	18.3	20.1	20.3	20.2	20.3	20.4	20.5	20.7	20.9	21	21.3	21.7	22	21.9	20.7	19	17.3	15
-25	12	10.5	13.5	15.2	16.5	17.9	18.8	19.4	19.8	19.9	19.9	19.8	19.6	19	18.6	17.9	16.9	15.2	10.5	17.7	19.2	19.2	19	19	19	19.1	19.2	19.4	19.4	19.7	20	20.3	19.7	18.5	17	15.3	13.3
-20	13.9	12.5	11.4	14.3	15.5	16.8	17.6	18.1	18.4	18.5	18.5	18.3	18	17.6	17	16.4	15.4	13.7	11	17.1	17.9	17.8	17.7	17.6	17.6	17.6	17.7	17.7	17.9	18.1	18.4	18.7	17.4	15.8	14.2	12.4	9.62
-15	14.7	14.2	12.4	12.5	14.7	15.8	16.6	17.1	17.2	17.3	17.1	16.9	16.6	16.2	15.6	15	14	12.4	11.3	16.2	16.7	16.4	16.3	16.2	16.1	16.1	16	16.1	16.3	16.5	16.8	16.4	14.6	13.1	11	8.57	6.15
-10	14	13.4	12.2	10.9	12.9	15	15.7	16.1	16.1	16.1	15.9	15.6	15.3	14.9	14.4	13.6	12.9	0	0	0.43	1.45	15.1	14.9	14.7	14.7	14.5	14.5	14.7	14.8	15	15.3	13.8	11.8	9.95	7.17	5.15	2.62
-5	10.4	9.49	8.12	9.4	11.3	13.6	15	15.3	15.4	15.1	7.64	6.17	4.91	3.29	2.09	0.46	0	0	0	0	0	0.39	0.94	1.79	2.5	3.23	4.11	13.2	13.4	13.6	12.5	10.7	8.55	6.06	3.65	1.5	0
0	5.64	4.21	5.7	8.12	9.93	12.1	12.4	11.2	9.56	8.07	6.2	4.84	3.37	1.72	0.52	0	0	0	0	0	0	0	0	0	0.6	1.35	2.13	2.94	3.94	3.99	2.74	1.38	0	0	0	0	0
5	0.76	2.5	4.72	7.01	8.71	10.8	10.4	9.74	8.51	6.91	4.93	3.5	1.99	0.47	0	0	0	0	0	0	0	0	0	0	0	0	0.34	1.16	1.35	0	0	0	0	0	0	0	0
10	0.17	1.8	3.89	6.05	7.64	9.25	8.65	8.01	7.14	5.99	3.88	2.37	0.8	0	0	0	0	0	0	0	0	0	0	0	0	0	0	0	0	0	0	0	0	0	0	0	0
15	0	1.24	3.2	5.23	6.72	7.72	7.02	6.27	5.31	4.69	3.09	1.48	0	0	0	0	0	0	0	0	0	0	0	0	0	0	0	0	0	0	0	0	0	0	0	0	0
20	0	0.81	2.64	4.55	5.94	6.49	5.7	4.68	3.81	2.94	2.09	1.06	0	0	0	0	0	0	0	0	0	0	0	0	0	0	0	0	0	0	0	0	0	0	0	0	0
25	0	0.52	2.23	4.01	5.31	5.24	4.36	3.25	2.46	1.52	0.42	0	0	0	0	0	0	0	0	0	0	0	0	0	0	0	0	0	0	0	0	0	0	0	0	0	0
30	0	0.38	1.96	3.62	4.82	4.31	3.34	2.13	1.27	0.09	0	0	0	0	0	0	0	0	0	0	0	0	0	0	0	0	0	0	0	0	0	0	0	0	0	0	0
35	0	0.41	1.86	3.4	4.49	3.54	2.48	1.17	0.07	0	0	0	0	0	0	0	0	0	0	0	0	0	0	0	0	0	0	0	0	0	0	0	0	0	0	0	0

Table 8.17: α acquisition table for α = 0°, 01.30 pm orbit, , 4th month of the year.

8.3.3. 01.30 pm, ALT 180° configuration

A best/worst case scenario for ACT acquisitions made at α =180° is given in Table *8.18* and 9.20 , respectively.

MCV/MOON	90	85	80	75	70	65	60	55	50	45	40	35	30	25	20	15	10	5	0	-5	-10	-15	-20	-25	-30	-35	-40	-45	-50	-55	-60	-65	-70	-75	-80	-85	-90
-35	0	0.1	0.4	0.5	0.7	1.1	1.6	2.1	2.7	3.6	3.8	3.5	17	16	16	15	14	12	15	22	21	20	19	18	18	5.2	4.8	4.5	4.4	4.4	4.3	0	0	0	0	0	0
-30	0	2.2	2.4	2.6	2.6	3	3.4	4	4.4	5.2	4.6	4	3.6	17	16	15	14	12	13	21	20	19	18	18	4.9	4.5	4.4	4.4	4.2	4.3	1.3	0	0	0	0	0	0
-25	0	4.3	4.4	4.6	4.7	4.9	5.2	5.6	6.1	5.9	5	4.5	3.9	3.3	16	16	15	13	12	19	19	18	17	4.4	4.1	4	4	4.1	4.1	2.4	0	0	0	0	0	0	0
-20	0	6.3	6.4	6.4	6.7	6.6	6.9	7.1	7.5	6.4	5.5	4.7	3.9	3.4	2.6	16	15	13	11	18	17	17	3.3	3.2	3.2	3.2	3.3	3.5	2.7	0.1	0	0	0	0	0	0	0
-15	0	8.5	8.4	8.4	8.5	8.3	8.4	8.7	8.2	7	5.8	4.8	3.8	3.2	2.3	1.6	0.7	13	9.7	17	2.2	2	2	2	2.2	2.3	2.7	2.9	0.6	0	0	0	0	0	0	0	0
-10	0	10	10	10	10	10	9.9	9.9	8.8	7.4	5.9	4.8	3.6	2.7	1.8	1	0.1	0	0	0.6	0.6	0.5	0.7	0.8	1.1	1.5	1.7	1.5	0	0	0	0	0	0	0	0	0
-5	0.6	12	12	12	12	12	11	11	9.1	7.5	5.9	4.7	3.4	2.1	1	0.2	0	0	0	0	0	0	0	0	0	0.3	0.7	0.1	0	0	0	0	0	0	0	0	0
0	2.3	14	14	14	13	13	13	11	9	7	5.2	3.9	2.5	1.4	0.4	0	0	0	0	0	0	0	0	0	0	0	0	0	0	0	0	0	0	0	0	0	0
5	9.6	17	16	15	15	14	14	11	8.6	6.3	4.3	2.9	1.3	0.2	0	0	0	0	0	0	0	0	0	0	0	0	0	0	0	0	0	0	0	0	0	1.8	6.4
10	12	33	32	26	17	16	14	10	7.5	5	2.8	1.3	0	0	0	0	0	0	0	0	0	0	0	0	0	0	0	0	0	0	0	0	0	0	4.8	5.2	6.8
15	14	36	35	34	32	17	13	8.9	5.9	3.1	1	0	0	0	0	0	0	0	0	0	0	0	0	0	0	0	0	0	0	0	0	0	5.7	5.4	5.3	6.1	7.8
20	16	39	38	37	35	17	11	6.1	3.1	0.5	0	0	0	0	0	0	0	0	0	0	0	0	0	0	0	0	0	0	0	0	0	0	6.3	6.1	6	6.7	8.7
25	17	41	40	39	38	19	6.7	2.2	0	0	0	0	0	0	0	0	0	0	0	0	0	0	0	0	0	0	0	0	0	0	0	0.7	7	6.7	6.9	7.6	9.7
30	18	44	42	41	39	15	1	0	0	0	0	0	0	0	0	0	0	0	0	0	0	0	0	0	0	0	0	0	0	0	0	2.2	6.7	7.5	7.9	8.7	11
35	20	46	44	43	24	5.9	0	0	0	0	0	0	0	0	0	0	0	0	0	0	0	0	0	0	0	0	0	0	0	0	0	0.7	5.3	5.9	6.9	8.6	11

Table 8.18: ALT acquisition table for α = 180°, 01.30 pm orbit, , 11th month of the year.

MCV/MOON	90	85	80	75	70	65	60	55	50	45	40	35	30	25	20	15	10	5	0	-5	-10	-15	-20	-25	-30	-35	-40	-45	-50	-55	-60	-65	-70	-75	-80	-85	-90
-35	5.66	6.29	6.96	7.59	7.57	6.51	5.73	5.39	5.2	5.22	5.35	5.6	31.2	29.2	27.9	26.7	25.6	25.3	7.07	24	23.1	22.4	22	21.7	21.5	2.38	1.4	0.37	0	0	0	0	0	0	0	0	0
-30	7.17	7.68	8.24	8.77	9.41	7.98	6.5	5.72	5.19	5	4.96	4.9	5.29	28.5	27.1	25.7	24.7	24.1	6.03	22.3	21.6	20.9	20.6	20.3	1.92	0.86	0.1	0	0	0	0	0	0	0	0	0	0
-25	8.86	9.24	9.67	10.1	10.6	10.6	7.1	5.62	4.63	4.22	4	3.84	3.98	23.5	26	24.6	23.4	22.5	4.87	20.7	20	19.6	19.1	1.31	0.36	0	0	0	0	0	0	0	0	0	0	0	0
-20	10.9	11	11.3	11.6	11.9	12.1	7.8	5.02	3.5	2.93	2.62	2.59	2.39	2.63	2.93	23.1	21.8	20.8	3.29	19.1	18.5	18.1	0.71	0	0	0	0	0	0	0	0	0	0	0	0	0	0
-15	13	13.1	13.2	13.2	13.4	13.7	7.93	2.55	0.95	0.35	0.22	0.34	0.57	0.73	0.91	1.33	1.74	18.7	3.86	17.6	1.18	0	0	0	0	0	0	0	0	0	0	0	0	0	0	0	0	0
-10	15.5	15.3	15.3	15.2	15.2	15.2	3.89	0	0	0	0	0	0	0	0	0	0	0	0	0.62	0	0	0	0	0	0	0	0	0	0	0	0	0	0	0	0	0	0
-5	16.4	17.9	17.6	17.5	15.4	11.7	5.03	0	0	0	0	0	0	0	0	0	0	0	0	0	0	0	0	0	0	0	0	0	0	0	0	0	0	0	0	0	0	0
0	17.1	19.4	19.1	17.2	14.2	10.8	5.82	1.42	0	0	0	0	0	0	0	0	0	0	0	0	0	0	0	0	0	0	0	0	0	0	0	0	0	0	0	0	0	0
5	16.5	17.6	18.6	17.2	14	11	6.71	3.06	0	0	0	0	0	0	0	0	0	0	0	0	0	0	0	0	0	0	0	0	0	0	0	0	0	0	0	0	0	17.1
10	14.5	15.5	16.6	17.4	14.6	11.6	7.79	4.5	0.18	0	0	0	0	0	0	0	0	0	0	0	0	0	0	0	0	0	0	0	0	0	0	0	0	0	0	12.8	13.8	14.9
15	12.7	13.6	14.6	15.5	15.5	12.7	9.15	5.89	1.89	0	0	0	0	0	0	0	0	0	0	0	0	0	0	0	0	0	0	0	0	0	0	0	6.92	10.7	11.4	12.3	13.4
20	10.9	11.8	12.8	13.7	14.7	14.2	10.9	7.75	3.81	0.42	0	0	0	0	0	0	0	0	0	0	0	0	0	0	0	0	0	0	0	0	0	0	9.07	9.68	10.3	11.2	12.3
25	9.06	9.94	11	11.9	13	13.8	12.6	10.1	6.28	2.75	0	0	0	0	0	0	0	0	0	0	0	0	0	0	0	0	0	0	0	0	0	0	8.34	8.97	9.62	10.6	11.7
30	7.24	8.09	9.13	10.1	11.3	12.3	11.4	9.39	7.13	5.31	0.85	0	0	0	0	0	0	0	0	0	0	0	0	0	0	0	0	0	0	0	0	0	7.9	8.57	9.26	10.3	11.5
35	5.38	6.23	7.29	8.31	9.64	10.7	9.81	7.96	5.89	4.35	2.46	0	0	0	0	0	0	0	0	0	0	0	0	0	0	0	0	0	0	0	0	0	7.73	8.44	9.19	10.3	11.6

Table 8.19: ALT acquisition table for α = 180°, 01.30 pm orbit, , 11th month of the year.

8.4. 01.30 am orbit

8.4.1. 01.30 am, ACT 270° configuration

A best/worst case scenario for ALT acquisitions made at α =270° is given in Table *8.18* and 9.22 , respectively.

MCV/MOON	90	85	80	75	70	65	60	55	50	45	40	35	30	25	20	15	10	5	0	-5	-10	-15	-20	-25	-30	-35	-40	-45	-50	-55	-60	-65	-70	-75	-80	-85	-90
-35	43	44	45	46	47	48	48	48	48	48	48	46	43	40	36	33	29	27	0	15	15	16	17	18	19	19	19	18	15	14	15	13	11	9.5	8	5.7	3.6
-30	44	44	45	46	46	47	48	48	48	48	48	46	43	38	33	30	26	24	0	13	14	14	15	15	16	17	17	17	16	14	13	17	15	13	11	9	6.6
-25	44	44	44	45	47	48	48	48	48	48	48	48	42	34	28	24	22	20	0	13	13	13	13	13	14	15	15	14	14	14	12	12	18	16	14	12	9.8
-20	43	43	46	47	47	48	48	48	48	48	48	48	41	27	21	18	17	17	0	12	11	11	11	12	12	13	13	12	11	11	11	11	8.4	20	18	15	13
-15	45	46	46	47	47	48	48	48	48	48	48	48	24	16	14	13	13	14	0	11	10	10	10	10	11	11	12	10	8.8	7.8	6.9	7.2	9.2	7.1	21	19	16
-10	46	46	47	47	48	48	48	48	48	49	48	18	11	9	8.4	8.3	8.9	10	0	10	9.3	9.1	9	9.2	9.4	9.8	10	9.3	7.2	5.5	4.1	3.4	3.2	5.2	6.1	22	19
-5	47	47	47	47	48	48	48	48	49	48	23	12	8.1	5.7	5.7	5.1	5.3	0	0	0	8.6	8.4	8.4	8.5	8.5	8.7	9	6.4	4.8	3.6	2.1	0.7	0	0	0.3	4.7	22
0	48	48	48	48	48	48	49	49	48	25	16	12	9.2	7.8	8.2	8.1	0	0	0	0	0	9	9	9	9.1	9.3	7.8	5.2	3.9	2.5	1.1	0.2	0	0	0.3	2.2	26
5	49	49	49	49	48	48	47	41	27	19	14	12	11	11	11	0	0	0	0	0	0	0	9	9.1	9.2	9.4	9.6	10	11	9.2	6.8	5	3.7	2.8	2.5	2.9	4.5
10	49	49	49	49	49	48	40	29	20	16	14	13	13	13	0	0	0	0	0	0	0	0	0	8.9	9	9	9.2	9.6	10	11	11	10	7.8	6.2	5.1	4.5	4.5
15	49	49	49	49	49	46	29	22	17	15	14	14	14	0	0	0	0	0	0	0	0	0	0	0	8.4	8.6	8.8	9.1	9.5	10	11	12	12	9.7	8.1	6.5	5.6
20	49	49	49	49	49	32	22	18	16	15	15	15	0	0	0	0	0	0	0	0	0	0	0	0	0	8	8.1	8.4	8.8	9.3	9.9	11	12	13	11	8.9	6.9
25	49	49	49	49	49	22	17	16	15	15	16	0	0	0	0	0	0	0	0	0	0	0	0	0	0	0	7.3	7.6	8	8.4	9	9.8	11	12	14	11	8.7
30	49	49	49	49	20	16	14	14	15	4.3	0	0	0	0	0	0	0	0	0	0	0	0	0	0	0	0	0	0	7	7.3	7.9	8.6	9.6	11	13	14	10
35	49	49	49	15	13	12	13	13	0	0	0	0	0	0	0	0	0	0	0	0	0	0	0	0	0	0	0	0	0	6.2	6.7	7.4	8.3	9.6	11	15	12

Table 8.20: ACT acquisition table for α = 270°, 01.30 am orbit, , 6th month of the year.

MCV/MOON	90	85	80	75	70	65	60	55	50	45	40	35	30	25	20	15	10	5	0	-5	-10	-15	-20	-25	-30	-35	-40	-45	-50	-55	-60	-65	-70	-75	-80	-85	-90
-35	17.8	19.3	21.1	22.6	24.1	25.3	26.1	26.6	26.8	26.6	26.4	26.1	25.6	25	24.3	23.7	22.6	21	15.1	16.7	19.2	20.2	20.6	21	21.5	22	22.7	23.3	23.4	22.9	21.8	20.5	19.2	17.8	16.7	15.4	14.6
-30	18.3	19.8	21.6	23	24.4	25.5	26.2	26.5	26.6	26.5	26	25.5	24.9	24.2	23.4	22.8	21.9	20.2	15.3	14.8	17.4	18.4	18.8	19.4	19.8	20.4	21.1	21.8	22.2	21.8	21.3	20.2	19	17.7	16.5	15.1	14.2
-25	18.7	20.2	21.9	23.2	24.5	25.5	26.1	26.3	26.3	26	25.5	24.8	24	23.2	22.4	21.7	20.8	19.5	15.2	13.2	15.6	16.7	17.1	17.7	18.2	18.6	19.4	20.1	20.9	20.9	20.3	19.9	19.3	17.9	16.5	15.3	14.3
-20	19	20.4	22	23.2	24.5	25.3	25.8	25.9	25.7	25.3	24.6	23.9	23.1	22.2	21.3	20.5	19.7	18.5	15	11.8	14	15	15.5	15.9	16.4	17	17.5	18.3	19.1	20	19.8	19.3	18.9	18.4	17.2	15.8	14.7
-15	19.1	20.4	21.9	23.1	24.2	24.9	25.2	25.2	24.8	24.2	23.4	22.6	21.6	20.7	19.7	19	18.3	17.3	14.6	10.6	12.6	13.5	13.9	14.2	14.7	15.2	15.7	16.4	17.1	18	19	18.9	18.6	18.1	17.5	16.5	15.7
-10	18.9	20.2	21.6	22.7	23.6	24.2	24.3	24.1	23.6	22.8	21.9	21	19.9	18.9	18	17.4	16.7	16.2	14	9.63	11.3	12.1	12.5	12.7	13.1	13.5	14.1	14.5	15.2	16	17	18	18.3	17.9	17.4	16.8	16.3
-5	18.5	19.7	21	21.9	22.7	23.1	23	22.7	21.9	21	20	19.1	18	17.2	16.4	15.8	15.3	1.65	0	0	10.3	10.9	11	11.3	11.6	12	12.5	13	13.4	14.1	14.9	15.9	17	17.8	17.4	16.8	16.3
0	17.8	18.9	20	20.8	21.3	21.5	21.3	20.8	19.9	18.9	17.9	17	16.2	15.3	14.5	14	1.27	0	0	0	0	9.9	9.95	10.2	10.4	10.7	11.1	11.5	11.8	12.4	13.1	13.9	14.9	15.9	17.1	17	16.5
5	16.8	17.7	18.6	19.2	19.6	19.5	19.1	18.6	17.7	16.7	15.7	15.1	14.2	13.5	12.8	0.81	0	0	0	0	0	0	0	9.12	9.28	9.44	9.64	9.78	10.1	10.5	11	11.5	12.2	13	13.9	14.9	16	16.7
10	15.3	16	16.8	17.2	17.4	17.3	16.8	16.2	15.4	14.6	13.7	13	12.3	11.7	0.26	0	0	0	0	0	0	0	0	0	8.61	8.55	8.7	8.92	9.18	9.49	9.86	10.3	10.8	11.5	12.2	13	13.9	14.7
15	13.5	14	14.6	14.9	15.1	14.9	14.5	14.1	13.4	12.7	12	11.5	10.9	0.14	0	0	0	0	0	0	0	0	0	0	0	8.08	8.18	8.34	8.53	8.77	9.07	9.42	9.84	10.3	10.9	11.5	12.2	12.8
20	11.4	11.8	12.3	12.6	12.8	12.8	12.5	12.2	11.7	11.2	10.7	10.3	0.45	0	0	0	0	0	0	0	0	0	0	0	0	0	7.92	8.03	8.17	8.35	8.58	8.86	9.18	9.56	9.99	10.5	11	11.4
25	9.2	9.66	10.2	10.5	10.9	11	10.9	10.8	10.5	10.2	9.78	1.02	0	0	0	0	0	0	0	0	0	0	0	0	0	0	0	7.97	8.07	8.2	8.37	8.59	8.84	9.12	9.44	9.79	10.1	10.4
30	7.18	7.7	8.32	8.83	9.32	9.64	9.79	9.79	9.66	4.39	1.3	0	0	0	0	0	0	0	0	0	0	0	0	0	0	0	0	0.66	8.3	8.43	8.58	8.77	8.98	9.21	9.46	9.69	9.85
35	5.46	6.08	6.87	7.53	8.2	8.71	9.03	9.16	4.01	2.14	0.52	0	0	0	0	0	0	0	0	0	0	0	0	0	0	0	0	0	1.46	8.72	8.83	8.96	9.11	9.26	9.41	9.54	9.61

Table 8.21: ACT acquisition table for α = 270°, 01.30 am orbit, , 10th month of the year.

8.4.2. 01.30 am, ALT 0° configuration

A best/worst case scenario for ACT acquisitions made at α =0° is given in Table *8.18* and 9.24 , respectively.

MCV/MOON	90	85	80	75	70	65	60	55	50	45	40	35	30	25	20	15	10	5	0	-5	-10	-15	-20	-25	-30	-35	-40	-45	-50	-55	-60	-65	-70	-75	-80	-85	-90
-35	45.92	47.39	47.98	48	48.01	47.73	46.42	45.14	43.57	42.07	38.28	34.87	32.2	29.93	27.55	25.6	23.67	21.09	14.58	13.52	17.47	19.18	20.06	20.83	21.61	22.46	23.4	23.66	22.99	21.53	19.93	17.23	14.52	11.34	9.266	6.946	4.172
-30	45.7	47.18	48.06	48.07	48.08	48.21	46.59	45.19	43.47	41.88	36.16	32.71	30.04	27.82	25.55	23.7	21.9	19.41	12.92	13.88	17.16	18.52	19.19	19.78	20.4	21.05	21.83	22.9	22.25	21.46	21.08	18.45	16.36	12.67	10.16	7.773	5.128
-25	45.42	46.92	48.14	48.15	47.98	48.16	46.76	45.23	43.38	41.71	34.06	30.59	27.94	25.78	23.61	22.04	20.35	17.78	11.45	14.03	16.73	17.77	18.27	18.72	19.02	19.68	20.32	21.23	21.45	20.51	19.85	18.45	17.29	13.74	10.92	8.61	5.93
-20	45.03	46.6	48.21	48.21	48.21	48.22	46.95	45.27	43.29	41.55	32.15	28.67	25.9	23.81	21.75	20.28	18.68	16.19	10.33	14.01	16.17	16.94	17.29	17.61	17.79	18.32	18.85	19.62	20.4	19.32	18.56	17.05	16.47	14.88	11.56	9.301	6.574
-15	44.49	46.18	47.56	48.28	48.28	48.28	47.16	45.31	43.19	41.57	30.1	26.64	24.09	22.07	19.95	18.57	17.06	14.68	10.04	13.81	15.49	16.01	16.23	16.27	16.53	16.95	17.39	18.05	18.73	18.04	17.01	15.4	14.9	14.08	12.07	9.85	7.059
-10	42.06	42.76	43.38	44.17	44.51	45.17	44.73	43.01	41.25	39.75	28.09	24.66	22.17	20.23	18.38	16.92	1.997	0.056	0	0	0	14.98	14.92	15.05	15.23	15.56	15.93	16.5	17.09	16.48	15.53	13.99	13.07	12.35	11	10.43	7.545
-5	38.48	38.9	39.2	39.4	39.4	39.57	39.03	36.54	33.78	26.78	7.238	5.765	4.388	3.343	2.081	1.237	0	0	0	0	0	0	0	0	0	0	0	14.96	15.5	14.79	13.61	11.98	11.14	10.51	9.331	10.26	8.023
0	33.73	33.42	32.56	17.26	16.78	16.23	15.28	12.09	9.049	6.822	4.902	3.551	2.423	1.134	0.145	0	0	0	0	0	0	0	0	0	0	0	0	0	0	0	0	0	0	0	7.498	8.591	8.315
5	17.28	16.64	15.99	15.49	14.9	14.39	13.68	10.02	6.485	4.37	2.48	1.214	0.183	0	0	0	0	0	0	0	0	0	0	0	0	0	0	0	0	0	0	0	0	0	0	0	0
10	16.18	15.38	14.58	13.93	13.23	12.42	11.79	8.139	4.208	1.896	0.073	0	0	0	0	0	0	0	0	0	0	0	0	0	0	0	0	0	0	0	0	0	0	0	0	0	0
15	15.16	14.18	13.21	12.41	11.59	10.82	9.909	6.131	1.83	0	0	0	0	0	0	0	0	0	0	0	0	0	0	0	0	0	0	0	0	0	0	0	0	0	0	0	0
20	14.22	13.05	12.07	10.94	10.16	9.092	8.238	4.347	0	0	0	0	0	0	0	0	0	0	0	0	0	0	0	0	0	0	0	0	0	0	0	0	0	0	0	0	0
25	13.56	12.18	10.83	9.689	8.613	7.579	6.447	2.745	0	0	0	0	0	0	0	0	0	0	0	0	0	0	0	0	0	0	0	0	0	0	0	0	0	0	0	0	0
30	12.89	11.43	9.854	8.347	7.296	5.954	4.878	3.958	0	0	0	0	0	0	0	0	0	0	0	0	0	0	0	0	0	0	0	0	0	0	0	0	0	0	0	0	0
35	12.62	10.86	9.007	7.268	6.057	4.564	3.374	2.336	0	0	0	0	0	0	0	0	0	0	0	0	0	0	0	0	0	0	0	0	0	0	0	0	0	0	0	0	0

Table 8.22: ALT acquisition table for α = 0°, 01.30 am orbit, , 11th month of the year.

MCV/MOON	90	85	80	75	70	65	60	55	50	45	40	35	30	25	20	15	10	5	0	-5	-10	-15	-20	-25	-30	-35	-40	-45	-50	-55	-60	-65	-70	-75	-80	-85	-90
-35	38	42	43	44	45	46	47	48	48	48	48	48	48	25	15	8.7	11	20	23	21	20	19	19	20	20	19	19	17	14	16	20	24	23	22	21	19	18
-30	38	41	42	43	45	47	48	48	48	48	48	32	24	19	15	11	5.6	16	21	20	19	18	18	19	19	20	21	20	17	15	16	19	23	25	24	22	21
-25	38	41	42	43	46	48	48	48	48	48	28	23	20	18	16	13	8.1	13	19	19	18	18	18	18	18	19	19	20	20	18	16	16	18	21	26	25	24
-20	37	39	40	42	46	48	48	48	48	26	23	21	20	18	17	16	11	8.7	17	18	17	17	17	17	17	18	18	19	20	21	19	16	14	16	19	22	27
-15	35	37	38	41	44	45	46	26	22	21	21	20	20	18	17	15	13	4.6	15	17	16	16	16	16	16	16	17	17	18	19	20	19	17	15	12	9.8	7.2
-10	32	32	32	33	41	20	14	14	15	16	17	18	18	17	15	14	0	0	0.2	1.4	0.5	15	15	15	15	15	16	16	17	18	18	20	19	17	15	13	10
-5	28	26	24	20	13	4.8	6.2	8.3	9.5	10	0	0	0	0	0	0	0	0	0	0	0	0	0	0	0	0	0	11	15	16	17	18	19	19	18	16	14
0	22	20	16	12	6	0.3	0	0	0	0	0	0	0	0	0	0	0	0	0	0	0	0	0	0	0	0	0	0	0	0	0	0	0	0	18	17	14
5	18	14	11	6.9	2.2	0	0	0	0	0	0	0	0	0	0	0	0	0	0	0	0	0	0	0	0	0	0	0	0	0	0	0	0	0	0	0	0
10	14	11	7.3	3.6	0	0	0	0	0	0	0	0	0	0	0	0	0	0	0	0	0	0	0	0	0	0	0	0	0	0	0	0	0	0	0	0	0
15	12	8.1	4.6	1	0	0	0	0	0	0	0	0	0	0	0	0	0	0	0	0	0	0	0	0	0	0	0	0	0	0	0	0	0	0	0	0	0
20	9.8	5.7	2.1	0	0	0	0	0	0	0	0	0	0	0	0	0	0	0	0	0	0	0	0	0	0	0	0	0	0	0	0	0	0	0	0	0	0
25	8.1	3.4	0	0	0	0	0	0	0	0	0	0	0	0	0	0	0	0	0	0	0	0	0	0	0	0	0	0	0	0	0	0	0	0	0	0	0
30	6.2	0.7	0	0	0	0	0	0	0	0	0	0	0	0	0	0	0	0	0	0	0	0	0	0	0	0	0	0	0	0	0	0	0	0	0	0	0
35	3.2	0	0	0	0	0	0	0	0	0	0	0	0	0	0	0	0	0	0	0	0	0	0	0	0	0	0	0	0	0	0	0	0	0	0	0	0

Table 8.23: ALT acquisition table for α = 0°, 01.30 am orbit, , 11th month of the year.

8.4.3. 01.30, ALT 180°

A best/worst case scenario for ACT acquisitions made at α =180° is given in Table *8.24* and Table *8.25* Table *8.18* and , respectively.

MCV/MOON	90	85	80	75	70	65	60	55	50	45	40	35	30	25	20	15	10	5	0	-5	-10	-15	-20	-25	-30	-35	-40	-45	-50	-55	-60	-65	-70	-75	-80	-85	-90
-35	2.2	2.45	2.77	2.99	3.44	3.95	4.54	5.21	5.13	4.68	4.35	4.16	19.9	18.8	17.5	16.5	15	11.7	18.1	22.4	21.4	20.5	19.8	19.2	18.7	4.84	4.4	4.21	4.11	3.91	3.64	0	0	0	0	0	0
-30	4.09	4.14	4.41	4.75	5.14	5.59	6.1	6.51	5.95	5.36	4.9	4.42	4.26	19	17.7	16.8	15.3	12.4	16.3	20.9	20.1	19.4	18.9	18.4	4.41	4.18	3.88	3.8	3.82	3.91	0.42	0	0	0	0	0	0
-25	5.99	6	6.22	6.49	6.65	7.02	7.44	7.65	6.66	5.91	5.15	4.54	4.11	3.6	17.9	16.8	15.3	12.8	14.7	19.5	18.8	18.2	17.9	3.9	3.53	3.42	3.4	3.42	3.55	1.42	0	0	0	0	0	0	0
-20	7.91	7.86	8.02	8.21	8.28	8.56	8.71	8.45	7.25	6.32	5.41	4.65	3.96	3.49	2.81	16.6	15.3	13	13.3	18	17.5	17.1	2.78	2.62	2.54	2.54	2.62	2.89	2.12	0	0	0	0	0	0	0	0
-15	9.83	9.73	9.64	9.75	9.73	9.9	9.94	9.12	7.69	6.55	5.47	4.4	3.77	3.06	2.47	1.67	0.78	13	12	16.6	1.78	1.46	1.32	1.43	1.44	1.69	1.85	2.03	0.35	0	0	0	0	0	0	0	0
-10	11.8	11.6	11.4	11.3	11.3	11.2	11.3	9.63	7.91	6.7	5.29	4.07	3.18	2.4	1.77	1.11	0.1	0	0	0	0.08	0.02	0	0.14	0.22	0.53	0.76	0.83	0	0	0	0	0	0	0	0	0	0
-5	13.7	13.4	13.2	12.9	12.7	12.6	12.3	9.89	7.83	6.2	4.79	3.6	2.64	1.48	0.66	0.01	0	0	0	0	0	0	0	0	0	0	0	0	0	0	0	0	0	0	0	0	0	0
0	15.9	15.4	15.1	14.7	14.2	13.9	12.8	9.76	7.31	5.43	3.87	2.43	1.44	0.61	0	0	0	0	0	0	0	0	0	0	0	0	0	0	0	0	0	0	0	0	0	0	0	0
5	27.5	21.7	17.1	16.5	15.9	15.2	13	8.99	6.14	4.06	2.44	0.84	0	0	0	0	0	0	0	0	0	0	0	0	0	0	0	0	0	0	0	0	0	0	0	0	0	3.56
10	32.5	31.9	30.9	26	17.5	16.6	12.4	7.3	4.05	1.79	0.28	0	0	0	0	0	0	0	0	0	0	0	0	0	0	0	0	0	0	0	0	0	0	0	2.61	8.37	8.82	6
15	35.9	35.4	34.6	33.5	30.9	18	9.16	4	0.91	0	0	0	0	0	0	0	0	0	0	0	0	0	0	0	0	0	0	0	0	0	0	0	0	8.63	8.68	9.08	11	14.7
20	36.6	38.3	37.4	36.2	34.5	15.9	2.78	0	0	0	0	0	0	0	0	0	0	0	0	0	0	0	0	0	0	0	0	0	0	0	0	0	0	9.15	9.29	10	12.7	17.8
25	34.5	35.2	39.8	38.4	36.7	0.36	0	0	0	0	0	0	0	0	0	0	0	0	0	0	0	0	0	0	0	0	0	0	0	0	0	0	9.3	9.96	10.7	13.5	12.9
30	31.6	30.3	27.1	17.5	6.15	0	0	0	0	0	0	0	0	0	0	0	0	0	0	0	0	0	0	0	0	0	0	0	0	0	0	1.88	7.59	8.85	10.5	14.5	15.4
35	27.7	24.1	17.3	9.13	3.09	0	0	0	0	0	0	0	0	0	0	0	0	0	0	0	0	0	0	0	0	0	0	0	0	0	0	0	6.23	7.35	8.85	12.6	15.8

Table 8.24: ALT acquisition table for α = 180°, 01.30 am orbit, , 7th month of the year.

MCV/MOON	90	85	80	75	70	65	60	55	50	45	40	35	30	25	20	15	10	5	0	-5	-10	-15	-20	-25	-30	-35	-40	-45	-50	-55	-60	-65	-70	-75	-80	-85	-90
-35	0	0	0	0	0	0	0	0	0	0	0	0	8.5	9.4	10	11	9.1	0	20	21	19	18	17	16	15	5.2	5.4	5.3	5.4	5.4	5.6	5.8	6	5.4	0	0	0
-30	0	0	0	0	0	0	0	0	0	0	0	0	0.7	12	12	12	11	0.2	18	20	18	17	17	16	5	5.2	5.3	5.4	5.6	5.7	6.1	6.3	6.7	1.2	0	0	0
-25	0	0	0	0	0	0.7	0.8	0.9	1.3	1.3	1.9	2.3	2.5	1.8	13	13	12	9	16	18	17	17	16	4.7	4.7	4.8	5	5.2	5.5	5.9	6.3	6.6	3.2	0	0	0	0
-20	0	0	0	0	1.7	3.1	3.2	3.3	3.4	3.4	3.8	3.9	3	2	1.3	13	13	11	15	17	16	16	3.6	3.8	4	4.4	4.7	5	5.4	5.9	6.5	4.3	0.9	0	0	0	0
-15	0	0	0	1.1	3.8	5.3	5.4	5.2	5.2	5.5	5.4	4.4	3.4	2.3	1.2	0.3	0	11	13	16	2.1	2.5	2.7	3	3.4	3.7	4.1	4.7	5.1	5.8	4.4	2.2	0	0	0	0	0
-10	0	0	0.4	3.1	5.7	7.3	7.2	7.1	7	7	5.9	4.6	3.5	2.3	1.4	0.1	0	0	0	0.7	0.8	1.2	1.6	2	2.6	3	3.5	4.2	4.7	4.8	2.6	0.8	0	0	0	0	0
-5	0	0	2.3	5	7.6	9.2	9	8.8	8.4	7.8	6.1	4.7	3.5	2.2	1.1	0	0	0	0	0	0	0	0.3	1	1.6	2.1	2.8	3.5	4.2	2.9	1.4	0	0	0	0	0	0
0	0	1.7	4.1	6.8	9.2	11	11	10	9.4	7.9	6.3	4.7	3.3	1.7	0.5	0	0	0	0	0	0	0	0	0.4	1	1.7	2.6	3.3	1.8	0.4	0	0	0	0	0	0	0
5	1.5	3.4	5.8	8.4	11	12	12	11	9.6	7.8	6	4.3	2.7	1.2	0	0	0	0	0	0	0	0	0	0	0	0	0.7	1.4	2.1	0.8	0	0	0	0	0	0	0
10	3.9	5.1	7.4	9.8	12	14	13	12	9.2	7.4	5.2	3.3	1.7	0.2	0	0	0	0	0	0	0	0	0	0	0	0	0	0.3	1.1	0.3	0	0	0	2.3	1	0	0
15	5.7	6.6	8.8	11	13	15	14	11	8.4	6.4	4.1	2	0.5	0	0	0	0	0	0	0	0	0	0	0	0	0	0	0	0.1	0	0	0	3.9	2.6	1.4	0.1	0
20	7.1	7.9	10	12	15	16	13	10	7.3	5	2.6	0.6	0	0	0	0	0	0	0	0	0	0	0	0	0	0	0	0	0	0	0	0	4	2.9	1.9	0.8	0
25	8.1	9.2	11	13	16	15	12	8.3	5.3	2.9	0.6	0	0	0	0	0	0	0	0	0	0	0	0	0	0	0	0	0	0	0	0	0	4.2	3.2	2.4	1.4	0.3
30	8.8	10	12	14	14	13	9.4	5.7	2.5	0.2	0	0	0	0	0	0	0	0	0	0	0	0	0	0	0	0	0	0	0	0	0	4.8	4.6	3.9	3.1	2.2	1.1
35	9.7	11	13	13	11	9.8	5.7	2.2	0	0	0	0	0	0	0	0	0	0	0	0	0	0	0	0	0	0	0	0	0	0	0	0	3.5	3.7	3.7	2.9	1.8

Table 8.25: ALT acquisition table for α = 180°, 01.30 am orbit, , 11th month of the year.

8.4.4. 01.30 am, one-year analysis

Evolution of feasible acquisition durations over one year are given in Figure *8.1*, Figure *8.2*, Figure *8.3* for α = 270°, 0° and 180°, respectively, for the 01.30 am orbit.

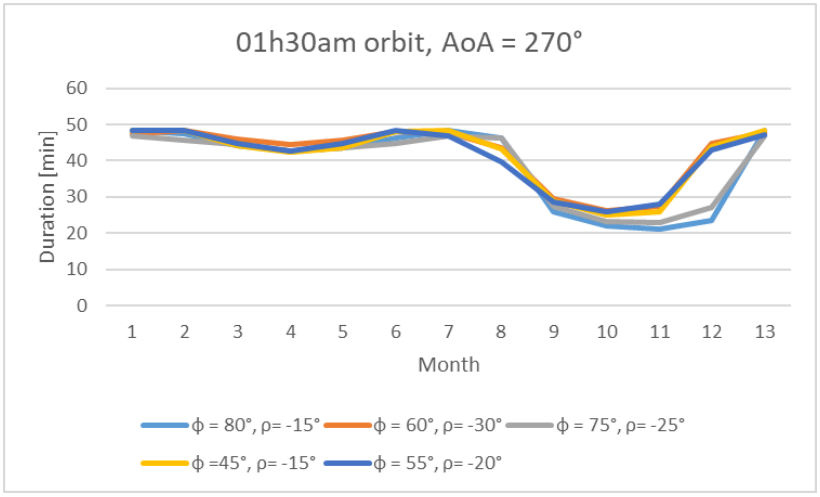

Figure 8.1: One-year evolution of acquisitions for α 270° configuration on 01.30 am orbit.

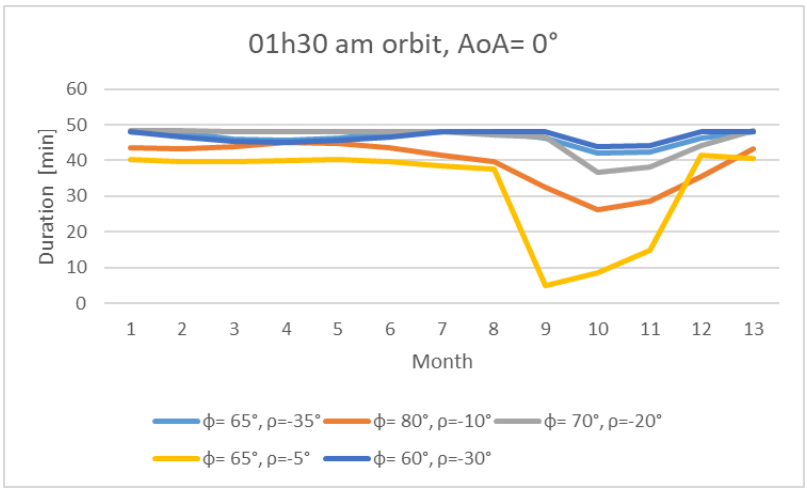

Figure 8.2: One-year evolution of acquisitions for α = 0° configuration on 01.30 am orbit.

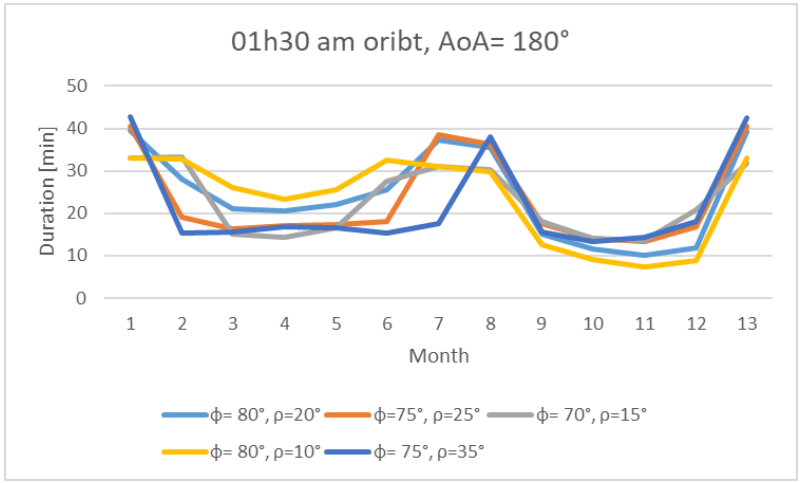

Figure 8.3: One-year evolution of acquisitions for α = 0° configuration on 01.30 am orbit.

9. References

[1] Stocker TF, Qin D et al. 2013. *Climate Change 2013: The Physical Science Basis*.

[2] Friedlingstein P, Jones M, et al., 2019. *Global Carbon Budget 2019.*

[3] Lucht W, Schaphoff S et al, 2006. *Terrestrial vegetation redistribution and carbon balance under climate change.*

[4] Schneising O, Bremen I, 2013*. Terrestrial carbon sink observed fromspace: variation of growth rates and seasonal cycle amplitudes in response to interannual surface temperature variability.* Institute of Environmental Physics (IUP), University of Bremen.

[5] Kort EA et al, 2012. *Space-based observations of megacity carbon dioxide*. Geophys. Res. Lett.

[6] JAXA. *GOSAT-2 project.* https://www.gosat-2.nies.go.jp/about/observation/.

[7] Frankenberg C, Pollock R, 2014. *Spectrometer performance evaluation using pre-launch direct sun measurement.* Jet Propulsion Laboratory.

[8] Chen W et al., 2020. *The Tansat mission: global CO2 observation an monitoring.* s.l. : Institute of Atmospheric Physics, 2020.

[9] *EO Portal Directory,* 2013. https://directory.eoportal.org/web/eoportal/satelliteissions/m/microcarb.

[10] Courtois M, Marcus V, 2015. *Contre-expertise de l'évaluation socio-économique du projet MicroCarb.*

[11] CNES, 2019 *CARB-SYST-ST-896-CNES Besoins de guidage et de programmation mission MicroCarb.*

[12] —. 2017. *MicroCarb Mission Specifications.*

[13] —. 2019. *MicroCarb System requirement Specifications.*

[14] —. MicroCarb Website. */microcarb.cnes.fr.* https://microcarb.cnes.fr/fr/.

[15] —. *Baffle Thermique CARB-SYS-MEM-1389-CNES_0101.*

[16] CNES. Polaris user manual. *gitlab.cnes.fr.* [En ligne] https://gitlab.cnes.fr/Polaris/Polaris/-/blob/master/doc/UserManuals/UserManual-Polaris-Maniac.md.

[17] —. *Modélisation du MCV 20170926*.

[18] Clough SA, Iacono MJ, 1995. *Line-by-line calculation of atmospheric fluxes and cooling rates: 2. Application to carbon dioxide, ozone, methane, nitrous oxide and the halocarbons.*

[19] JPL, NASA. OCO-2 mission. https://ocov2.jpl.nasa.gov/mission/.

[20] NASA. The Afternoon Constellation. *nasa.gov.* https://atrain.nasa.gov/.